JOURNAL OF PETROLOGY | VOLUME 47 | NUMBER 8 | PAGES 1467–1507 | 2006 | doi:10.1093/petrology/egl015

Evidence of Magma Mixing in the 'Daly Gap' of Alkaline Suites: a Case Study from the Enclaves of Pantelleria (Italy)

PAOLO FERLA* AND CARMELINA MELI

DIPARTIMENTO DI CHIMICA E FISICA DELLA TERRA ED APPLICAZIONI ALLE GEORISORSE E AI RISCHI NATURALI (CFTA), UNIVERSITÀ DEGLI STUDI DI PALERMO, VIA ARCHIRAFI N, 36-90123 PALERMO, ITALY

RECEIVED APRIL 24, 2004; ACCEPTED MARCH 7, 2006; ADVANCE ACCESS PUBLICATION MARCH 31, 2006

The island of Pantelleria consists of trachytes, pantellerites and minor mildly alkaline basalts. Rocks of intermediate composition (falling in the so-called 'Daly Gap') such as mugearites, benmoreites and mafic trachytes occur only in the form of enclaves in trachytes and pantellerites inside the main caldera of the island (Caldera 'Cinque Denti'), which collapsed during the 'Green Tuff' ignimbrite eruption at ~50 ka. The enclaves include volcanic, subvolcanic and intrusive rock types. The enclaves in host trachyte contain traces of glass; devitrified glass occurs within enclaves in host pantellerites. Minerals in the enclaves show regular compositional variations with whole-rock silica content. Glass present in the medium-grained samples is interpreted to be the result of incipient melting. The major and trace element compositions of the enclaves show regular and linear variations between an evolved mafic magma (hawaiite) and a felsic end-member similar to the 'Green Tuff' trachyte. Fractional crystallization modelling of compatible and incompatible trace elements (V, Ni, Zr, La, Sm, Lu, Nb, Y, Th) does not reproduce the observed trends. Rocks of intermediate composition within the 'Daly Gap' can be explained only by magma mixing between an already differentiated mafic magma (hawaiite) and an anorthoclase-rich trachytic melt in the lower and higher parts, respectively, of a stratified magmatic chamber. Medium-grained enclaves are interpreted as the result of fragmentation of solidified mixing layers in the roof of the magma chamber during the eruption of the 'Green Tuff', when the collapse of the caldera took place. Diffusion calculations suggest a residence time of <5 days for the enclaves in their host magmas.

KEY WORDS: *Daly Gap; enclaves; magma mixing; Pantelleria*

INTRODUCTION

Pantelleria is a Pleistocene volcanic island located in the Sicily Channel Rift Zone (Fig. 1) in which transtensional tectonics along the northern margin of the African plate have been active since the middle Pliocene. The island is constructed on crust constituting the foreland of the northern African plate, consisting of a deformed cover sequence (Tertiary–Pleistocene) overlying a Mesozoic carbonate succession and a thinned and unknown continental basement (Colombi *et al.*, 1973; Reuther & Eisbacher, 1985; Catalano *et al.*, 1993; Berrino & Capuano, 1995). The subaerial part of the island consists of trachytes, pantellerites and minor alkaline to transitional basalts (Villari, 1974; Cornette *et al.*, 1983; Civetta *et al.*, 1984, 1988; Mahood & Hildreth, 1986).

As frequently observed in many mildly alkaline suites in continental and oceanic areas, the erupted products lack rocks of intermediate composition, a phenomenon known as the 'Daly Gap' (Chayes, 1963, 1977; Yoder, 1973). A number of non-conclusive petrogenetic models have been proposed to explain the Daly Gap (e.g. Baker, 1968; Cann, 1968; Clague, 1978; Lowenstern & Mahood, 1991; Bonnefoi *et al.*, 1995; Mungall & Martin, 1995; Bohrson & Reid, 1997; Peccerillo *et al.*, 2003; Avanzinelli *et al.*, 2004).

Important petrogenetic problems in the context of Pantelleria include: explaining the origin of the peralkaline silicic rocks, their relationship with the basaltic magmas, and the reasons for the scarcity of intermediate compositions in the volcanic sequence.

*Corresponding author. Telephone: +39 091 6161516. Fax: +39 091 6168376. E-mail: pferla@unipa.it, applina2@katamail.com

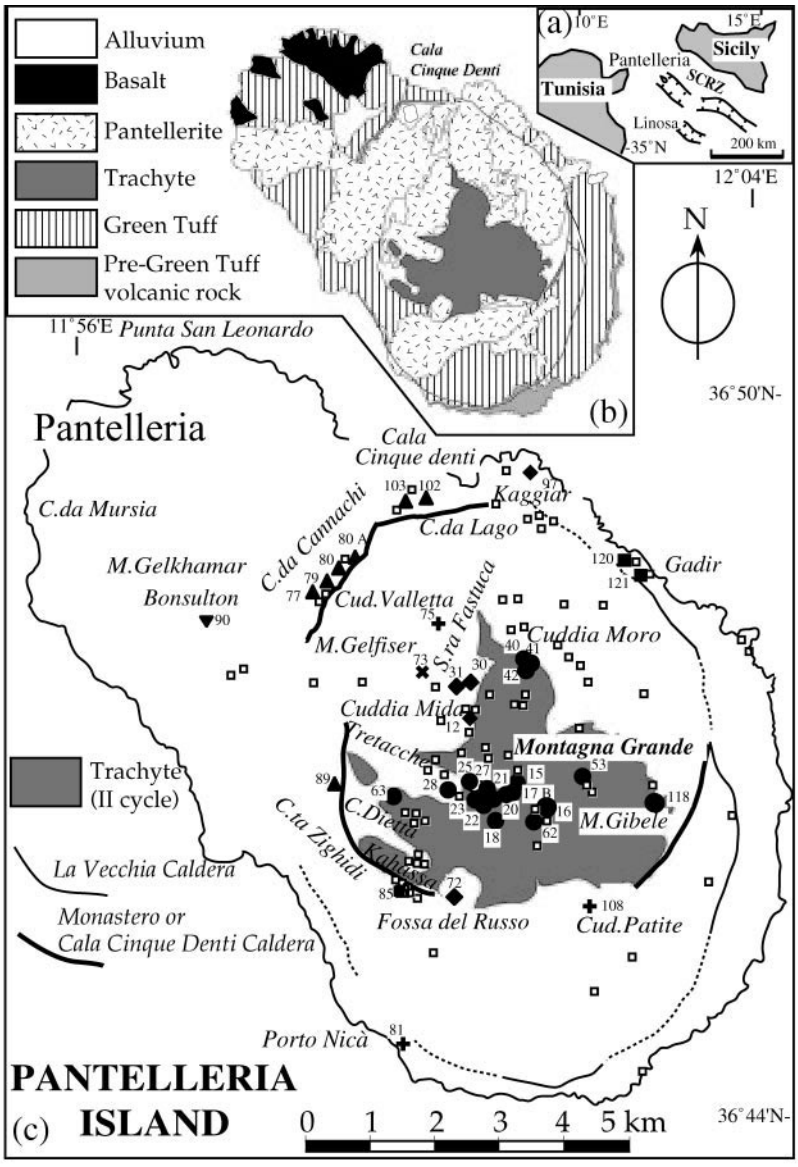

	stratigraphic section	age ka B.P.	host rock unit	host rock type (h)	enclave (x) (d)
	Basalts	<9 ka	Mursia	basalt	
◆	VI silicic cycle	9-5 ka	Cuddia Mida-Khaggiar	pantellerite	30,31,72
✖	V silicic cycle	13 ka	C.da Gadir	pantellerite	73
✚	IV silicic cycle	20-15 ka	Cuddie Patite-M.Gelfiser	pantellerite	75,81,108
▼	III silicic cycle	22 ka	Gelkhamar-Bonsulton	pantellerite	90
	Basalts	29 ka	Punta S.Leonardo	basalt	
●	II silicic cycle	44-29 ka	Montagna Grande-M.Gibele	trachyte	15,16B,17B,18,20,21,22,23,25,27A, 28,40,41,42,62A,62B,63,74,118
■	I silicic cycle	50-45 ka	Green Tuff	trachyte pantellerite	85,120,121
▲	Palaeo-Pantelleria	50 ka - 324 ka	Pre-Green Tuff volcanic rocks	pantellerite, trachyte basalt	77,79,80A,80C,89,102,103
❒					chemically not analysed

Fig. 1. Sketch map of the island of Pantelleria. (a) Location of Pantelleria within the Sicily Channel Rift Zone (SCRZ) between Sicily and Tunisia in the central Mediterranean Sea. (b) Geological sketch map of the volcanic island of Pantelleria. (c) Schematic map showing the locations of the sampled enclaves and the relative age of their host-rocks. The calderas have been redrawn from Mahood & Hildreth (1983) and Orsi *et al.* (1991); the trachytic outcrops of Montagna Grande are taken from the same sources. The sampled enclaves (filled symbols) are classified according to the age of the host-rock [Roman numbers in (d)], according to Civetta *et al.* (1984). (d) Schematic stratigraphic section to show the main eruptive cycles, with approximate ages according to Civetta *et al.* (1984), the horizons from which the enclaves were collected and analysed and the related host-rock types. The Palaeo-Pantelleria deposits according to Avanzinelli *et al.* (2004) comprise the pre-Green Tuff volcanic activity.

The study of magmatic enclaves from a suite of lavas characterized by a 'Daly Gap' can help to reveal the process responsible for the genesis of these particular rock fragments and can contribute to an understanding of the lack of intermediate erupted magmas at Pantelleria. The island is a favourable locality for this purpose because the erupted products are dominated by mafic (basalts–trachybasalts or hawaiites) and evolved (trachytes–pantellerites) rocks containing many enclaves of different composition.

In 1991, field research forming part of a geothermal project was carried out at Pantelleria during which magmatic enclaves were systematically collected. In this paper, we report on the petrological and geochemical study of these magmatic enclaves. Compositional data for whole-rocks and minerals are discussed with the aim of placing constraints on the genesis of the enclaves and explaining the transition between the mafic and felsic groups of magmatic rocks.

Geological setting

The island of Pantelleria consists mainly of lavas and welded ignimbrites of trachyte to pantellerite composition with subordinate basalts, and is the type locality for pantellerite and peralkaline volcanic rocks (Washington, 1913–1914). Large magnetic anomalies around the island suggest the presence of abundant basalt or gabbro intrusions at depth (Mahood & Hildreth, 1983; Berrino & Capuano, 1995).

The oldest exposed rocks are pantellerite lavas and ignimbrites with ages up to 324 ka. These are truncated by the La Vecchia caldera, which is dated at about 114 ka (Mahood & Hildreth, 1986). Post-caldera activity includes lavas, ignimbrites and pumice falls. Eruption of the 'Green Tuff', dated at ~45 ka, led to the formation of the younger Cinque Denti caldera (Mahood & Hildreth, 1986), which, however, according to Civetta *et al.* (1988, 1998), is coincident with the northern part of the older La Vecchia caldera and the younger Monastero caldera (Fig. 1). The 'Green Tuff' is a unit compositionally zoned from pantellerite to trachyte and considered by Mahood & Hildreth (1986) and Civetta *et al.* (1988, 1998) as the result of a large eruption from a stratified magmatic reservoir. It is a major marker horizon representative of the first of six silicic eruptive cycles (Civetta *et al.*, 1988, 1998), which lasted until 5·5 ka. Volcanic cycles I–VI are indicated in a schematic stratigraphic section in Fig. 1d. Subsequent eruptions filled the pre-existing caldera through several eruptive vents, the principal of which was at Monte Gibele; this volcanic edifice was subsequently tectonically uplifted and tilted to form Montagna Grande, the highest summit of the island (Washington, 1913–1914; Mahood & Hildreth, 1986). On the basis of K–Ar geochronological data, Mahood & Hildreth (1986) considered the Monte Gibele–Montagna Grande volcanic activity as a continuation of the 'Green Tuff' eruptive cycle; however, according to Civetta *et al.* (1988) the Montagna Grande is the result of eruptive cycle II. Considering the Pantelleria post-Green Tuff activity, mildly alkali basalts erupted sporadically (29 ka and <9 ka) solely from outside the calderas.

Sample collection and analytical methods

Samples of enclaves were grouped according to host-rock age based on the sequence of magmatic cycles proposed by Civetta *et al.* (1988). Enclaves were found and sampled almost exclusively from lavas that erupted in the area of the Cinque Denti caldera.

From 133 collected samples, often of small dimensions, 38 enclaves (x) and 22 host-rocks (h) were selected for detailed study on the basis of the following criteria (for the enclaves): greater size, lack of clay mineral alteration, negligible macroscopic interaction with the host-magma, hand specimen characteristics (colour, grain size) and the age of host-rocks (Tables 1 and 2). Among the widespread felsic enclaves <18 ka in age (Mahood & Hildreth, 1986; De Vivo *et al.*, 1993), only a few representative samples were considered.

The absence of secondary alteration in the enclaves was verified by X-ray diffraction (XRD) analysis using a Philips 1200 diffractometer at the Dipartimento CFTA of the University of Palermo (Italy); <2 μm oriented slides of water-centrifuged ground powders were analysed after natural, ethylene glycol, 300°C and 600°C heating treatments, respectively. For small enclaves, the host-rock was also analysed.

Modal proportions of minerals in the enclave and in the representative host-rock were determined by point counting involving 1631–2054 points covering the entire area of a thin section at 0·1 mm spacing with a 2–3% precision.

Mineral compositions were determined by electron microprobe analysis (EMPA) on an ARL-SEMQ at the Centro Studi Geominerari e Mineralurgici, CNR of Cagliari (Italy), with instrument settings at 24 kV accelerating voltage and 23 nA beam current with a diameter of 1 μm and counting times of 10 s. Brass and ZAF corrections were made using the MAGIC IV program (Colby, 1967) with precision better than 5%. Glass and feldspar were analysed with a 10 μm defocused beam on a vibrated sample to avoid analytical bias on the Na determination by EMPA (Spray & Rae, 1995; Olmi, 1997). For Cl, Sr, Ba, and F determination the detection limit was >30–40 ppm.

Whole-rock analyses were carried out on samples initially washed in distilled water to minimize the effect of marine aerosol. Major and trace elements were determined by X-ray fluorescence (XRF) at the Dipartimento

Table 1: Enclaves from Pantelleria volcanic rocks: sample description

Sample no	Host-rock type[1]	H.r. cycle	Size (cm)	Shape	Contact	Grain size	Composition	SiO_2% (wr)	Rock type[2]	TAS classification[3]	Modal proportion (vol. %)	Groundmass	Glass
103x	trach-(103 h)	>50 ka	7	rounded	graded	fg-mg	mafic	48·07	dolerite	hawaiite–tephrite	Ol(3) + Cpx(13) + Feld(69) + Te–Fe(3) + (Ap)		12
77x	pantell.-(77 h)	>50 ka	15	angular	sharp	fg-mg-po	felsic	66·20	microsyenite	trachyte	Cpx(2) + Anc(17) + Te–Fe(tr)	81	
80Cx	trachyte	>50 ka	16	angular	sharp	fg-po	felsic	66·73	trachyte	trachyte	Cpx(2) + Anc(14) + Te–Fe(tr)	84	tr
80Ax	trach-(80Ah)	>50 ka	6	rounded	graded	fg	felsic	70·11	microgranite	pantellerite	Af(56) + Qz(23) + Bi + Te–Fe[4]		tr
89x	trach-(89 h-)	>50 ka	16	rounded	graded	fg-po	felsic	70·44	microgranite	pantellerite	Af(60) + Qz(22) + Bi + Te–Fe[4]		tr
79x	pantell-(79 h)	>50 ka	6	rounded	sharp	fg	felsic	71·04	microgranite	pantellerite	Af63) + Qz(26) + Bi + Te–Fe[4]		tr
102x	trach-(102 h)	>50 ka	10	rounded	graded	fg-po	felsic	71·89	microgranite	pantellerite	Af(47) + Qz(35) + Bi + Te–Fe[4]		tr
121x	pantellerite	I	4	angular	sharp	fg-mg-po	interm.	59·98	trachyte	trachyte	Cpx(2) + Anc(18) + Te–Fe(1)	79	tr
120x	pantell-(120 h)	I	10	angular	sharp	fg-mg-po	interm.	62·60	trachyte	trachyte	Cpx(2) + Anc(19) + Te–Fe(1) + Ol(tr)	78	tr
85x	pantellerite	I	12	angular	sharp	fg-mg-po	interm.	64·60	microsyenite	trachyte	Feld(34) + Anc(tr) + Te–Fe(tr)	66	tr
21x	trachyte	II	9	rounded	graded	fg-mg-po	interm.	49·22	dolerite	hawaiite	Ol(10) + Cpx(33) + Feld(35) + Te–Fe(5) + (Ap)		17
28x	trachyte	II	8	rounded	graded	fg-mg-po	interm.	50·78	dolerite	hawaiite	Ol(5) + Cpx(21) + Feld(61) + Te–Fe(4) + (Ap)		9
20x	trachyte	II	4	rounded	graded	fg	interm.	52·85	microsyeno-gabbro	mugearite	Ol(5) + Cpx(22) + Feld(59) + Te–Fe(4) + (Ap)		10
16Bx	trach-(16Bh)	II	6	rounded	graded	fg-mg-po	interm.	53·57	syenogabbro	mugearite	Ol(4) + Cpx(25) + Feld(63) + Te–Fe(8) + (Ap)		tr
118x	trach-(118 h)	II	7	rounded	graded	fg-mg	interm.	53·94	syenogabbro	mugearite	Ol(6) + Cpx(23) + Feld(52) + Te–Fe(8) + (Ap)		11
62Bx	trach-(62Bh)	II	5	rounded	graded	fg-mg	interm.	54·10	syenogabbro	mugearite	Ol(6) + Cpx(17) + Feld(72) + Te–Fe(3) + (Ap)		2
62Ax	trach-(62Ah)	II	7	rounded	graded	fg-mg	interm.	54·41	syenogabbro	mugearite	Ol(7) + Cpx(20) + Feld(68) + Te–Fe(3) + (Ap)		2
18x	trachyte	II	6	rounded	graded	fg-mg	interm.	55·23	syenodiorite	benmoreite	Ol(3) + Cpx(10) + Feld(81) + Te–Fe(4) + (Ap)		2
27Ax	trachyte	II	5	rounded	graded	fg-mg	interm.	55·56	syenodiorite	benmoreite	Ol(6) + Cpx(14) + Feld(56) + Te–Fe(3) + (Ap)		21
27Bx	trachyte	II	6	rounded	graded	fg-mg	interm.	55·56	syenodiorite	benmoreite	Ol(4) + Cpx(11) + Feld(61) + Te–Fe(5) + (Ap)		19
42x	trachyte	II	7	rounded	graded	fg-mg	interm.	55·63	syenodiorite	benmoreite	Ol(8) + Cpx(22) + Feld(60) + Te–Fe(6) + (Ap)		4
17Bx	trachyte	II	6	rounded	graded	fg-mg	interm.	55·88	syenodiorite	benmoreite	Ol(3) + Cpx(10) + Feld(53) + Te–Fe(4) + (Ap)		30
63x	trachyte	II	17	rounded	graded	fg-mg	interm.	55·95	syenodiorite	benmoreite	Ol(5) + Cpx(17) + Feld(65) + Te–Fe(4) + (Ap)		9
15x	trachyte	II	5	rounded	graded	fg-mg	interm.	56·11	syenodiorite	benmoreite	Ol(2) + Cpx(15) + Feld(66) + Te–Fe(3) + (Ap)		14
23x	trachyte	II	5	rounded	graded	fg-mg	interm.	56·54	syenodiorite	benmoreite	Ol(2) + Cpx(10) + Feld(67) + Te–Fe(4) + (Ap)		17
41x	trachyte	II	6	rounded	graded	fg-mg	interm.	56·55	syenodiorite	benmoreite	Ol(3) + Cpx(16) + Feld(75) + Te–Fe(3) + (Ap)		3
40x	trachyte	II	5	rounded	graded	fg-mg	interm.	57·14	syenodiorite	benmoreite	Ol(5) + Cpx(17) + Feld(69) + Te–Fe(5) + (Ap)		4
22x	trachyte	II	9	rounded	graded	fg-mg	interm.	58·11	syenodiorite	benmoreite	Ol(2) + Cpx(10) + Feld(61) + Te–Fe(3) + (Ap)		24
25x	trachyte	II	5	rounded	graded	fg-mg	interm.	58·29	syenodiorite	benmoreite	Ol(5) + Cpx(6) + Feld(49) + Te–Fe(4) + (Ap)		36
74nax	trachyte	II	5	rounded	graded	fg-mg	interm.	n.a.	n.a.	n.a.	Ol(1) + Cpx(11) + Feld(79) + Te–Fe(9) + (Ap)		tr
90x	90 h-pantell.	III	4	rounded	sharp	fg-po	felsic	67·50	trachyte	trachyte	Cpx(1) + Anc(26) + Te–Fe(1)	72	
75x	75 h-trach.	IV	9	angular	sharp	fg-po	interm.	61·54	trachyte	trachyte	Cpx(2) + Anc(19) + Te–Fe(1)	78	tr
81x	81 h-pantell.	IV	10	angular	sharp	cg	interm.	62·65	syenite	trachyte	Ol(2) + Cpx(7) + Anc(88) + Te–Fe(1) + Amph(2)	—	—
108x	108 h-pantell.	IV	11	angular	sharp	fg-mg-po	felsic	65·99	trachyte	trachyte	Anc(25) + Cpx(tr) + Te–Fe(tr) + Ol(tr)	75	
73x	73 h-pantell.	V	8	angular	sharp	cg	felsic	66·27	syenite	trachyte	Cpx(6) + Anc(84) + Te–Fe(1) + Amph(3) + Qz(6)	—	—
31x	31 h-pantell.	VI	6	angular	sharp	fg-mg-po	interm.	56·50	syenodiorite	benmoreite	Ol(2) + Cpx(8) + Feld(72) + Te–Fe(4) + Amph(3)	11[5]	
30x	30 h-trach.	VI	10	rounded	sharp	fg-po	felsic	69·61	pantellerite	pantellerite	Cpx(1) + Anc(20) + Te–Fe(tr) + Co(tr)		79

[1]Chemical (with suffix h) or microscopic analysis.
[2]Nomenclature after MacKenzie *et al*. (1982).
[3]Le Maitre *et al*.(1989) classification.
[4]Normative calculation.
[5]Biotite + aegirine–augite + Fe oxides.
H.r. cycle, host-rock volcanic cycles after Civetta *et al*. (1988). cg, coarse-grained; mg, medium-grained; fg, fine-grained; po, porphyritic; interm., intermediate; wr, whole rock; teph, tephrite; Ol, olivine; Cpx, clinopyroxene; Feld, feldspar; Anc, anorthoclase; Af, alkali feldspar; Ti–Fe, Ti–Fe oxide; Amph, amphibole; Co, cossyrite; Qz, quartz; tr, trace; Bi, biotite.

Table 2: Volcanic rocks from Pantelleria : sample description

Sample no.	Locality	Volcanic cycle	TAS classification	Macdonald classification	Volcanic rock-type	Phenocryst mineralogy	Glass
80Ah	C.da Cannachi	>50 ka	trachyte	comenditic-trachyte	pyroclastic	Anc + Cpx + Te−Fe	n.a.
103 h	C.da Lago	>50 ka	trachyte	comenditic-trachyte	lava	Anc + Cpx + Te−Fe + (Ol)	n.a.
102 h	C.da Lago	>50 ka	trachyte	comenditic-trachyte	lava	Anc + Cpx + Te−Fe + (Ol)	n.a.
89 h	Costa Zighidi	>50 ka	trachyte	pantellerite	lava	Anc + Cpx + Te−Fe	n.a.
77 h	C.da Cannachi	>50 ka	pantellerite	pantellerite	lava	Anc + Cpx + Co	n.a.
79 h	C.da Cannachi	>50 ka	pantellerite	pantellerite	lava	Anc + Cpx + Co	n.a.
120 h	Gadir	I	pantellerite	pantellerite	pyroclastic	Anc + Cpx + Co	n.a.
16Bh	Montagna Grande	II	trachyte	comenditic-trachyte	lava	Anc(30) + Cpx(4) + Te−Fe(2) + (Ol)	64
18 h	Montagna Grande	II	trachyte	comenditic-trachyte	lava	Anc(39) + Cpx(5) + Te−Fe(2) + Ol(1)	54
23 h	Montagna Grande	II	n.a.	n.a.	lava	Anc(29) + Cpx(6) + Te−Fe(2)	64
28 h	Montagna Grande	II	n.a.	n.a.	lava	Anc(21) + Cpx(5) + Te−Fe(2) + Ol(1)	72
62Ah	Montagna Grande	II	trachyte	comenditic-trachyte	lava	Anc + Cpx + Te−Fe + (Ol)	n.a.
62Bh	Montagna Grande	II	trachyte	comenditic-trachyte	lava	Anc + Cpx + Te−Fe	n.a.
74 h	Montagna Grande	II	n.a.	n.a.	lava	Anc(27) + Cpx(2) + Te−Fe(tr)	69
118 h	M. Gibele	II	trachyte	comenditic-trachyte	lava	Anc + Cpx + Te−Fe + (Ol)	n.a.
90 h	Bonsulton	III	pantellerite	pantellerite	pyroclastic	Anc + Cpx + Co	n.a.
75 h	Cuddia Valletta	IV	trachyte	pantelleritic-trachyte	lava	Anc + Cpx + Te−Fe	n.a.
81 h	Porto Nicà	IV	pantellerite	pantellerite	lava	Anc(4) + Cpx(tr) + Co(1)	95
108 h	Cuddie Patite	IV	pantellerite	pantellerite	pyroclastic	Anc(9) + Cpx(tr) + Co(tr)	91
73 h	Serra Fastuca	V	pantellerite	pantellerite	pyroclastic	Anc + Cpx + Co	n.a.
30 h	Cuddia Mida	VI	trachyte	pantellerite	pyroclastic	Anc(20) + Cpx(1) + Te−Fe(tr)	79
12 h	Cuddia Mida	VI	trachyte	pantellerite	pyroclastic	Anc + Cpx + Te−Fe	n.a.
97 h	Khaggiar	VI	trachyte	pantellerite	lava	Anc + Cpx + Te−Fe	n.a.
72 h	Fossa Russo	VI	pantellerite	pantellerite	pyroclastic	Anc + Cpx + Co	n.a.
31 h	Cuddia Mida	VI	pantellerite	pantellerite	pyroclastic	Anc + Cpx + Co	n.a.

C.da, Contrada; M., Monte; Anc, anorthoclase; Cpx, clinopyroxene; (Ol), trace of Fe-olivine; Co, cossyrite; Ti−Fe, Ti−Fe oxides. TAS classification is from Le Maitre *et al*. (1989). Macdonald classification is from Macdonald (1974). Volcanic cycles after Civetta *et al*. (1988).

CFTA of the University of Palermo, on pressed pellets using a wavelength-dispersive XRF Philips PW 1400 spectrometer with Cr and Rh tubes. A matrix effect correction procedure was performed using the experimentally determined coefficients (Franzini *et al.*, 1975; Leoni & Saitta, 1976; Leoni *et al.*, 1982). Nb was measured by a step-by-step slow scan. The uncertainty for major elements is <1% for Si, Al and Na, <3% for Ti, K, Fe and Ca, and <10% for Mg, Mn and P. The uncertainty for trace elements is estimated to be <7% for Rb, Nb, Y, Sr and V, and <15% for Zr, La, Ce, Ba, Ni, Cr and Cl.

Several trace elements for some II Cycle enclaves, selected according to the available amount of sample, were determined by inductively coupled plasma mass spectrometry (ICP-MS) at the Dipartimento ITAF of the University of Palermo, using a Hewlett Packard 4500. The precision is 2–10% for trace element contents in the range 10–150 ppm and 5–30% for trace element contents in the range 0·1–5 ppm. Loss on ignition (LOI) was determined by gravimetric methods. mg-number = $Mg/(Mg + Fe^{2+})$ and Fe^{3+}/Fe^{2+} ratio were calculated according to the method of Kilinc *et al.* (1983).

Volcanic enclaves were classified according to the total alkali–silica (TAS; Le Maitre *et al.*, 1989) and Macdonald (1974) schemes; medium-grained enclaves were classified according to De la Roche *et al.* (1980) and MacKenzie *et al.* (1982) diagrams.

PETROGRAPHIC DESCRIPTIONS

Size and shape

The enclaves vary in size from centimetres to decimetres and show irregular, rounded or ellipsoidal shapes. There appears to be no relation between the shape of the

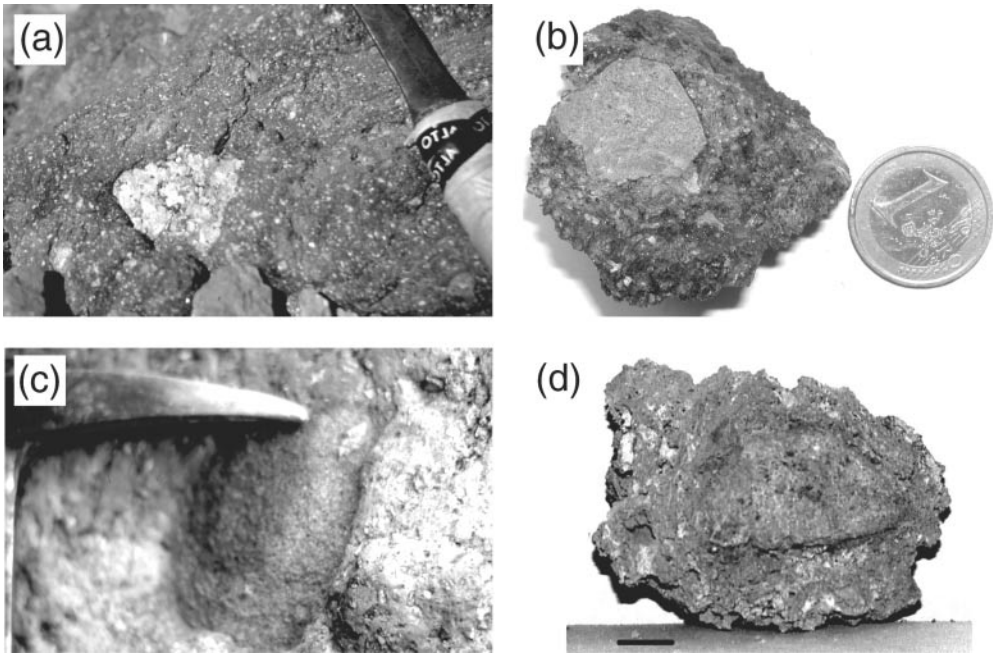

Fig. 2. (a) Coarse-grained felsic enclave shows irregular and sharp contact with the pantellerite host-rock of cycle V. (b) Microgranite enclave showing sharp contact with the pantellerite host-rock. (c) Rounded syenogabbro enclave within the trachyte host lava of Montagna Grande. (d) Syenodiorite enclave within the trachyte host lava of Montagna Grande; the enclave is rounded and has a gradational contact with the host-rock. Scale bar represents 1 cm.

enclaves and their internal structure, suggesting that they were solid fragments when incorporated in the host magma. Enclaves hosted in trachyte and pantellerite seem to have different shapes and sizes; the former exhibit margins grading into the host-rock and are frequently rounded, whereas the latter display sharp edges and have irregular shapes (Fig. 2).

Texture

Textures in the enclaves vary from holocrystalline, fine- to medium-grained, to porphyritic; some contain traces of glass. Enclaves have been grouped according to their texture, into volcanic, fine- to medium-grained and medium- to coarse-grained types. As noted above, there is a distinction between enclaves in pantellerite hosts and enclaves in trachyte hosts. Within the glass-bearing types it is possible to distinguish those with glass with abundant microlites, glass with few microlites, and clear to dark glass without microlites.

Modal mineralogy of the enclaves

The results of the modal analysis for selected enclaves within the trachytes and pantellerites are presented in Table 1. Enclaves within trachytes have the following mineralogy: (a) mafic enclaves: Ol (10–3), Cpx (33–13), Feldspar (65–33), Fe–Ti oxides (5–3), Apatite (tr; trace), glass (17–9); (b) intermediate composition enclaves: Ol (8–2), Cpx (25–6), Feldspar (79–49), Fe–Ti oxides (9–3), Apatite (tr), glass (36–tr); (c) felsic enclaves: (c1) trachyte enclaves: Cpx (2–0), Anorthoclase (20–17), groundmass (81–78); (c2) microgranite enclaves: Feldspar (60–47), Qz (35–22), Bi (tr), Fe–Ti oxides (tr), glass (tr), quartz and feldspars are normative; syenite and pantellerite enclaves were not found. Enclaves within pantellerites are as follows: (a) trachyte enclaves: Cpx (2–1), Anorthoclase (26–18), Fe–Ti oxides (tr), Ol (tr), groundmass (72–79); (b) syenite enclaves: Ol (2–0), Cpx (7–tr), Anorthoclase (88–17), Amph (3–0), Bi (tr), Fe–Ti oxides (tr), groundmass (81–0); (c) pantellerite enclaves (one sample) Anorthoclase (20), Cpx (1), Fe–Ti oxides (tr), Cossyrite (tr), glass (79); (d) microgranite enclaves (one sample) Alkali feldspar (63), Qz (26), Bi (tr), Fe–Ti oxides (tr), quartz and feldspars are normative. Enclaves of intermediate composition in host pantellerite were sporadically found in the intra-caldera ignimbritic pantellerite, e.g. sample 31x, which is very similar to the intermediate enclaves in the trachytes. We emphasize, in this context, the wide glass content variation from 0% up to 36% in the medium-grained sample 25x. Glass is generally more abundant towards the margin of the enclaves. The result of modal analyses for representative enclave host-rocks are presented in Table 2.

Enclave types

Volcanic enclaves

These include rock types similar to the common volcanic rock types of Pantelleria, including both trachytic and pantelleritic compositions.

Fine- to medium-grained enclaves

Although traces of interstitial glass occur in some fine- to medium-grained enclaves, the majority have textures similar to those of sub-volcanic rocks.

The more felsic types have textures ranging from granophyric to porphyritic and show some similarity to trachytes and pantellerites, except for their crystalline groundmass. They contain phenocrysts of zoned anorthoclase, subordinate Na–Fe-hedenbergitic clinopyroxene, fayalitic olivine and cossyrite in a microcrystalline groundmass of Na-sanidine, quartz, cossyrite, green aegirine-rich clinopyroxene, opaque minerals and apatite.

The more mafic enclaves have textures ranging from doleritic to porphyritic with phenocrysts of equant, forsteritic, olivine in an sub-ophitic groundmass of labradorite–andesine plagioclase, Ti-augite, Ti-magnetite, ilmenite, apatite and interstitial dark glass (Fig. 3a). Enclaves of hawaiitic composition contain spongy centimetre-sized xenocrysts of anorthoclase (Fig. 3a) and are found in volcanic rocks >50 ka in age, from the II, IV and VI cycles. These enclaves are similar, apart from the crystallization state, to the mafic sample 33MB from C.da Mursia of Mahood & Baker (1986) considered 'a result of basalt contamination by trachyte or syenite or of a mixing process with a trachytic magma'.

Medium- to coarse-grained enclaves

These rocks include alkaline granites, syenites, syenodiorites and syenogabbros with crystals of millimetre size. They resemble intrusive rocks but sometimes have interstitial glass.

The alkaline granites have porphyritic textures with zoned anorthoclase, hedenbergitic pyroxene with an aegirine-rich rim, quartz, alkali amphibole and biotite.

The syenites are common in the host trachytes of the earliest pre-Green Tuff volcanic eruptions, as well as the I and IV cycles. They consist of zoned anorthoclase with a resorbed core and green, zoned, hedenbergitic clinopyroxene, fayalitic olivine, interstitial Fe–Ti oxides, apatite, aegirine–augite, green to reddish brown pleochroic amphibole, biotite and quartz.

The syenodiorites show textural similarities to orthocumulates (Fig. 3d). Such enclaves, found in the II and VI cycle rocks from the Monastero caldera, were previously described as 'benmoreites' (Villari, 1974; Civetta *et al.* 1984). They show different mineral generations (e.g. relics of equant olivine with opaque inclusions and zoned elongate to skeletal olivine). The clinopyroxenes occur either as lobate augite with opaque inclusions and Ti-rich rims, or as clear, Fe-rich, zoned pyroxenes with augitic cores. Green, aegirine-rich rims are locally observed. Most feldspar is zoned with a clear, twinned, plagioclase core and a rim of zoned to xenomorphic alkali-feldspar. Ti-magnetite, ilmenite and needles of apatite are also present.

Syenogabbro and monzonitic gabbro enclaves are rare in the oldest pantellerites. They are similar to the syenodiorites with a comparable intercumulus assemblage of pleochroic alkaline amphibole, acicular aegirine-rich clinopyroxene and biotite.

Glass–enclave relations

The enclaves contain a variety of types of glass (Figs 3 and 4):

(1) clear to dark glass with microlites, occurring as localized areas in the outermost parts of the enclaves, suggests leakage of the host magma into the enclave;
(2) brown glass with few microlites, often exhibiting feathery crystallization, quench skeletal or radial crystals, locally with bifid edges, is distributed along grain boundaries in the enclaves; this kind of glass is often found close to mafic minerals;
(3) clear glass in contact with brown to dark glass occurs in the interiors of the enclaves, without microlites.

Enclave–host magma relations

The granular enclaves within pantellerite lavas (e.g. the syenite sample with amphibole 81x, the microgranite 79x, and the syenodiorite enclave 31x) do not contain glass. In the fine-grained types, portions of the mesostasis in trachyte and pantellerite enclaves show traces of rapid devitrification of the glass into globular or fibrous clusters of Na-sanidine, quartz, aegirine-rich clinopyroxene and cossyrite. Fibrous feldspars nucleate around the rims of anorthoclase phenocrysts (Fig. 3 h), which are often broken along cleavage planes or fragmented into small subidiomorphic quadrate grains. In holocrystalline medium-grained and hypidiomorphic types, alkali feldspar shows antiperthite exsolution.

Enclaves in trachytes are commonly characterized by the presence of interstitial glass and deformations of crystals, but show distinctive differences according to the enclave type: (1) The enclaves with a bulk-rock composition of pantellerite (only in pre-Green Tuff trachytes) contain glass varying from colourless to dark brown, in some cases, similar to the glass derived from the host magma; (2) in the mafic doleritic enclaves, glass develops as inclusions in spongy anorthoclase xenocrysts and

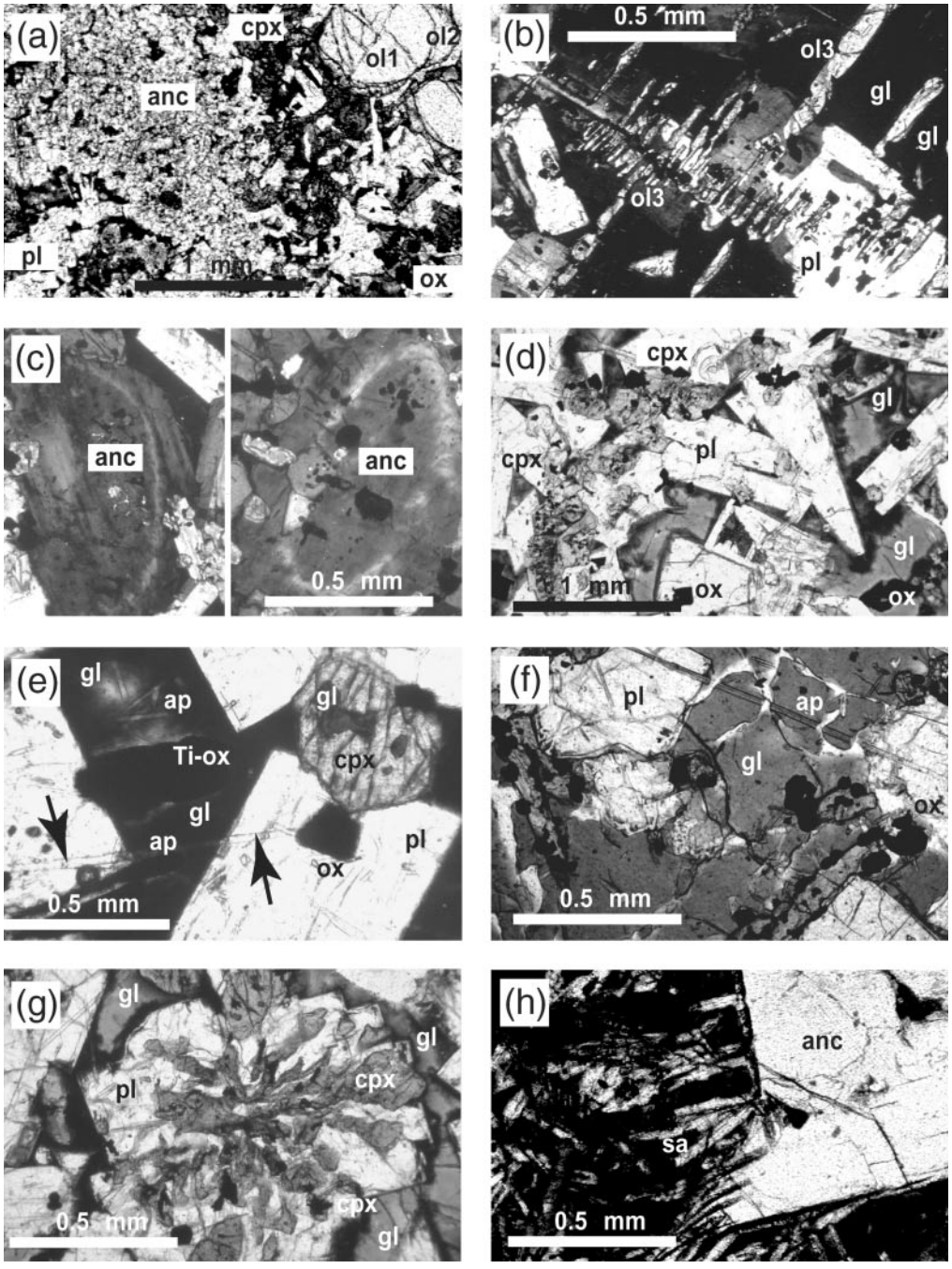

Fig. 3. Textural characteristics of enclaves within host trachyte and pantellerite. (a) 21x: mafic enclave with equant olivine xenocrysts with Fo_{86} cores (ol1), euhedral rims Fo_{79} (ol2) and spongy anorthoclase (anc) in a sub-ophitic groundmass of plagioclase (pl) and clinopyroxene (cpx) (plane-polarized light). (b) 22x: skeletal Fo_{39} olivine (ol3), plagioclase (pl) and glass (gl) in enclave of intermediate composition (cross-polarized light). (c) Ovoid core to anorthoclase within 27x (left) and 17x (right) intermediate enclaves (cross-polarized light). (d) 17Ax enclave of intermediate composition, which shows intra-crystalline glass (gl) between euhedral Ca-rich plagioclase (pl). The same glass area appears zoned in colour with dark glass close to the minerals and clear glass in the interior part of the glassy area (plane-polarized light). (e) 22x: intermediate enclave with glass (gl) formed by incipient melting within clinopyroxene and between plagioclase (pl), ilmenite (Ti-ox) and apatite (ap); the apatite needle, marked by the arrows, intersects two plagioclase crystals separated by glass (plane-polarized light). (f) 22x: skeletal apatite needles crossing the glass and two resorbed plagioclase (oligoclase) crystals (plane-polarized light). (g) 17Ax: clinopyroxene and plagioclase feldspars in radial intergrowth; note the intra-crystalline partial melt (gl), which retains the euhedral shape of the zoned plagioclase (plane-polarized light). (h) Sanidine needles (sa) surrounding an anorthoclase phenocryst (anc) in a trachytic enclave within a host pantellerite (cross-polarized light).

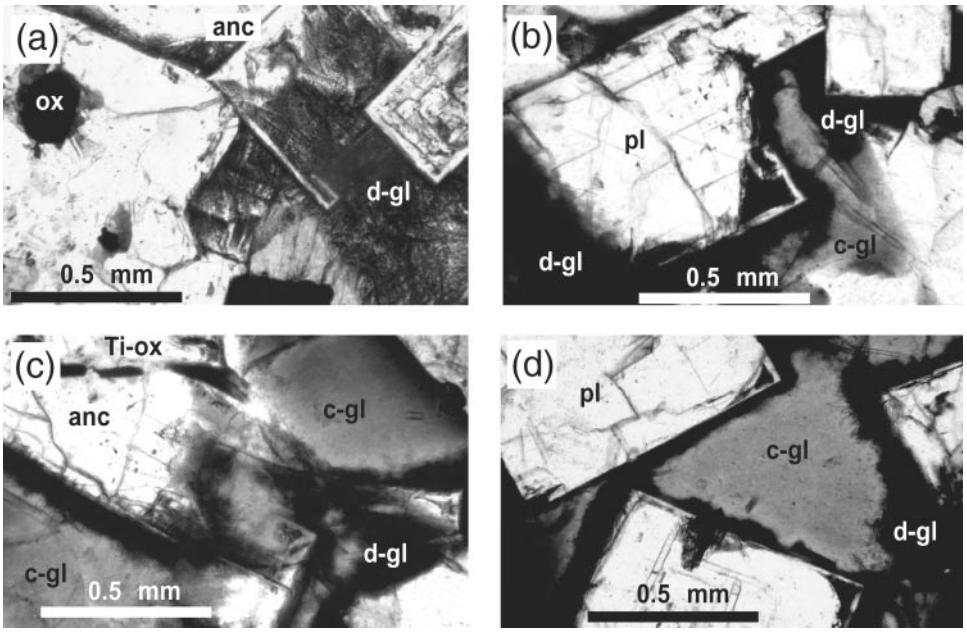

Fig. 4. Microscopic texture of feldspar crystals in contact with glass (gl) in the intermediate composition enclaves within the trachyte host-rocks of the II volcanic cycle of Montagna Grande. The crystal shapes of the almost totally resorbed anorthoclase (anc) and of the partially resorbed rim of the plagioclase (pl) are interpreted as the result of partial melting of the enclaves by heating from the host lavas. (a) 14x enclave (chemically not analysed): the glass shows incipient devitrification. (b), (c) and (d) 17Ax enclave (plane-polarized light).

interstitially in the groundmass; (3) the medium- to coarse-grained enclaves exhibit glass very similar to the residual intra-crystalline melt, changing from colourless to darkish brown. The sharp colour change occurs on a $<10\,\mu m$ interval, which is indicative of very low interdiffusion of elements between the two different glasses (Figs 3 and 4). These enclaves are poly-crystalline aggregates with allotriomorphic-granular textures in which radial intergrowths (MacKenzie *et al.*, 1982) of pyroxenes and feldspars are occasionally observed; however, the side of these feldspar crystals in contact with the surrounding glass is idiomorphic with sharp boundaries (Fig. 3 g). Feldspar crystals in contact with the glass show evidence of rim resorption and euhedral, more anorthitic, cores (Figs 3d,e and 4). Both crystals and interstitial glassy areas are crossed by needles of skeletal olivine, pyroxene and even apatite (Fig. 3e and f). According to Ferla *et al.* (1978) and Harris & Bell (1982), all these textures are consistent with heating and partial remelting of the enclaves by the host magma. Glass in the enclaves is nearly absent when the host trachyte is holocrystalline, as in some Montagna Grande trachytic rocks.

Bulk-rock geochemistry of the enclaves

Bulk-rock chemical analyses of the enclaves and their host lavas are reported in Tables 3–5 and compared with available published data for Pantelleria rocks in Fig. 5a–c (Carmichael, 1962, 1967; Rittmann, 1967; Romano, 1969; Macdonald, & Bailey, 1973; Villari, 1974; Civetta *et al.*, 1984, 1988, 1998; Mahood & Baker, 1986; Mahood & Stimac, 1990; Esperança & Crisci, 1995; Avanzinelli *et al.*, 2004). According to the TAS classification diagram (Le Maitre *et al.*, 1989) the enclaves span the compositional range between the mafic and felsic volcanic rocks, corresponding to the 'Daly Gap', typically found between basalts and trachytes (Fig. 6). Volcanic or medium- to coarse-grained enclaves of trachytic and pantelleritic composition are also present.

The volcanic rocks of Pantelleria typically show a bimodal distribution of compositions with hawaiites and trachytes as mafic and felsic end-members, respectively, and a wide 'Daly Gap' between 52% and 63% SiO_2. The host-rocks to the enclaves are trachytes with at least 61% SiO_2, almost exclusively of the II cycle, and subordinate pantellerites. Enclaves of basaltic composition or mafic cumulates have not been found.

Element variations with silica content and rock type.

Major and trace element Harker variation diagrams for enclaves with SiO_2 ranging from 48% to 65% display, with few exceptions, distinctive linear and regular trends that are different from those of the erupted volcanic rocks (Fig. 5). Among the enclaves and volcanic rocks of Pantelleria we have, therefore, distinguished three chemical groups based on SiO_2 content: mafic (45–48 wt %

Table 3. Representative bulk-rock analyses of enclaves within the volcanic rocks of Pantelleria

Sample no.:	103x	77x	80Cx	80Ax	89x	79x	102x	121x	120x	85x	16Bx	118x	62Ax	18x
Locality:	C.da Lago	C.da Cannachi	C.da Cannaxchi	C.da Cannachi	C.da Zighidi	C.da Cannachi	C.da Lago	Gadir	Gadir	C.da Kahassa	M. Grande	M. Grande	M. Grande	M. Grande
Rock type:	dolerite	microsyenite	trachyte	microgranite	microgranite	microgranite	microgranite	trachyte	trachyte	microsyenite	syenogabbro	syenogabbro	syenogabbro	syenodiorite
H.r. type:	trachyte	pantellerite	trachyte	trachyte	trachyte	pantellerite	trachyte	pantellerite	pantellerite	pantellerite	trachyte	trachyte	trachyte	trachyte
H.r. volc. cycle:	>50 ka	>50 ka	>50 ka	>50 ka	>50 ka	>50 ka	>50 ka	I	I	I	II	II	II	II
wt %														
SiO_2	48·07	66·20	66·73	70·11	70·44	71·04	71·89	59·98	62·60	64·60	53·57	53·94	54·41	55·23
TiO_2	3·85	1·02	0·73	0·66	0·53	1·02	0·54	1·48	1·04	1·04	2·37	2·28	2·22	2·09
Al_2O_3	15·80	15·37	14·75	10·69	11·37	12·99	11·51	16·24	16·34	15·41	15·19	17·69	16·64	15·85
FeO*	11·09	4·58	5·08	8·08	6·30	5·83	6·64	6·93	5·58	5·22	9·99	8·70	9·26	9·84
MnO	0·26	0·22	0·21	0·20	0·23	0·20	0·23	0·23	0·23	0·23	0·27	0·25	0·24	0·27
MgO	3·85	0·58	0·28	0·36	0·30	0·16	1·91	1·28	0·87	0·97	4·20	2·45	2·03	1·89
CaO	8·73	1·03	0·69	0·42	0·35	0·40	0·07	3·30	2·41	1·55	6·93	6·31	5·89	5·35
Na_2O	5·69	7·08	6·65	5·00	5·73	4·94	1·64	7·50	7·10	6·88	5·00	5·45	6·48	6·26
K_2O	1·39	3·92	4·82	4·43	4·73	3·30	5·54	2·53	3·61	3·84	1·88	2·13	1·86	2·34
P_2O_5	1·27	0·02	0·07	0·02	0·01	0·11	0·01	0·53	0·22	0·25	0·58	0·78	0·97	0·90
LOI	1·79	0·97	0·39	2·60	1·65	1·65	1·30	0·54	0·92	0·60	1·07	1·34	0·36	0·84
Cl		0·04	0·05	0·10	0·15	0·02	0·06	n.a.	0·09	0·06	0·10	0·14	0·07	0·09
AI	0·69	1·03	1·09	1·22	1·28	0·90	0·76	0·93	0·95	1·00	0·68	0·64	0·76	0·81
ppm														
Rb	59	41	45	53	114	35	72	32	44	43	20	20	12	12
Sr	369	88	32	85	2	29	27	286	173	94	322	354	332	223
Y	35	29	19	72	85	72	82	45	61	138	16	32	47	9
Zr	136	472	375	442	956	432	630	196	313	306	212	261	194	54
Nb	36	102	99	88	179	77	116	60	73	68	80	51	52	35
Ba	n.a.	n.a.	718	n.a.	n.a.	n.a.	n.a.	n.a.	n.a.	n.a.	867	n.a.	n.a.	1469
La	n.a.	n.a.	118	n.a.	n.a.	n.a.	n.a.	n.a.	n.a.	n.a.	71	n.a.	n.a.	58
Ce	n.a.	n.a.	169	n.a.	n.a.	n.a.	n.a.	n.a.	n.a.	n.a.	134	n.a.	n.a.	114
Cr	n.a.	n.a.	3	n.a.	n.a.	n.a.	n.a.	n.a.	n.a.	n.a.	114	n.a.	n.a.	4
Ni	n.a.	n.a.	2	n.a.	n.a.	n.a.	n.a.	n.a.	n.a.	n.a.	58	n.a.	n.a.	3
V	n.a.	n.a.	16	n.a.	n.a.	n.a.	n.a.	n.a.	n.a.	n.a.	181	n.a.	n.a.	112

Sample no.:	27Ax	42x	15x	23x	22x	25x	90x	75x	108 x	73x	31x	72x	30 x
Locality:	Mont. Grande	Cuddia Moro	M. Grande	M. Grande	M. Grande	M. Grande	Bonsulton	Cuddia Valletta	Cuddie Patite	Serra Fastuca	Cuddia Mida	Fossa Russo	Cuddia Mida
Rock type:	syenodiorite	syenodiorite	syenodiorite	syenodiorite	syenodiorite	syenodiorite	trachyte	trachyte	trachyte	syenite	syenodiorite	trachite	pantellerite
H.r. type:	trachyte	trachyte	trachyte	trachyte	trachyte	trachyte	pantellerite	trachyte	pantellerite	pantellerite	pantellerite	pantellerite	trachyte
H.r.volc. cycle:	II	II	II	II	II	II	III	IV	IV	V	VI	VI	VI
wt %													
SiO_2	55·56	55·63	56·11	56·54	58·11	58·29	67·50	61·54	65·99	66·27	56·50	65·11	69·61
TiO_2	2·11	2·25	2·00	1·92	1·57	1·81	0·69	1·25	0·65	0·54	1·83	0·66	0·49
Al_2O_3	16·45	16·16	16·09	16·09	16·55	16·03	14·82	16·12	14·39	15·32	15·92	14·12	10·15
FeOt	9·08	9·10	9·24	8·89	7·92	8·06	4·08	5·60	6·68	4·24	8·47	6·99	8·31
MnO	0·24	0·24	0·31	0·28	0·29	0·27	0·22	0·24	0·24	0·23	0·24	0·23	0·29
MgO	1·83	2·05	1·82	1·69	1·64	1·63	0·50	1·21	0·01	0·28	2·10	0·22	0·01
CaO	5·45	5·54	5·23	5·07	4·44	4·06	0·73	2·65	0·90	0·90	4·93	1·01	0·46
Na_2O	6·17	6·22	6·26	6·30	6·38	6·15	6·59	7·08	6·36	6·99	6·40	6·76	6·34
K_2O	2·19	2·22	2·25	2·37	2·59	2·85	4·81	3·80	4·79	5·18	2·60	4·83	4·36
P_2O_5	0·79	0·60	0·70	0·79	0·43	0·64	0·05	0·27	0·01	0·04	1·01	0·05	0·01
LOI	0·54	0·22	1·19	0·25	0·84	0·94	1·04	0·63	1·67	0·91	1·20	1·38	1·35
Cl	0·10	0·04	0·15	0·12	0·14	0·21	0·04	0·24	0·14	0·21	0·15	0·68	0·21
AI	0·76	0·78	0·79	0·80	0·80	0·82	1·08	0·98	1·09	1·12	0·84	1·16	1·49
ppm													
Rb	20	12	15	23	26	37	68	65	41	100	63	59	114
Sr	264	276	326	248	293	290	24	159	30	42	245	10	32
Y	47	35	21	17	13	19	53	52	9	46	52	51	63
Zr	175	176	207	163	186	238	472	362	360	464	135	434	1478
Nb	52	56	74	58	61	83	95	89	116	105	75	101	238
Ba	n.a.	n.a.	1583	1426	1416	1105	n.a.	n.a.	234	n.a.	n.a.	n.a.	322
La	n.a.	n.a.	64	67	45	77	n.a.	n.a.	52	n.a.	n.a.	n.a.	n.a.
Ce	n.a.	n.a.	149	139	108	140	n.a.	n.a.	133	n.a.	n.a.	n.a.	411
Cr	n.a.	n.a.	3	4	8	5	n.a.	n.a.	1	n.a.	n.a.	n.a.	4
Ni	n.a.	n.a.	6	4	6	6	n.a.	n.a.	1	n.a.	n.a.	n.a.	4
V	n.a.	n.a.	125	124	112	98	n.a.	n.a.	11	n.a.	n.a.	n.a.	10

*Total Fe as FeO.
Major (wt %) and trace elements (ppm) by XRF. Analyses were recalculated to 100% on an anhydrous basis and corrected for NaCl. H.r. volc. cycle, host-rock volcanic cycle after Civetta *et al.* (1988). LOI, loss on ignition. AI, Agpaitic Index [molar($Na_2O + K_2O$)/Al_2O_3)]. n.a., not analysed.

Table 4: Selected bulk-rock analyses of the enclaves of intermediate composition

Sample no.:	21x	28x	20x	62Bx	27Bx	17Bx	63x	41x	40x	81x
Locality:	Mont. Grande	Mont. Grande	Mont. Grande	Mont. Grande	Mont. Grande	Mont. Grande	C. Dietta	Cuddia Moro	Cuddia Moro	Porto Nicà
Rock type:	dolerite	dolerite	microsy.gab.	sy.gabbro	syenodiorite	syenodiorite	syenodiorite	syenodiorite	syenodiorite	syenite
H.r. type:	trachyte	trachyte	trachyte	trachyte	trachyte	trachyte	trachyte	trachyte	trachyte	pantellerite
H.r. volcanic cycle:	II	II	II	II	II	II	II	II	II	IV
wt %										
SiO_2	49·22	50·78	52·85	54·10	55·56	55·88	55·95	56·55	57·14	62·65
TiO_2	2·81	2·67	2·71	2·32	2·09	2·21	2·11	1·99	1·97	0·86
Al_2O_3	15·17	16·05	15·57	15·95	15·94	16·16	15·68	15·87	16·27	15·80
FeOt	10·26	10·17	10·68	10·17	9·35	8·79	9·45	9·06	8·25	6·36
MnO	0·26	0·21	0·32	0·31	0·30	0·23	0·29	0·30	0·25	0·29
MgO	7·39	4·86	2·57	2·04	1·98	2·22	2·10	1·77	1·71	0·29
CaO	8·99	8·68	6·59	5·97	5·52	5·18	5·33	4·93	4·99	1·64
Na_2O	4·14	4·49	5·81	6·27	6·20	6·02	6·10	6·42	6·20	6·83
K_2O	1·18	1·47	1·75	1·91	2·25	2·55	2·25	2·40	2·45	5·11
P_2O_5	0·59	0·63	1·13	0·97	0·82	0·77	0·75	0·71	0·77	0·17
LOI	0·45	1·48	0·78	0·93	1·24	1·01	0·91	0·27	0·62	1·24
Cl	0·16	0·16	0·13	0·04	0·26	0·38	0·14	0·06	0·05	0·19
Al	0·53	0·56	0·74	0·78	0·79	0·78	0·79	0·83	0·79	1·06
ppm										
Cs	0·19	0·68	0·20	0·14	0·34	0·37	0·20	0·27	0·10	0·12
Rb	20	24	14	13	20	37	16	12	23	45
Sr	395	386	315	363	313	280	285	285	273	46
Y	33	18	14	23	23	16	17	16	35	10
Zr	227	193	176	214	231	221	137	199	203	111
Nb	47	57	62	72	69	76	54	66	57	68
Ba	612	706	1251	1280	1190	1005	1531	1503	1194	671
La	68	65	72	76	72	66	73	70	96	73
Ce	121	122	130	146	115	124	123	131	178	148
Nd	40·3	46·3	38·0	34·0	41·9	41·3	35·7	40·1	38·8	38·1
Sm	9·63	9·85	8·96	9·54	10·08	7·32	9·14	8·52	10·23	7·98
Eu	3·37	3·26	4·01	3·26	3·74	2·98	3·09	3·46	3·52	3·41
Gd	8·56	8·75	9·47	10·34	9·63	10·12	9·85	9·53	9·64	10·02
Dy	9·27	12·32	10·87	14·13	10·8	11·99	10·65	11·91	11·25	9·5
Er	5·83	6·33	6·4	6·2	6·04	5·73	5·72	5·62	8·15	5·65
Yb	4·55	5·08	3·98	3·36	3·84	4·4	3·84	5·35	5·79	5·18
Lu	0·49	0·58	0·39	0·34	0·47	0·42	0·46	0·52	0·48	0·52
Sc	16	31	29	24	17	16	20	24	25	16
Cr	6	196	8	10	10	17	2	7	13	4
Ni	12	72	7	7	11	6	7	6	14	1
V	176	286	214	180	153	167	133	154	104	32
Cu	35	96	58	68	39	45	39	44	70	32
Ga	52	64	49	58	38	39	36	55	67	65
Hf	8·98	8·67	7·29	9·02	5·78	13·56	4·73	7·67	9·25	8·99
Ta	4·85	3·62	5·8	6·21	6·06	5·69	3·71	6·71	7·18	4·63
Pb	3	5	3	4	2	4	4	4	7	6
Th	8·15	7·28	3·24	5·40	3·71	8·57	2·00	5·09	9·05	4·34
U	1·93	1·90	1·10	1·78	1·82	1·81	0·86	1·50	1·15	0·75
$(Ce/Yb)_N$	6·896	6·231	8·451	11·268	7·715	7·268	8·290	6·323	7·972	7·394
(Eu/Eu*	1·112	1·052	1·322	0·998	1·145	1·058	0·990	1·170	1·068	1·166
$(Gd/Yb)_N$	1·518	1·390	1·920	2·483	2·024	1·856	2·071	1·436	1·344	1·561

Major elements (wt %) by XRF, trace elements (ppm) by ICP-MS. REE normalization (indicated by subscript N) after Boynton (1984).

Table 5: Representative analyses of the host-rocks containing the enclaves

Sample no.:	80Ah	103 h	102 h	89 h	77 h	79 h	120 h	16Bh	18 h	62Ah	118 h
Locality:	C.da Cannachi	C.da Lago	C.da Lago	Costa Zighidi	C.da Cannachi	C.da Cannachi	Gadir	M. Grande	M. Grande	M. Grande	M. Gibele
Rock type TAS:	trachyte	trachyte	trachyte	trachyte	pantellerite	pantellerite	pantellerite	trachyte	trachyte	trachyte	trachyte
Rock type Macd:	comenditic-trach.	comenditic-trach.	comenditic-trach.	pantellerite	pantellerite	pantellerite	pantellerite	comenditic-trach.	comenditic-trach.	comenditic-trach.	comenditic-trach.
Volcanic cycle:	>50 ka	>50 ka	>50 ka	>50 ka	>50 ka	>50 ka	I	II	II	II	II
wt %											
SiO_2	66·20	67·47	67·92	68·99	69·56	70·93	70·63	59·03	60·32	61·66	61·74
TiO_2	0·98	0·55	0·55	0·49	0·67	0·59	0·60	1·33	1·30	1·11	0·81
Al_2O_3	15·24	14·61	14·41	11·04	11·03	10·21	10·49	16·94	15·98	15·30	19·22
FeOt*	5·96	4·49	4·62	5·78	7·84	7·71	7·79	7·00	6·90	6·76	5·24
MnO	0·23	0·20	0·23	0·20	0·22	0·18	0·23	0·28	0·29	0·27	0·23
MgO	0·86	0·30	0·35	0·54	0·52	0·15	0·45	1·58	1·43	1·14	0·54
CaO	0·69	0·83	0·75	0·43	0·39	0·35	0·50	2·82	2·85	2·24	1·94
Na_2O	5·76	7·03	6·45	8·08	5·19	5·36	4·82	7·14	6·86	7·24	6·48
K_2O	3·90	4·47	4·68	4·42	4·56	4·51	4·48	3·51	3·66	3·99	3·64
P_2O_5	0·17	0·05	0·04	0·01	0·01	0·01	0·01	0·37	0·42	0·28	0·17
LOI	0·63	0·99	1·98	2·88	1·73	2·26	2·61	1·59	1·42	1·21	2·50
Cl			0·05	0·06	1·23	0·12		0·41	0·04	0·09	0·04
AI	0·90	1·12	1·09	1·64	1·22	1·34	1·22	0·92	0·95	1·06	0·76
ppm											
Rb	103	66	69	118	92	89	102	30	46	42	32
Sr	8	39	36	4	10	3	19	163	174	98	184
Y	62	59	70	76	30	39	81	14	24	17	36
Zr	918	504	575	1075	852	1061	1377	270	297	205	431
Nb	174	102	111	196	149	157	245				86
Ba	n.a.	n.a.	n.a.	n.a.	n.a.	n.a.	n.a.	1349	1331	1370	n.a.
La	n.a.	n.a.	n.a.	n.a.	n.a.	n.a.	n.a.	80	71	84	n.a.
Ce	n.a.	n.a.	n.a.	n.a.	n.a.	n.a.	n.a.	143	146	146	n.a.
Cr	n.a.	n.a.	n.a.	n.a.	n.a.	n.a.	n.a.	6	7	5	n.a.
Ni	n.a.	n.a.	n.a.	n.a.	n.a.	n.a.	n.a.	6	8	5	n.a.
V	n.a.	n.a.	n.a.	n.a.	n.a.	n.a.	n.a.	59	57	46	n.a.

Sample no.:	62Bh	90h	75h	81h	108h	73h	30 h	12h	97h	72h	31h
Locality Mida:	M. Grande	Bonsulton	Cuddia Valletta	Porto Nicà	Cuddie Patite	Serra Fastuca	Cuddia Mida	Cuddia Mida	Khaggiar	Fossa Russo	Cuddia Mida
Rock type TAS:	trachyte	pantellerite	trachyte	pantellerite	pantellerite	pantellerite	trachyte	trachyte	trachyte	pantellerite	pantellerite
Rock type Macd:	comenditic-trach.	pantellerite	pantelleritic-trach.	pantellerite	pantellerite	pantellerite	pantellerite	pantellerite	pantellerite	pantellerite	pantellerite
Volcanic cycle:	II	III	IV	IV	IV	V	VI	VI	VI	VI	VI
SiO_2	63·07	69·30	66·97	70·12	70·21	69·68	66·95	67·41	68·60	69·13	69·19
TiO_2	1·09	0·65	0·56	0·50	0·45	0·51	0·54	0·54	0·54	0·54	0·51
Al_2O_3	15·17	11·19	12·73	8·94	8·51	9·85	11·46	10·00	10·23	9·87	10·21
FeOt	6·53	8·44	6·91	8·01	8·40	7·88	7·81	8·38	8·05	8·72	7·85
MnO	0·23	0·22	0·23	0·28	0·29	0·21	0·30	0·32	0·23	0·21	0·22
MgO	0·76	0·38	0·23	0·20	0·20	0·02	0·25	1·16	0·21	0·10	0·14
CaO	2·13	0·50	0·74	0·30	0·32	0·47	0·62	0·56	0·51	0·47	0·52
Na_2O	6·73	4·77	6·87	7·30	7·30	6·87	7·54	7·34	7·05	6·53	6·89
K_2O	4·01	4·52	4·74	4·33	4·32	4·50	4·50	4·30	4·57	4·41	4·44
P_2O_5	0·26	0·01	0·03	0·01	0·01	0·01	0·02	0·01	0·01	0·01	0·01
LOI	0·65	2·88	1·51	1·12	1·90	1·00	1·77	0·88	0·82	1·71	1·75
Cl	0·46	n.a.	0·27	n.a.	n.a.	n.a.	n.a.	1·04	n.a.	n.a.	n.a.
Al	1·02	1·14	1·29	1·87	1·96	1·64	1·51	1·67	1·62	1·57	1·58
ppm											
Rb	46	108	95	140	150	132	98	126	126	139	149
Sr	77	9	8	28	23	5	28	26	3	9	10
Y	50	104	89	69	86	129	48	73	132	135	150
Zr	341	1135	767	1856	2441	1076	996	1814	1053	1278	1405
Nb	73	216	157			230			222	260	277
Ba	n.a.	n.a.	n.a.	307	308	n.a.	347	303	n.a.	n.a.	n.a.
La	n.a.	n.a.	n.a.	n.a.	n.a.	n.a.	271	n.a.	n.a.	n.a.	n.a.
Ce	n.a.	n.a.	n.a.	493	511	n.a.	345	414	n.a.	n.a.	n.a.
Cr	n.a.	n.a.	n.a.	1	1	n.a.	1	n.a.	n.a.	n.a.	n.a.
Ni	n.a.	n.a.	n.a.	6	4	n.a.	4	6	n.a.	n.a.	n.a.
V	n.a.	n.a.	n.a.	56	8	n.a.	11	10	n.a.	n.a.	n.a.

*Total Fe as FeO.
Major (wt %) and trace elements (ppm) by XRF. Analyses were recalculated to 100% on an anhydrous basis and corrected for NaCl. TAS, Le Maitre *et al*. (1989) classification. Macd, Macdonald (1974) classification. Volcanic cycles after Civetta *et al*. (1988). Trach., trachyte.

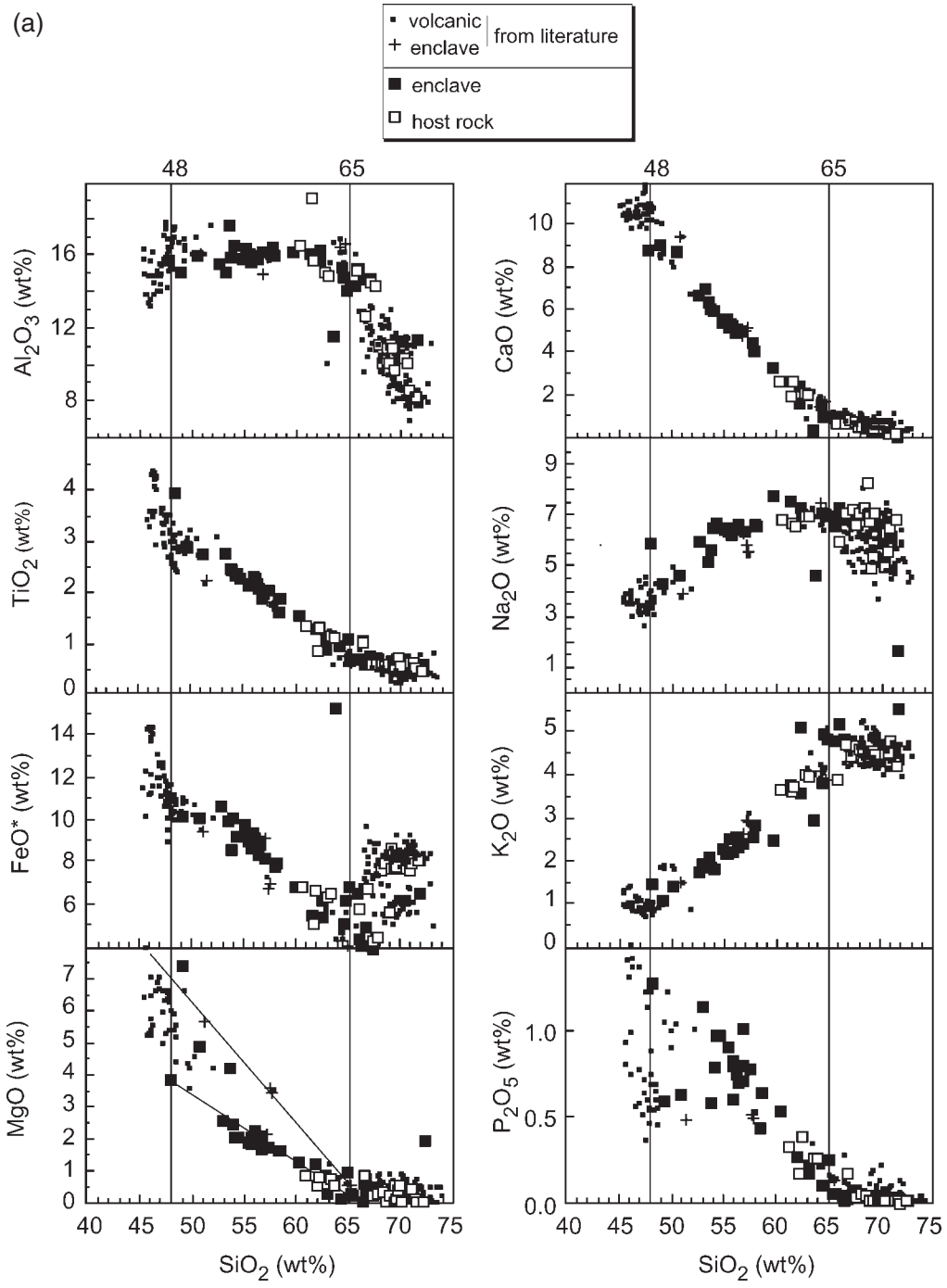

Fig. 5. (a) Major element oxide (wt %) contents for the analysed enclaves and volcanic host-rocks vs SiO_2 (wt %). Data from the literature for volcanic rocks from Pantelleria and for enclaves are also plotted from Carmichael (1962, 1967), Rittmann (1967), Romano (1969), Macdonald & Bailey (1973), Villari (1974), Civetta *et al.* (1984, 1988, 1998), Mahood & Baker (1986), Mahood & Stimac (1990), Esperança & Crisci (1995) and Avanzinelli *et al.* (2004). (b) Agpaitic index [molecular $(Na_2O + K_2O)/Al_2O_3$], Cl (wt %) and selected trace element (ppm) contents in the analysed enclaves and volcanic host-rocks vs SiO_2 (wt %). Symbols are as in (a). (c) Variation of select trace elements (ppm) vs wt % SiO_2. Theoretical Rayleigh fractionation model curves are shown for comparison. A step-by-step magmatic differentiation model was performed through high confidence (sum of squares of the residuals ΣR^2 <0·3) mass-balance calculations for major oxides (Table 11), subtracting the corresponding original phenocryst phases from 1MB basalt, 2x hawaiite, 16Bx mugearite, 22x benmoreite and 108x trachyte. Distribution coefficients from Luhr & Carmichael (1980), Villemant *et al.* (1981), Villemant (1988) and Peccerillo *et al.* (2003). Symbols are as in (a).

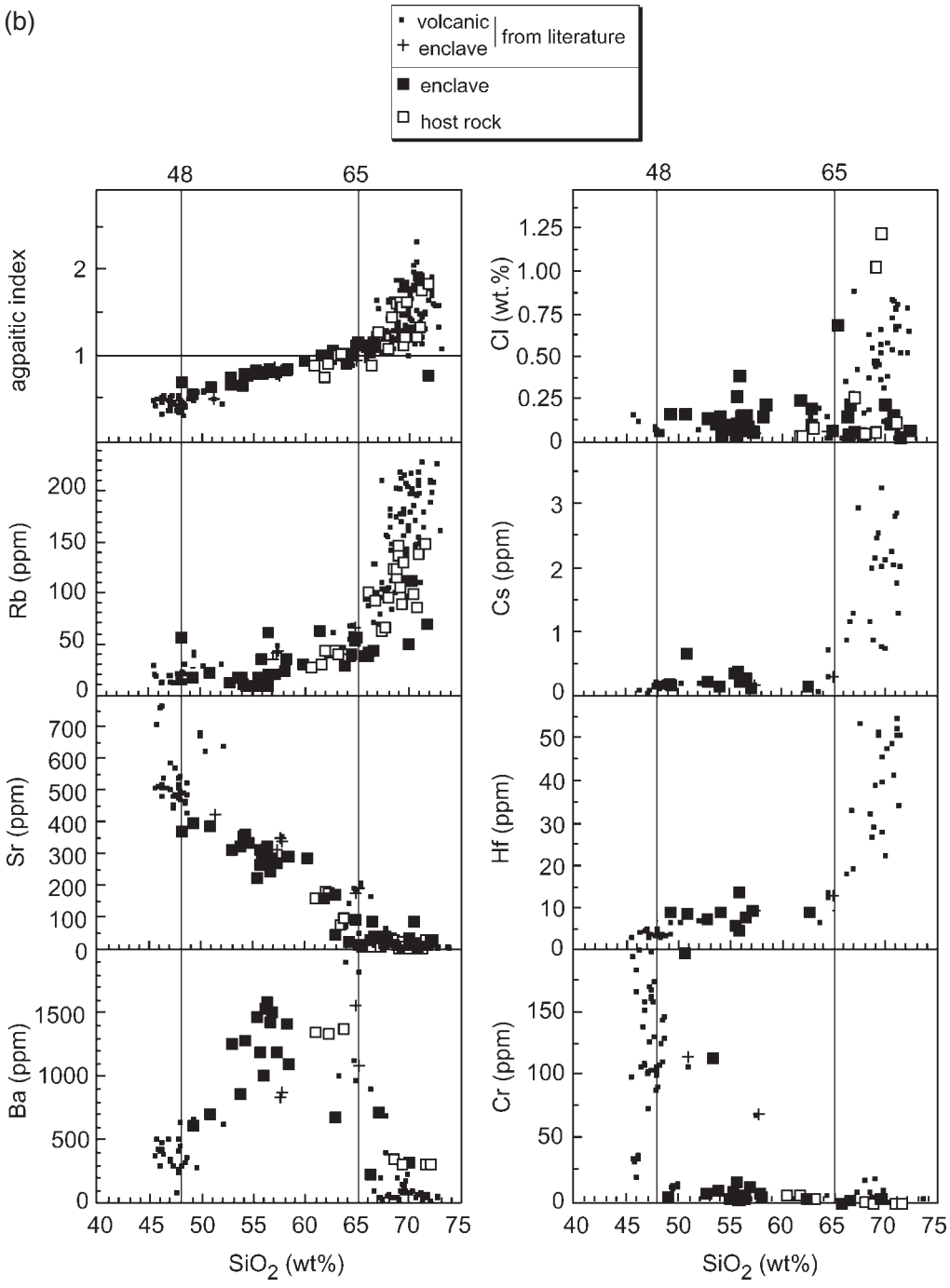

Fig. 5. Continued

SiO_2), intermediate (48–65 wt % SiO_2) and felsic (65–73 wt % SiO_2) (Figs 5 and 6). A plot of the agpaitic index (AI) [molecular $(Na_2O + K_2O)/Al_2O_3$) vs SiO_2 (whole-rock per cent)] for the enclaves (Fig. 5b) shows a linear trend for AI values <1, varying from AI ≈0·5 for mafic enclaves to AI ≈1·1 for enclaves with 65 wt % SiO_2. The felsic volcanic rocks show a different trend, with progressively increasing peralkalinity (AI >1) with increasing silica content. The majority of the enclaves fall within the intermediate composition range, whereas the majority of the volcanic rocks are felsic (comenditic trachytes and pantellerites). We emphasize that the enclaves of intermediate composition (intermediate enclaves) practically are hosted solely in the II cycle trachytic volcanic

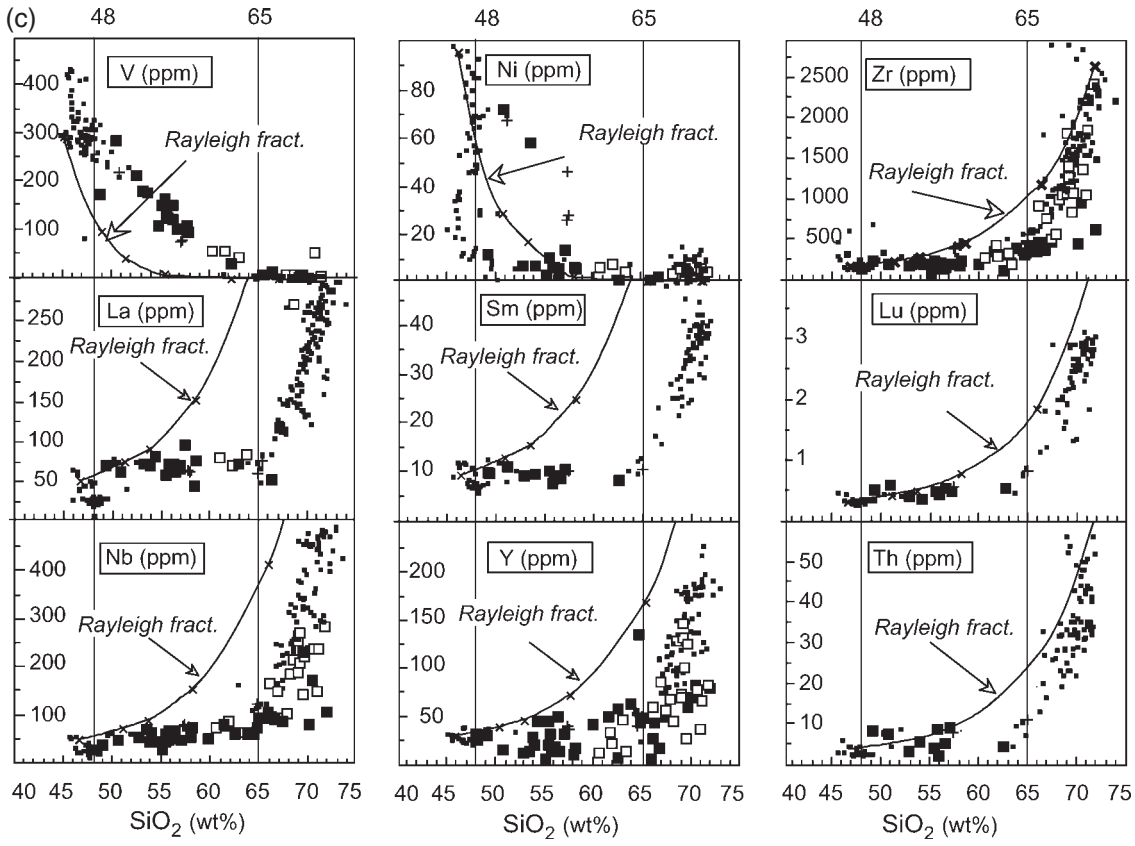

Fig. 5. Continued

rocks; however, the felsic end-member of the intermediate group is a syenite (81x) within a pantellerite host-rock.

Mineral chemistry and mineral–melt equilibria in the enclaves

The chemistry of minerals from the studied enclaves was compared with that for the volcanic rocks of Pantelleria available from the literature.

Olivine

Olivines with the highest Fo (Table 6, Fig. 7) contents correspond to the cores of crystals or to euhedral olivines coexisting with skeletal olivines. The skeletal crystals have lower Fo contents. Excluding the relict equant olivine ($Fo_{86–84}$), the rim or skeletal olivines of the last generations to crystallize vary in composition with increase in whole-rock silica from $Fo_{79–80}$ and 49·22 wt % whole-rock SiO_2 (21x) to $Fo_{2–6}$ in syenite (81x).

The Mg-rich cores of olivine in enclave 21x (Fo_{86}) (ol1 in Fig. 3a) are compatible with crystallization from a fairly primitive melt with mg-number ≈0·65 (Snyder & Carmichael, 1992) and a calculated temperature of crystallization, on the basis of the olivine–liquid geothermometer, of 1230°C [applying the method of Roeder & Emslie (1970)], or of 1215°C [according to Sisson & Grove (1993*b*)], under dry conditions and low pressure. In comparison, the basalts of Pantelleria exhibit a mg-number range from 0·58–0·54 (Mahood & Baker, 1986). The calculated liquid (FM-1) in equilibrium with the (Fo_{79}) olivine rim from sample 21x (ol2 in Fig. 3a; Table 6), which contains anorthoclase, has mg-number 0·56 and a temperature of 1193°C, according to the liquid geothermometer of Sisson & Grove (1993b). This value is similar to that for the less-evolved basalt 38 of Mahood & Baker (1986), for which a liquidus temperature of 1181 ± 5°C was experimentally calculated at low pressure: the reliability of the Sisson & Grove (1993*b*) liquid geothermometer was also tested on basalt 38MB composition, for which the same temperature value of 1181°C has been calculated.

The estimated temperature of crystallization for the intermediate composition unzoned olivines (ol3 in Figs 3b and 7, and Table 6), calculated according to the olivine–liquid geothermometer of Sisson & Grove (1993*b*), varies from 1082° to 948°C with increasing silica

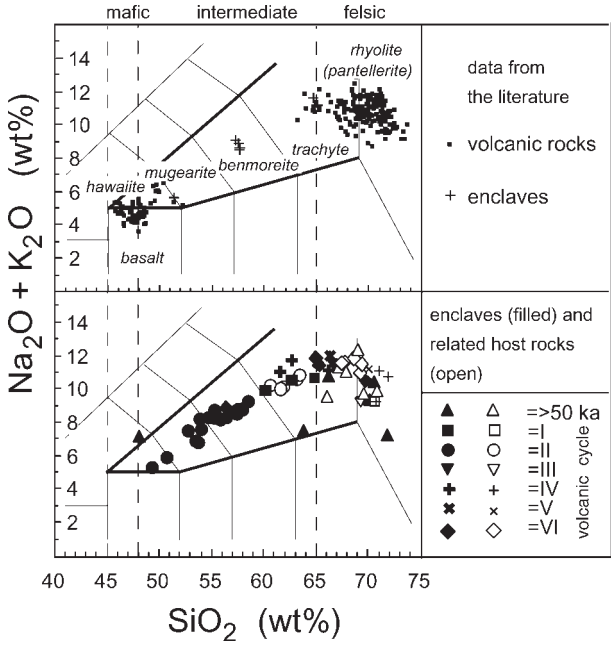

Fig. 6. Total Alkali–Silica (TAS) (Le Maitre *et al.*, 1989) diagrams. Enclaves (filled symbols) and related host-rocks (open symbols) are plotted. All available published data for Pantelleria rocks are plotted for comparison: volcanic rocks (small filled squares), enclaves (crosses).

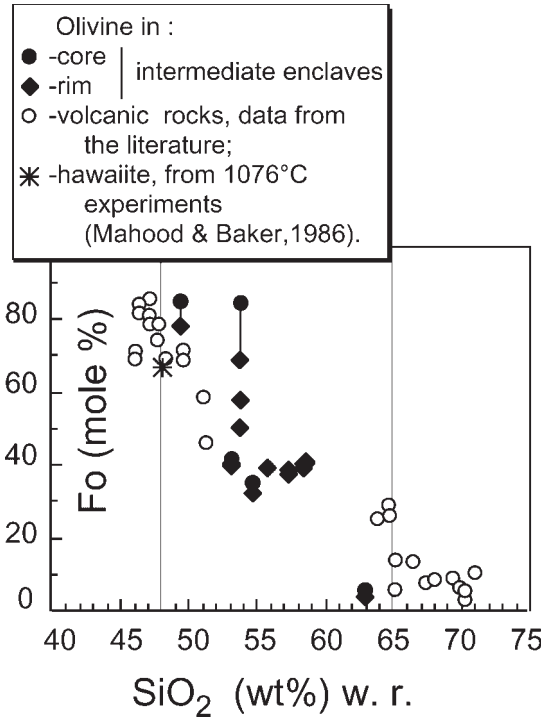

Fig. 7. Olivine compositions (Fo mol %) vs SiO_2 (wt %) content of the enclave whole-rocks (w.r.). Data from the literature for olivine in volcanic rocks from Pantelleria and that crystallized at 1075°C in the experimental products of differentiation of a basaltic liquid by Mahood & Baker (1986) are also plotted. (For sources of olivine data from the literature see text and Fig. 5a.)

content of the host-enclave; these olivines have ${}^{Fe/Mg}K_{Dol\text{-}w.r.} > 0{\cdot}3$, in agreement with the Carmichael & Ghiorso (1990) calculations for olivine with Fo <58. Temperature values close to 855 ± 10°C were calculated for the skeletal olivine and the adjacent surrounding glass, and can account for a not-approached equilibrium or for the probable limit of the olivine–liquid geothermometer, in agreement with that reported by Sisson & Grove (1993*b*).

The calculated liquid (FM-1) can be obtained by mass-balance calculations subtracting a 5 (wt %) of Fo_{79} olivine (rim) and a further 20 (wt %) of trachyte composition, from the 21x whole-rock. The primitive melt composition (FM-0) with mg-number ≈0·65 can tentatively be obtained by mass-balance calculations adding a 10 (wt %) of Fo_{86} olivine (core) to the FM-1 calculated liquid (Table 6). As a consequence of these calculations it is possible to assert that the 21x doleritic enclave, and also the 16x enclave, display traces of olivine xenocrysts of a more mafic basaltic parental magma.

Clinopyroxenes

Different kinds of clinopyroxene crystals are present in the enclaves. Some are partially resorbed, subhedral, equant crystals containing opaque micro-inclusions; more frequently, they show prismatic, elongated shapes, which can coexist with equant types. Sometimes skeletal clinopyroxenes occur in radial intergrowths with plagioclase (Fig. 3 g). Similar to the olivine trend (Fig. 7), except for the relict crystals, the rims or skeletal pyroxene of the last generations to crystallize vary in composition with an increase in whole-rock silica (Table 7, Fig. 8). Compositions range from Ca-rich clinopyroxene in dolerite to ferro-augite to Na-ferrohedenbergite in intermediate enclaves and aegirine–augite in syenite and felsic volcanic rocks. An increase of Fe/Mg and MnO (wt %) and a decrease of Al_2O_3 (wt %) and TiO_2 (wt %) was observed in clinopyroxenes with increasing whole-rock silica content (Fig. 8). The doleritic enclaves contain sub-ophitic pyroxenes with high Al and Ti contents; these are typically indicative of high rates of crystallization (Feeley & Dungan, 1996).

Clinopyroxenes with mg-number >0·7 ['basaltic' according to Nimis (1995)], are present in the more mafic enclaves, both as cores of zoned crystals and as xenocrysts coexisting with pyroxenes that have a higher Fe/Mg ratio. In many cases we have noted an inverse zoning pattern with a sudden increase of Al and Ti followed by an equally strong decrease of the same elements towards the rims of the pyroxenes. If we consider ${}^{Fe/Mg}K_{Dcpx\text{-}liq} = 0{\cdot}22 \pm 0{\cdot}04$, according to Sisson & Grove (1993*a*, 1993*b*), the Mg-rich cores of some Cpx

Table 6: Selected electron microprobe analyses of olivines from enclaves of intermediate composition and calculated analyses of primitive basalts

Sample/spot:	21x core	21x rim	20x	mega 16x/83 core	mega 16x/84 rim	16x	62Bx/14	27x/15	40x	22x	25x/57	74x/67	81x/47 core	81x/38 rim	Sample:	FM-0 primitive	38MB	FM-1	21x
Rock type:	dolerite	dolerite	sy. gabbro	sy. gabbro	sy. gabbro	sy. gabbro	sy. gabbro	sy. diorite	sy. diorite	sy. diorite	sy. diorite	n.a.	syenite	syenite	TAS clas.	basalt	basalt	basalt	hawaiite
H.r. type:	trachyte	trachyte	trachyte	trachyte	trachyte	trachyte	trachyte	trachyte	trachyte	trachyte	trachyte	trachyte	pantellerite	pantellerite	type	calc.[1]		calc.[2]	enclave
H.r. cycle:	II	II	II	II	II	II	II	II	II	II	II	II	IV	IV					
wt %															*wt %*				
SiO_2	40·99	38·99	33·76	39·56	37·30	35·03	33·91	33·88	33·99	32·73	33·31	33·50	29·98	29·87	SiO_2	45·45	46·00	45·95	49·22
FeO	13·15	18·87	44·83	14·72	26·50	37·23	48·59	45·37	45·60	45·42	44·31	46·15	63·15	63·03	TiO_2	3·19	3·50	3·54	2·81
MnO	0·23	0·37	2·16	0·20	0·66	0·99	2·43	2·33	1·95	2·27	2·08	2·39	4·04	4·79	Al_2O_3	14·34	14·90	15·93	15·17
MgO	46·22	40·66	17·75	45·53	35·03	24·89	13·99	17·59	16·80	17·50	18·02	16·85	1·60	1·00	FeOt	11·23	11·30	11·02	10·26
CaO	0·31	0·30	0·31	0·28	0·23	0·22	0·45	0·35	0·31	0·35	0·31	0·32	0·17	0·18	MnO	0·26	0·18	0·26	0·26
Total	100·90	99·19	98·81	100·29	99·72	98·36	99·37	99·52	98·65	98·27	98·03	99·21	98·94	98·87	MgO	10·90	7·01	6·98	7·39
															CaO	10·35	11·00	11·46	8·99
Cations per 4 oxygens															Na_2O	3·24	3·50	3·60	4·14
Si	1·009	1·006	1·000	1·000	1·000	1·000	1·000	1·000	1·000	0·993	1·003	1·006	1·010	1·011	K_2O	0·38	1·44	0·42	1·18
Fe^{2+}	0·271	0·407	1·135	0·305	0·589	0·900	1·270	1·141	1·171	1·153	1·116	1·160	1·778	1·783	P_2O_5	0·68	0·99	0·76	0·59
Mn	0·005	0·008	0·056	0·004	0·015	0·024	0·064	0·059	0·051	0·058	0·053	0·061	0·115	0·137	Total	100·02	99·82	99·92	100·01
Mg	1·697	1·564	0·800	1·683	1·389	1·070	0·651	0·788	0·769	0·792	0·809	0·755	0·080	0·050					
Ca	0·008	0·008	0·011	0·007	0·007	0·007	0·015	0·011	0·011	0·011	0·010	0·010	0·006	0·007	mg-no.	0·65	0·58	0·56	0·58
Sum M1	1·981	1·987	2·002	1·999	2·000	2·001	2·000	2·000	2·002	2·014	1·988	1·986	1·979	1·977					
Fo (mol %)	85·68	78·69	40·01	84·17	69·46	53·51	32·56	39·42	38·43	39·31	40·70	38·02	4·07	2·54					
Fa (mol %)	13·67	20·48	56·73	15·27	29·47	44·97	63·50	57·07	58·53	57·23	56·13	58·39	89·80	90·19					
Tp (mol %)	0·24	0·41	2·76	0·20	0·74	1·20	3·20	2·96	2·53	2·90	2·66	3·07	5·83	6·93					
Lar (mol %)	0·41	0·42	0·50	0·36	0·33	0·32	0·74	0·55	0·51	0·56	0·51	0·53	0·30	0·34					
Fe + Mg	1·97	1·97	1·93	1·99	1·98	1·97	1·92	1·93	1·94	1·95	1·93	1·92	1·86	1·83					
mg-no.	0·86	0·79	0·41	0·85	0·70	0·54	0·34	0·41	0·40	0·41	0·42	0·39	0·04	0·03					
SiO_2 wr	49·22	49·22	52·85	53·57	53·57	53·57	54·10	55·56	57·14	58·11	58·29	n.a.	62·65	62·65					

mg-number = $Mg/(Mg + Fe^{2+})$; wr, whole rock; h.r., host-rock; mega, phenocryst; sy.gabbro, syenogabbro; sy.diorite, syenodiorite. MB, Mahood & Baker (1986). FM, this study.

[1]Primitive basalt composition obtained by mass-balance calculation by adding 10 wt % of olivine Fo_{86} to the calculated basalt FM-1; the primitive liquid is in equilibrium with the core of the olivine from the 21x sample.

[2]Basalt composition obtained by mass-balance calculation subtracting 5 wt % of olivine/core Fo_{86} xenocryst and 20 wt % of trachyte composition from 21x hawaiitic enclave; the calculated liquid is in equilibrium with the rim of the olivine from the 21x sample.

Table 7: Representative electron microprobe analyses of clinopyroxenes and amphiboles from enclaves within the trachytes and the pantellerites

	Clinopyroxene																			Amphibole		
Sample/spot:	21x	20x/53	16Bx/87	mega 16Bx/88	mega 16Bx/10	16Bx/86	62Bx/m5	62Bx/32	27Ax/16	27Ax/20	27Ax/14	17Bx/m3	22x/9	22x/m3	74nax	81x/51	81x/35	73x/73	73x/79		81x	73x
	ground	rim	core	rim					core	rim		core	rim									
Rock type:	dolerite	sy. gabb.	sy. gabb.	sy. gabb.	sy. gabb.	sy. gabb.	sy. gabb.	sy. gabb.	sy. diorite	sy. diorite	sy. diorite	sy. diorite	sy. diorite	sy. diorite	sy. diorite	syenite	syenite	syenite	syenite		syenite	syenite
H.r. type:	trachyte	trachyte	trachyte	trachyte	trachyte	trachyte	trachyte	trachyte	trachyte	trachyte	trachyte	trachyte	trachyte	trachyte	trachyte	pantel.	pantel.	pantel.	pantel.		pantell.	pantell.
H.r. cycle:	II	II	II	II	II	II	II	II	II	II	II	II	II	II	II	IV	IV	V	V		IV	V
wt %																						
SiO_2	47·00	51·91	50·21	44·89	51·12	51·94	52·12	51·87	50·55	52·11	52·44	51·79	50·94	51·47	51·09	50·44	49·23	50·53	49·90	SiO_2	48·91	48·89
TiO_2	2·87	0·57	1·56	3·58	1·15	0·46	0·59	0·44	1·07	0·64	0·69	1·11	0·92	0·59	0·48	0·38	0·39	0·28	0·38	TiO_2	1·97	1·52
Al_2O_3	5·85	0·83	3·88	8·63	2·36	0·67	0·54	0·63	2·55	1·27	1·31	1·98	2·13	0·86	0·46	0·36	0·18	0·38	0·23	Al_2O_3	1·03	1·78
Cr_2O_3	b.d.l.	b.d.l.	0·30	0·23	b.d.l.	b.d.l.	b.d.l.	0·03	0·02	0·03	0·00	0·03	n.a.	b.d.l.	b.d.l.	b.d.l.	b.d.l.	b.d.l.	b.d.l.	Cr_2O_3	0·00	0·00
FeOt	8·51	12·42	6·46	8·16	11·27	14·50	13·71	19·09	11·00	11·96	12·52	10·10	10·33	12·65	15·35	19·81	24·25	16·49	27·07	FeOt	27·75	26·13
MnO	0·23	0·89	0·14	0·21	0·49	0·97	0·83	1·27	0·63	0·60	0·75	0·48	0·58	0·82	1·12	1·23	1·29	0·99	1·08	MnO	1·17	0·92
MgO	12·60	12·24	15·74	12·09	12·56	11·45	11·69	9·57	13·10	13·10	12·69	15·02	13·69	12·45	10·53	6·80	3·58	9·54	0·58	MgO	4·43	5·73
CaO	20·69	19·67	20·75	21·16	20·41	19·06	19·52	13·62	19·92	19·58	19·34	18·58	19·75	19·57	19·12	19·70	18·04	19·50	11·16	CaO	4·63	6·03
Na_2O	1·03	0·49	0·27	0·53	0·50	0·50	0·60	3·01	0·45	0·53	0·58	0·45	0·49	0·47	0·46	0·63	1·48	0·61	6·65	Na_2O	5·64	5·58
Total	98·78	99·02	99·31	99·48	99·86	99·55	99·60	99·53	99·29	99·82	100·32	99·54	98·83	98·88	98·61	99·35	98·44	98·32	97·05	K_2O	1·15	1·01
																				Total	96·68	97·59
Fe_2O_3	4·10	0·02	1·16	2·87	0·50	0·10	0·35	7·11	1·31	0·63	0·03	0·35	1·26	0·92	0·38	0·74	2·98	1·80	15·89			
FeO	4·81	12·40	5·42	5·58	10·81	14·41	13·39	12·68	9·81	11·39	12·49	9·78	9·19	11·82	15·01	19·14	21·57	14·87	12·76	*Cations per 23 oxygens*		
Total	99·19	99·02	99·42	99·76	99·91	99·56	99·63	100·23	99·41	99·88	100·32	99·57	98·95	98·97	98·64	99·42	98·74	98·50	98·63	Si	7·781	7·655
																				AlIV	0·193	0·329
																				Ti	0·026	0·016
Cations per 6 oxygens																						
Si	1·768	1·983	1·861	1·683	1·926	1·989	1·988	1·980	1·910	1·963	1·972	1·936	1·926	1·967	1·987	1·993	1·996	1·979	1·997	Sum T	8·000	8·000
AlIV	0·232	0·017	0·139	0·317	0·074	0·011	0·012	0·020	0·090	0·037	0·028	0·064	0·074	0·033	0·013	0·007	0·004	0·018	0·003	AlVI	0·000	0·000
Sum T	2·000	2·000	2·000	2·000	2·000	2·000	2·000	2·000	2·000	2·000	2·000	2·000	2·000	2·000	2·000	2·000	2·000	1·997	2·000	Ti	0·210	0·163
AlVI	0·027	0·020	0·030	0·064	0·031	0·019	0·012	0·008	0·024	0·020	0·030	0·023	0·021	0·006	0·008	0·010	0·004	0·000	0·008	Cr^{3+}	0·000	0·000
Ti	0·081	0·016	0·043	0·101	0·033	0·013	0·017	0·013	0·030	0·018	0·020	0·031	0·026	0·017	0·014	0·011	0·012	0·008	0·011	Fe^{3+}	0·000	0·000
Cr	0·000	0·000	0·009	0·007	0·000	0·000	0·000	0·001	0·001	0·001	0·000	0·001	0·000	0·000	0·000	0·000	0·000	0·000	0·000	Mg	1·050	1·337
Fe^{3+}	0·118	0·000	0·033	0·082	0·015	0·003	0·010	0·208	0·038	0·018	0·001	0·010	0·037	0·027	0·011	0·022	0·092	0·054	0·487	Fe^{2+}	3·692	3·421
Fe^{2+}	0·151	0·396	0·168	0·175	0·341	0·461	0·427	0·405	0·310	0·359	0·393	0·306	0·291	0·378	0·488	0·633	0·731	0·487	0·427	Mn^{2+}	0·048	0·079
Mn	0·007	0·029	0·004	0·007	0·016	0·031	0·027	0·041	0·020	0·019	0·024	0·015	0·019	0·027	0·037	0·041	0·044	0·033	0·037	Sum C	5·000	5·000

	Clinopyroxene																			Amphibole		
Sample/spot:	21x	20x/53	16Bx/87	mega 16Bx/88	mega 16Bx/10	16Bx/86	62Bx/m5	62Bx/32	27Ax/16	27Ax/20	27Ax/14	17Bx/m3	22x/9	22x/m3	74nax	81x/51	81x/35	73x/73	73x/79		81x	73x
	ground	rim	core	rim					core	rim		core	rim									
Rock type:	dolerite	sy. gabb.	sy. gabb.	sy. gabb.	sy. gabb.	sy. gabb.	sy. gabb.	sy. gabb.	sy. diorite	sy. diorite	sy. diorite	sy. diorite	sy. diorite	sy. diorite	sy. diorite	syenite	syenite	syenite	syenite		syenite	syenite
H.r. type:	trachyte	trachyte	trachyte	trachyte	trachyte	trachyte	trachyte	trachyte	trachyte	trachyte	trachyte	trachyte	trachyte	trachyte	trachyte	pantel.	pantel.	pantel.	pantel.		pantell.	pantell.
H.r. cycle:	II	II	II	II	II	II	II	II	II	II	II	II	II	II	II	IV	IV	V	V		IV	V
Mg	0·706	0·697	0·869	0·676	0·705	0·653	0·664	0·544	0·738	0·736	0·711	0·837	0·771	0·709	0·610	0·400	0·216	0·557	0·035	Mg	0·000	0·000
Ca	0·834	0·805	0·824	0·850	0·824	0·782	0·798	0·557	0·807	0·791	0·779	0·744	0·800	0·802	0·797	0·834	0·784	0·818	0·479	Fe^{2+}	0·000	0·000
Na	0·075	0·036	0·019	0·039	0·037	0·037	0·044	0·223	0·033	0·039	0·042	0·033	0·036	0·035	0·035	0·048	0·116	0·046	0·516	Mn^{2+}	0·110	0·043
Total M1+M2	1·999	1·999	1·999	2·001	2·002	1·999	1·999	2·000	2·001	2·000	2·000	2·000	2·001	2·001	2·000	1·999	2·000	2·003	2·000	Ca	0·789	1·012
																				NaB	1·101	0·945
Ca (at. %)	45·89	41·78	43·40	47·51	43·36	40·49	41·41	31·74	42·17	41·12	40·84	38·92	41·73	41·27	41·00	43·20	41·95	41·99	32·69	Sum B	2·000	2·000
Mg (at. %)	38·87	36·15	45·79	37·75	37·12	33·83	34·49	31·02	38·57	38·27	37·27	43·77	40·24	36·52	31·41	20·74	11·58	28·57	2·36	NaA	0·639	0·749
Fe* (at. %)	15·24	22·07	10·81	14·74	19·52	25·67	24·10	37·24	19·25	20·61	21·88	17·31	18·03	22·21	27·59	36·06	46·47	29·44	64·95	K	0·234	0·202
																				Sum A	0·873	0·951
Vc	440·41		439·44	440·29					440·59			439·21	440·25							Totals	15·873	15·951
VM1	11·69		11·80	11·61					11·95			11·94	11·95									
																				$(Ca+Na)_B$	1·890	1·957
mg-no.	0·82	0·64	0·84	0·79	0·67	0·54	0·61	0·57	0·70	0·67	0·64	0·73	0·73	0·65	0·56	0·39	0·23	0·53	0·07	mg-no.	0·22	0·28
SiO_2 wr	49·22	52·85	53·57	53·57	53·57	53·57	54·10	54·10	55·56	55·56	55·56	55·88	58·11	58·11	n.a.	62·65	62·65	66·27	66·27	SiO_2 wr	62·65	66·27

Vc and VM1 are crystallochemical volumes calculated on clinopyroxene with mg-number $\geq$0·7 according to the procedure proposed by Nimis (1995); b.d.l., below detection limit. Clinopyroxene formula after Papike *et al*. (1974). Amphibole formula after Leake *et al*. (1997); h.r., host-rock. mg-number = $Mg/(Mg + Fe^{2+})$; wr, whole-rock; $Fe^* = Fe^{2+} + Fe^{3+} + Mn$; ground., groundmass; sy.gabb., syenogabbro; sy.diorite, syenodiorite; pantel., pantellerite.

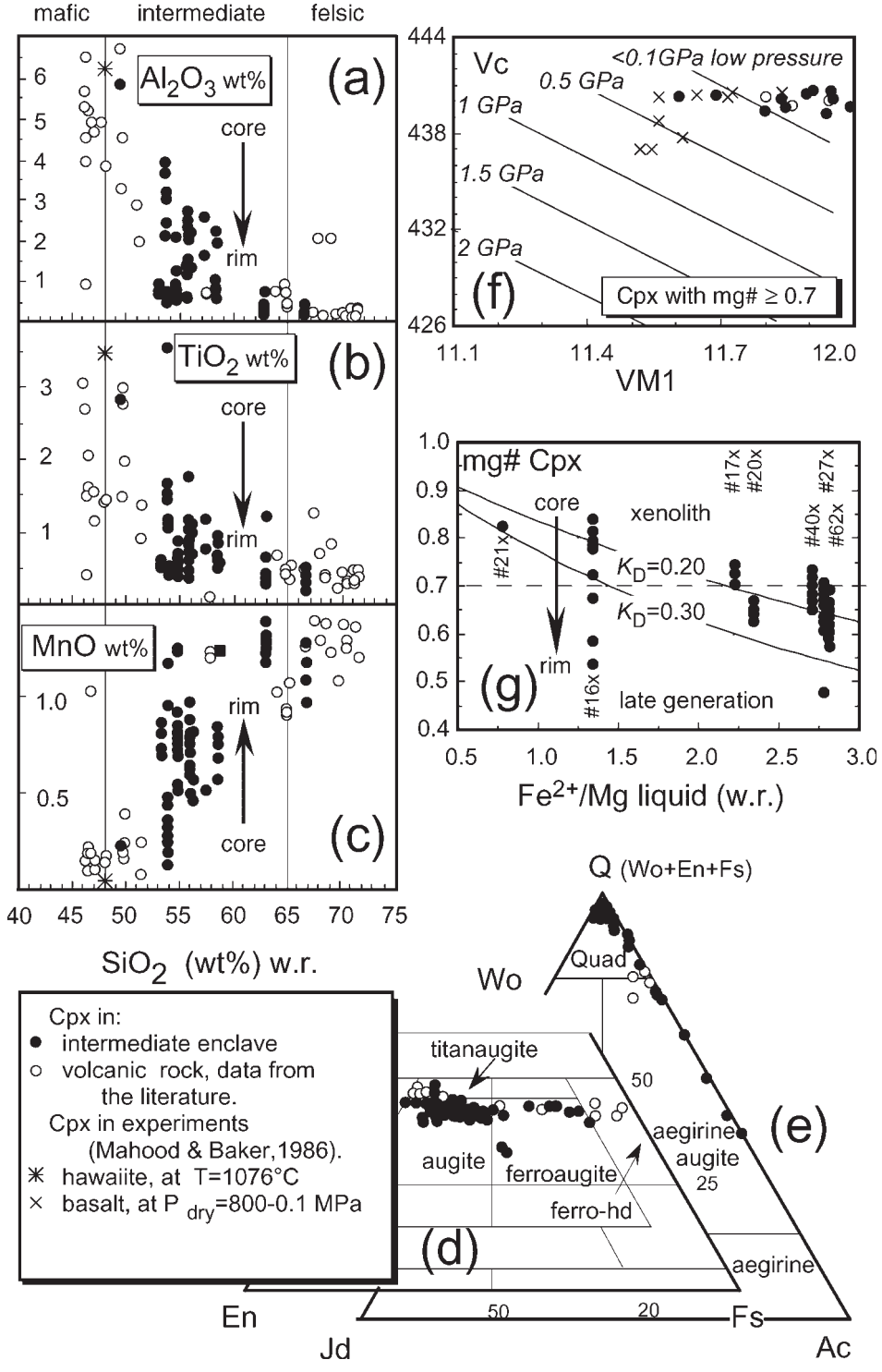

Fig. 8. Clinopyroxene compositions: (a) Al_2O_3 (wt %); (b) TiO_2 (wt %) and (c) MnO (wt %) vs SiO_2 (wt %) in the enclave whole-rock (w.r.). (d) Clinopyroxene compositions in the Morimoto (1988) Wo–En–Fs quadrilateral diagram. (e) Q–Jd–Ac diagram for the Na-rich pyroxenes (f) Pyroxene geobarometer: Vc and VM1 volumes of clinopyroxenes with mg-number ≥0·7 (Table 7) calculated according to Nimis (1995). (g) mg-number = Mg/(Mg + Fe^{2+}) of Cpx vs Fe^{2+}/Mg in enclave whole-rocks (after Kilinc *et al.*, 1983) at temperatures calculated from coexisting Fe–Ti oxides. Equilibrium curves for $^{Fe2+/Mg}K_{Dcpx\text{-}liq}$ values of 0·20 and 0·30 are indicated (Grove *et al.*, 1982; Baker & Eggler, 1983; Sisson & Grove, 1993*b*). (For sources of clinopyroxene data from the literature see text and Fig. 5a.)

in intermediate enclaves (Table 7) with mg-number >0·7 (e.g. 16B cpx), are not in equilibrium with the whole-rock (liquid). These xenocrysts, applying the geothermometer of Putirka *et al.* (1996), are in equilibrium ($K_D = 0·26$) with a calculated basaltic liquid FM-1 (Table 6) at about 1168 ± 2°C and <0·5 GPa pressure. A similar temperature was determined experimentally by Mahood & Baker (1986) for cpx crystallization from a Pantelleria basalt at low pressure. Applying the clinopyroxene geobarometer of Nimis (1995), pressures of <0·2 GPa were obtained for the cpx cores in syenogabbro and syenodioritic enclaves (Table 7).

The skeletal clinopyroxenes in the intermediate composition enclaves could be in equilibrium with a liquid represented by the whole-rock, at estimated temperatures varying from 1070° to 987°C with increasing whole-rock silica content, at low pressure, taking into account the uncertainty that derives from the estimated composition of the original liquid. The lowest equilibrium temperature range, for clinopyroxene in the syenodioritic enclaves, is 994–981°C. These values have been calculated for the Fe–Mn-rich rims of the zoned cpx and for the skeletal pyroxenes in radial intergrowths with the plagioclase (oligoclase), suggesting an equilibrium liquid with a composition similar to that of the intracrystalline glass (e.g. 22x). It must be noted that the estimated temperature ranges for intermediate clinopyroxenes and olivines give fairly comparable results, which are also confirmed by the olivine–augite geothermometer of Loucks (1996) with a 985 ± 6°C estimated temperature. The aegirine–augite clinopyroxene appears as a late skeletal crystallization product in devitrified glass.

Feldspars

Feldspar compositions vary with-whole rock silica content (Table 8, Fig. 9); they are $An_{58–50}$ in the dolerite enclaves. The plagioclases of the intermediate enclaves vary from andesine in the zoned euhedral cores to oligoclase or anorthoclase in the rims (e.g. An_{45}–An_{19}–An_6 range in 20x feldspar). Alkali feldspar (Or_{38}), close to the binary minimum (Carmichael & MacKenzie, 1963), is present in the syenitic enclaves on the rim of the anorthoclase and in the groundmass of the trachytic enclaves.

All enclaves with intermediate compositions between basalt and trachyte contain resorbed anorthoclase with ovoid cores that we consider xenocrysts (Fig. 3c). The enclaves without glass contain anorthoclase in the rim overgrowths on plagioclase and resorbed megacrysts of earlier-formed anorthoclase.

It must be noted that the alkali feldspar in the trachyte-hosted enclaves does not display the perthite textures that are observed in the enclaves within the pantellerites. Trachytes contain $An_{10–2}Or_{20–28}Ab_{65}$ anorthoclase and, in places, Na-sanidine in the groundmass. The Ba content in the feldspars of the enclaves increases while the An content progressively decreases (not shown). Feldspars show, in places, patchy-zoning: normally zoned feldspars (62x) coexist with crystals retaining rounded cores of ternary feldspar, euhedral external cores of An_{40} plagioclase and an outermost zone of clear alkali-feldspar. According to Sisson & Grove (1993*a*) and Feeley & Dungan (1996), the plagioclases from the intermediate enclaves could be in equilibrium with a liquid similar to the whole-rock composition, under almost dry conditions ($K_D = 1 – 2$) and at low pressure (<0·2 GPa) (Fig. 9b). However, the Ca-rich composition of the hypothesized liquid is probably due to the presence of traces of Ca-rich clinopyroxene and Ca-rich plagioclase (>An_{70}) xenocrysts. The andesine–labradorite plagioclases ($A_{58–38}$), in places occurring as resorbed feldspar cores, do not contain apatite inclusions and have compositions very similar to the plagioclase synthesized in the 1050 ± 25°C range in the experiments of Mahood & Baker (1986). For the radial textural intergrowth of oligoclase plagioclase $An_{20–18}$ and Fe–Mn-rich skeletal clinopyroxene the equilibrium temperature must be the same: the calculated temperature range for clinopyroxene is 994–981°C and is surprisingly very similar to the 990–960°C temperature range, calculated according to Mathez (1973), for oligoclase in equilibrium with a liquid with the intracrystalline glass composition (e.g. 22x) (Fig. 9c). The Ca-rich plagioclases are not in equilibrium with interstitial glass (Fig. 9c).

Fe–Ti oxides

Many researchers have reported the occurrence of coexisting Fe–Ti oxide pairs, ilmenite and magnetite, in all the rocks of the island. Only Fe–Ti oxide pairs with equilibrium Mn/Mg partitioning according to Bacon & Hirschmann (1988) were considered here (Table 9).

In a plot of T°C vs fO_2, calculated using the method of Ghiorso & Sack (1991) (Fig. 10), the enclave and volcanic rock data plot subparallel to the quartz–fayalite–magnetite (QFM) buffer for temperatures up to 1050°C, corresponding to the equilibrium conditions of mafic melts. The data display a decrease of ΔNNO (where NNO is the nickel–nickel oxide buffer), according to Carmichael (1991), from hawaiite to trachyte and trachypantellerite, and intercept the trend defined by the pantellerite data of Carmichael (1991) and Lowenstern *et al.* (1993), and the experimental data for samples from Ferdinandea Island (Graham Bank, Sicily Channel) reported by Carapezza *et al.* (1979). A temperature of 1075°C was determined by Mahood & Baker (1986) for an experimental differentiated mafic melt ($F_{liquid} = 0·47$, hawaiite); the highest temperature calculated for the intermediate composition enclaves is close to 1050°C (16x; mugearite). Temperatures of 1003–987°C

Table 8: Representative electron microprobe analyses of feldspars in enclaves of intermediate composition and host-rocks

Sample/spot:	21x/6	21x/7	20x/60	mega 20x/63	mega 20x/64	16Bx/68	16Bx/70	mega 16Bx/71	mega 16Bx/67	62Bx/10	62Bx/9	62Bx/11	62Bx/12	27x/31	27x/23
	core	rim	core	rim	core	ground.	rim	spongy	rim	core	core	rim	rim	core	core
Rock type:	dolerite	dolerite	sy.gabbro	sy.gabbro	sy.gabbro	sy.gabbro	sy.gabbro	sy.gabbro	sy.gabbro	sy.gabbro	sy.gabbro	sy.gabbro	sy.gabbro	sy.diorite	sy.diorite
H.r. type:	trachyte	trachyte	trachyte	trachyte	trachyte	trachyte	trachyte	trachyte	trachyte	trachyte	trachyte	trachyte	trachyte	trachyte	trachyte
H.r. cycle:	II	II	II	II	II	II	II	II	II	II	II	II	II	II	II
SiO_2	59·13	60·34	55·89	62·05	65·33	53·92	56·73	65·45	65·00	56·57	63·36	65·05	64·86	56·25	61·31
TiO_2	0·22	0·11	0·15	0·18	0·07	0·15	0·13	0·11	0·07	0·16	0·17	0·07	0·11	0·09	0·06
Al_2O_3	23·49	23·63	27·72	22·84	20·76	28·28	27·24	19·78	20·84	26·62	21·45	20·14	19·78	27·53	23·91
FeOt	0·79	0·47	0·20	0·21	0·28	0·72	0·71	0·43	0·34	0·28	0·27	0·27	0·32	0·31	0·26
MgO	0·05	0·05	n.d.	n.d.	n.d.	0·04	n.d.	n.d.	n.d.	n.d.	n.d.	n.d.	n.d.	0·02	n.d.
CaO	11·81	5·75	9·29	3·98	1·38	10·56	9·03	0·82	1·63	8·25	2·35	1·00	0·57	9·33	4·73
Na_2O	4·50	7·11	5·93	8·05	8·30	5·70	6·24	7·90	8·54	6·91	8·67	8·34	8·64	5·97	7·65
K_2O	0·31	1·30	0·44	1·67	3·73	0·41	0·50	4·57	3·39	0·41	2·98	4·69	4·42	0·48	1·28
SrO	n.a.	n.a.	n.a.	n.a.	n.a.	n.a.	n.a.	n.a.	n.a.	n.a.	n.a.	n.a.	n.a.	n.a.	n.a.
BaO	n.a.	n.a.	n.a.	n.a.	n.a.	n.a.	n.a.	n.a.	n.a.	n.a.	n.a.	n.a.	n.a.	n.a.	n.a.
Total	100·30	98·76	99·62	98·98	99·85	99·78	100·58	99·06	99·81	99·20	99·25	99·56	98·70	99·98	99·20
An mol %	58·11	28·52	45·23	19·39	6·63	49·43	43·18	3·97	7·72	38·82	10·88	4·62	2·64	45·07	23·53
Ab mol %	40·07	63·80	52·25	70·94	72·04	48·27	53·99	69·57	73·19	58·87	72·68	69·61	72·83	52·17	68·89
Or mol %	1·82	7·68	2·52	9·67	21·33	2·30	2·83	26·46	19·09	2·31	16·44	25·77	24·52	2·76	7·58
SiO_2 wr	49·22	49·22	52·85	52·85	52·85	53·57	53·57	53·57	53·57	54·10	54·10	54·10	54·10	55·56	55·56

Sample:	27x/27	27x/30	17x/38	17x/36	40x/94	40x/1	22x/16	22x/2	22x/14	25x/49	25x/48	25x/43	119MS	81 h/31	81 h/30
	rim	rim	core	rim	core	rim	core	core	rim	core	rim	microlite[1]	phen.	core phen.	rim phen.
Rock type:	sy.diorite	sy.diorite	sy.diorite	sy.diorite	sy.diorite	sy.diorite	sy.diorite	sy.diorite	sy.diorite	sy.diorite	sy.diorite	sy.diorite	trachyte	pantel.	pantel.
H.r. type:	trachyte	trachyte	trachyte	trachyte	trachyte	trachyte	trachyte	trachyte	trachyte	trachyte	trachyte	trachyte			
H.r. cycle:	II	II	II	II	II	II	II	II	II	II	II	II	II	IV	IV
SiO_2	63·59	65·74	62·87	64·34	60·19	66·08	59·22	61·98	65·09	64·25	64·49	64·49	64·67	66·37	65·87
TiO_2	0·07	0·03	0·07	0·13	0·11	0·13	0·09	0·12	0·06	0·06	0·05	0·11		0·21	0·16
Al_2O_3	21·39	20·30	22·71	20·07	24·91	18·33	26·28	23·35	21·37	21·10	21·50	21·27	20·35	18·16	18·30
FeOt	0·34	0·31	0·38	0·44	0·40	0·52	0·26	0·54	0·34	0·31	0·31	0·63	0·23	0·92	0·85
MgO	n.d.	n.d.	0·01	n.d.	n.d.	n.d.	n.d.	0·04	n.d.	n.d.	n.d.	n.d.		n.d.	n.d.
CaO	2·53	1·26	4·59	0·97	6·42	0·28	6·19	4·05	1·57	1·46	1·38	1·42	2·44	0·01	0·01
Na_2O	8·61	8·46	8·57	8·62	7·80	8·80	7·83	8·19	8·72	8·39	8·28	8·30	8·05	7·33	7·80
K_2O	2·78	3·98	1·45	4·44	0·75	5·02	0·96	1·83	3·47	3·73	3·67	3·95	3·60	6·76	6·65
SrO	n.a.	n.a.	n.a.	n.a.	n.a.	n.a.	0·20	0·10	0·04	0·06	0·11	0·07		n.a.	n.a.
BaO	n.a.	n.a.	n.a.	n.a.	n.a.	n.a.	0·35	0·34	0·37	0·50	0·36	0·52	0·28	n.a.	n.a.
Total	99·31	100·08	100·65	99·01	100·58	99·16	101·38	100·54	101·03	99·86	100·15	100·76	99·62	99·76	99·64
An mol %	11·80	5·92	21·04	4·43	29·95	1·25	28·78	19·24	7·31	6·92	6·66	6·72	11·46	0·06	0·06
Ab mol %	72·75	71·84	71·07	71·36	65·88	71·80	65·90	70·41	73·46	72·02	72·27	71·04	68·44	62·18	64·03
Or mol %	15·45	22·24	7·89	24·21	4·17	26·95	5·32	10·35	19·23	21·06	21·07	22·24	20·10	37·76	35·91
SiO_2 wr	55·56	55·56	55·88	55·88	57·14	57·14	58·11	58·11	58·11	58·29	58·29	58·29	63·50	70·12	70·12

Microprobe compositional range determined by 3–10 point analyses. wr, whole enclave; n.a., not analysed; n.d., not detected; phen., phenocryst; mega, megacryst.
[1]Microlite in glass within 25x syenodiorite enclave.

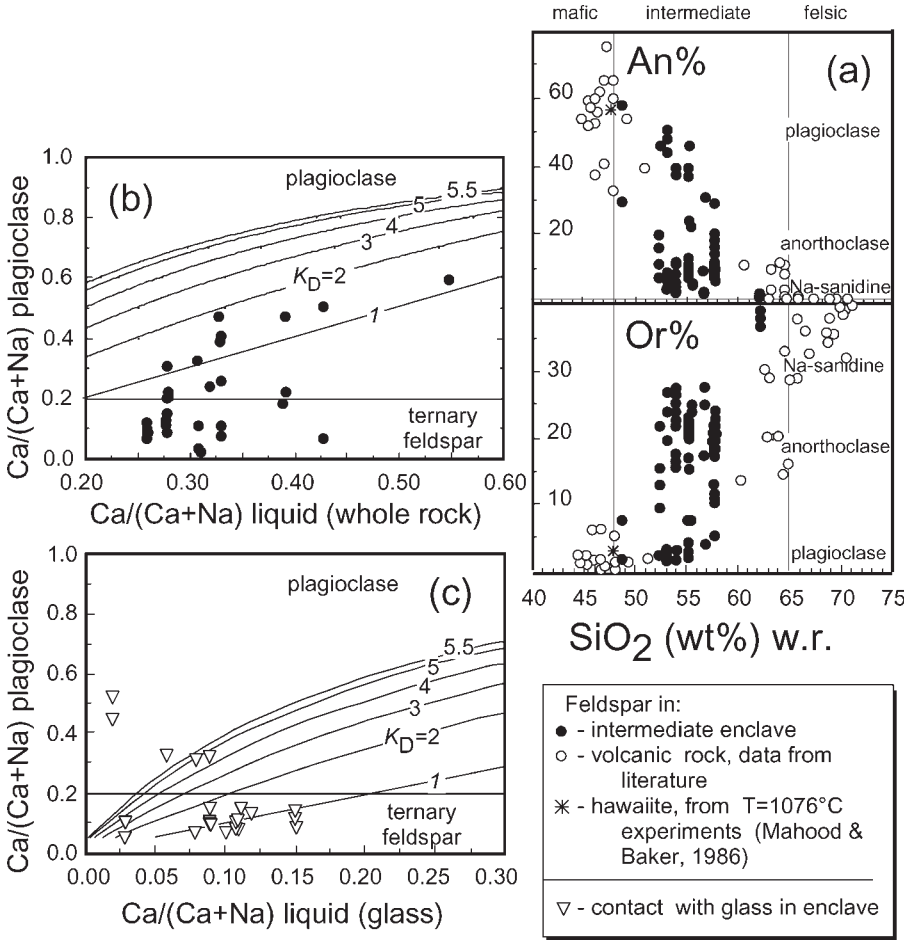

Fig. 9. Feldspar compositions: (a) feldspar composition (%An, %Or) vs whole-rock SiO_2 (wt %) content, (b) feldspar–melt equilibrium conditions: Ca/(Ca + Na) cationic ratio in plagioclase feldspar vs that in the liquid (enclave whole-rock) and (c) vs Ca/(Ca + Na) of the interstitial glass compared with the equilibrium compositions calculated on the basis of $^{Ca/Na}K_{Dfeld\text{-}liq} = 1$–5·5 according to Sisson & Grove (1993*b*) and Feeley & Dungan (1996). The plagioclase in the intermediate enclaves crystallized from a liquid under almost dry conditions ($K = 1$) or at very low water content ($K = 2$) if we modify the liquid composition by subtracting the modal Ca-rich xenocrysts; only ternary feldspar seems in equilibrium with the surrounding glass. (For sources of feldspar data from the literature see Fig. 5a.)

were calculated from Fe–Ti oxide pairs associated with Fe-augite pyroxene, and 886–864°C from oxide pairs associated with aegirine–augite pyroxene. All the analysed enclaves containing interstitial glass, enclosed within vitrophyric lavas of trachytic composition, give temperatures between 1000 and 950°C.

Amphiboles

Previous studies on the felsic volcanic rocks of Pantelleria revealed the presence of alkali amphiboles of barkevikite and arfvedsonite composition (Rittmann, 1967; Villari, 1974). Ti–Na-arfvedsonite and Fe-richterite have been found in trachytic pantellerite and pantellerite rocks, respectively (Avanzinelli *et al.*, 2004). Fe-richterite [classified according to Leake *et al.* (1997)] is also found in the comenditic trachytes (Civetta *et al.*, 1998). In the syenite enclaves we have found xenomorphic Fe-richterite with Na increasing towards the rims of the zoned crystals (Table 8).

Apatite

Apatite, in the intermediate composition enclaves, is found enclosed solely in the external parts of zoned feldspars and surrounding glass, but it is absent in plagioclase cores. In doleritic enclaves it is confined within a matrix containing brown glass. In medium-grained enclaves, syenogabbros and syenodiorites, apatite crystals are needle-shaped with a morphological axial ratio of *c*:*a* >50:1 (Fig. 3e and f), whereas in the syenite enclaves the apatite crystals have a more stumpy shape. The high rate of crystallization is responsible for the morphology of the acicular apatite (Frost & Mahood, 1987). In this context, the presence of needle-shaped apatite crystals as the only microlites in the glass should be noted (Fig. 3e).

Table 9: Representative electron microprobe analyses of Fe–Ti oxides from intermediate enclaves and of cossyrite from pantellerite host-rock

	magnetite						ilmenite						cossyrite	
Sample/spot:	20x	16Bx/75	62x	27x	17x/40	40x/91	20/x	16Bx/72	62x	27x/8	17x/43	40x/98		81 h/29
Rock type:	sy. gabbro	sy. gabbro	sy. gabbro	sy. diorite	sy. diorite	sy. diorite	sy. gabbro	sy. gabbro	sy. gabbro	sy. diorite	sy. diorite	sy. diorite		
H.r. type:	trachyte	trachyte	trachyte	trachyte	trachyte	trachyte	trachyte	trachyte	trachyte	trachyte	trachyte	trachyte		pantell.
H.r. cycle:	II	II	II	II	II	II	II	II	II	II	II	II		IV
SiO_2	0·20	0·20	0·15	0·28	0·22	0·26	0·16	0·14	0·15	0·20	0·17	0·21	SiO_2	40·21
TiO_2	22·45	23·50	23·73	21·51	21·99	26·07	48·39	48·61	50·06	47·69	47·85	50·12	TiO_2	8·63
Al_2O_3	1·14	1·15	0·63	0·92	1·08	0·23	0·09	0·05	0·05	0·11	0·07	0·05	Al_2O_3	0·63
FeO	69·24	70·00	69·86	71·62	70·40	69·70	46·27	46·30	45·50	46·00	46·50	45·50	Fe_2O_3[1]	1·27
MnO	1·28	0·73	1·29	1·30	1·11	0·90	1·45	0·84	1·56	1·46	1·26	1·30	FeO	38·93
MgO	1·73	1·29	1·27	1·70	2·39	0·89	2·56	2·74	2·04	2·50	3·00	2·03	MnO	1·17
CaO	0·02	0·15	0·06	0·06	0·04	0·04	0·10	0·13	0·04	0·14	0·03	0·16	MgO	0·53
Na_2O	0·00	0·00	0·00	0·00	0·00	0·00	0·00	0·00	0·00	0·00	0·00	0·00	CaO	0·51
K_2O	0·00	0·00	0·03	0·03	0·01	0·02	0·00	0·02	0·02	0·00	0·03	0·00	Na_2O	6·82
Cr_2O_3	0·03	0·01	0·00	0·01	0·08	0·00	0·00	0·02	0·02	0·00	0·03	0·00	K_2O	0·00
Total	96·09	97·03	97·02	97·43	97·32	98·11	99·02	98·85	99·44	98·10	98·94	99·37	Totals	98·70
Fe_2O_3	23·67	21·98	22·24	26·69	25·90	18·20	9·67	9·24	6·18	9·98	11·03	5·90	*Cations per 20 O*	
FeO	47·93	50·21	49·84	47·59	47·09	53·31	37·55	37·97	39·94	37·01	36·57	40·18	Si	5·852
Total	98·45	99·22	99·24	100·09	99·91	99·92	99·97	99·76	100·06	99·09	100·04	99·95	AlIV	0·108
													Fe^{3+}	0·040
Ulv%	65·13	68·48	67·48	60·84	61·91	73·58							Sum	6·000
R_2O_3							9·17	8·73	5·86	9·57	10·40	5·59	AlVI	0·000
log(Mg/Mn)	0·38	0·49	0·23	0·36	0·58	0·24	0·49	0·76	0·36	0·48	0·62	0·44	Fe^{3+}	0·099
													Ti	0·944
SiO_2 wr	52·85	53·57	54·41	55·56	55·88	57·14							Mg	0·114
													Fe^{2+}	4·736
T(°C)	1029	1050	886	1003	1048	939							Mn	0·144
$\log_{10}fO_2$	−10·58	−10·39	−13·84	−10·87	−10·01	−13·27							Ca	0·000
T(°C) range	1015–1043		864–916	987–1021		930–1019							Sum	6·037
													Ca	0·079
													Na	1·923
													K	0·000
													Sum	2·002
													Totals	14·039

wr, whole rock. T°C and fO_2 are calculated after Ghiorso & Sack (1991).
[1]Fe_2O_3 calculated assuming stoichiometry according to Deer *et al*. (1978).

Cossyrite and quartz

The mineral cossyrite (aenigmatite), named after the pre-Byzantine name of Pantelleria, Cossyra, was detected in the pantellerite hosting the syenite enclaves and shows an almost constant composition comparable with data from the literature (Carmichael, 1962; Zies, 1966; Wolff & Wright, 1981; Mahood & Stimac, 1990; Civetta *et al.*, 1998; Avanzinelli *et al.*, 2004) (Table 9). Quartz was observed in the syenite enclaves and in the more felsic rocks (based on X-ray data).

Glass composition

The small deficiency in the sum of some of the analyses, considering the total Fe as Fe_2O_3, might be due to the presence of unanalysed Cl, Fl, Sr and Ba (Table 10).

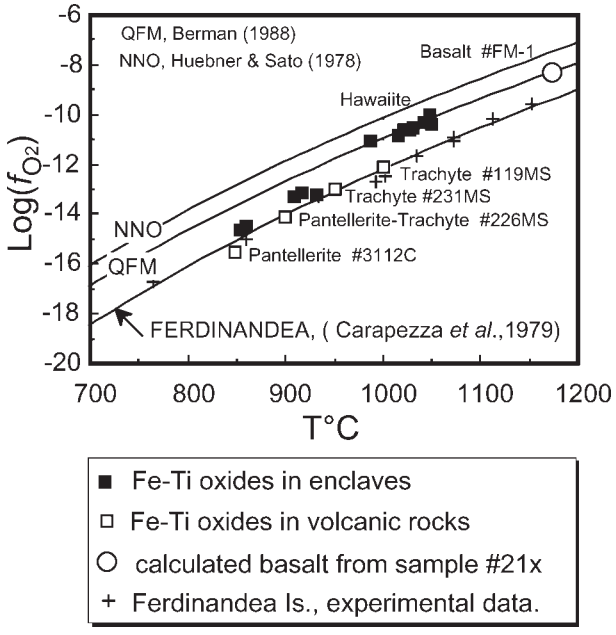

Fig. 10. Temperature (°C) vs log fO_2, calculated from coexisting Fe–Ti oxides in enclaves and volcanic rocks using the method of Carmichael & Ghiorso (1991). The oxides were selected according to criteria of Bacon & Hirschmann (1988). Data sources: Fe–Ti oxides in volcanic rocks (119MS, 231MS, 226MS) from Mahood & Stimac (1990); 3112C from Carmichael (1991). Experimental data for sample of mafic lava from Ferdinandea Island on Graham Bank in the Sicily Channel (Carapezza *et al.*, 1979) are shown for comparison. QFM, quartz–fayalite–magnetite buffer from Berman (1988); NNO, nickel–nickel oxide buffer from Huebner & Sato (1978).

The glass in the doleritic enclave (21x), with hawaiitic composition, is peralkaline and silica-undersaturated, with a higher TiO_2 content than the other analysed glasses. The 21x glass has the highest K_2O content of all the known rocks of Pantelleria and a K_2O/Na_2O ratio of 0·75, which is very similar to that of the glass in the trachytic and pantelleritic volcanic rocks studied by Mahood & Stimac (1990). This glass, representing 17·5 vol. % of enclave 21x (Table 10), has a particularly high F and Cl content; the value of 9400 ppm Cl detected in the glass corresponds to 1645 ppm in the bulk-rock enclave. This provides evidence of the incompatible behaviour of Cl, which is almost totally concentrated in the melt. The total Cl content of the 21x hawaiitic enclave is comparable with that of other mafic rocks (see Fig. 5b). Volcanic rocks with compositions similar to the glass in 21x have not been discovered on the island.

The glasses in the intermediate and medium-grained enclaves, syenogabbros and syenodiorites are silica-saturated with compositions ranging from metaluminous, alkaline to peralkaline quartz-trachyte to pantellerite on an R1–R2 diagram (not shown) after De la Roche *et al.* (1980). The glasses appear similar in composition to the felsic volcanic rocks of Pantelleria, with AI = 0·94 ± 0·21. Considering the measured whole-rock Cl content as all concentrated in the glass, the calculated equivalent bulk-rock contents are in agreement, according to Webster (1997), with the chlorine solubility in felsic melts, in the temperature range 800–1075°C and at pressures of 0·1 MPa to 0·2 GPa. There are significant heterogeneites within the glass in individual enclaves (Table 10). However, different colours are often observed in the same glass area (Figs 3 and 4) and do not appear to be related to compositional variations. Mg-rich olivine, Ca-rich pyroxene and Ca-rich plagioclase are not in equilibrium with the surrounding glass. Traces of glass with a very high silica content (SiO_2 74–76 wt %) were found in the syenogabbro (16Bx) enclave hosted in a trachyte. Syenite enclave (81x) within a hyalo-pantellerite host lava does not contain glass. We have found glass in the angular trachytic and pantelleritic wall-rock enclaves in host pyroclastic pantellerite. The glass within the spongy anorthoclase (22x) is similar to the external glass.

The behaviour of Sr in the Pantelleria magmas is strongly controlled by plagioclase crystallization, with a progressive lowering of Sr contents from basalts to trachytes, down to the very low concentration in the pantellerites. The Sr content of the analysed glass at the contact with the spongy anorthoclase enclaves (e.g. 22x) is variable and ranges from >1000 ppm down to below detection limits (<40 ppm); the latter corresponds to the low Sr content of the host lava.

Applying the liquid geothermometer of Sisson & Grove (1993*b*) to the analysed glass compositions and considering, for the original melt, H_2O content of 0·5–1·85 wt %, the results are 938–983 ± 14°C and ~876°C respectively for the trachytic and the more felsic glass compositions (e.g. the glass in 16Bx syenogabbro). The reliability of the Sisson & Grove (1993*b*) liquid geothermometer was also tested on pantellerite compositions: it must be noted in this context that the same temperature (~850°C) was calculated for the 81h and 32MS hyalopantellerites (Table 12), and for the 3112CG pantellerite, all with a pre-eruptive H_2O content of ~1·85 wt %, and that the same temperature value of 850°C was estimated from the Fe–Ti oxide geothermometer for 3112CG pantellerite (Carmichael & Ghiorso, 1990; Lowenstern *et al.*, 1993) with a pre-eruptive H_2O content of 1·4–2·1 wt % (Lowenstern & Mahood, 1991).

DISCUSSION OF MAGMA EVOLUTION

One of the main problems in studies of peralkaline suites, such as those of Pantelleria, is the need for an explanation for the lack of rocks of intermediate composition, constituting the so-called 'Daly Gap'. Among the several classes of hypotheses proposed to explain this distinctive feature, the most common are based on

Table 10: Representative electron-microprobe analyses of glasses from intermediate enclaves and host-rocks

Sample/spot:	21x/4	21x/3	22x/m	22x/38	22x/24	h.r. 22 h/19 +microlites	h.r. 119MS +microlites	17B/34 clear	17B/35 dark	17x/46
Rock type:	dolerite	dolerite	sy.diorite	sy.diorite	sy.diorite			sy.diorite	sy.diorite	sy.diorite
H.r. type:	trachyte	trachyte	trachyte	trachyte	trachyte	trachyte	trachyte	trachyte	trachyte	trachyte
H.r. cycle:	II	II	II	II	II	II	II	II	II	II
wt %										
SiO_2	58·47	59·30	64·47	64·90	66·71	64·53	64·80	64·65	65·39	69·42
TiO_2	1·23	1·36	0·88	0·88	0·91	0·91	0·59	1·01	1·24	1·19
Al_2O_3	16·47	16·94	14·50	14·80	17·67	14·52	14·70	14·07	14·06	14·28
Fe_2O_3t	5·53	5·87	6·19	6·27	6·55	6·19	5·59	5·98	6·12	6·45
MnO	0·00	0·11	0·22	0·23	0·26	0·21	0·20	0·21	0·25	0·22
MgO	0·74	0·92	0·52	0·49	0·52	0·54	0·40	0·75	0·68	0·71
CaO	1·02	1·22	1·16	1·18	1·26	1·15	1·15	1·00	1·13	1·11
Na_2O	8·16	7·37	6·53	5·22	2·19	5·07	5·93	6·41	5·59	1·59
K_2O	6·12	5·53	4·90	4·74	3·85	4·92	5·00	5·05	5·24	3·49
Cl	n.a.	0·94	0·58	0·58	0·58	n.a.	0·27	1·27	1·27	1·27
SrO	n.a.	n.a.	0·089	0·045	0·050	b.d.l.	0·006	n.a.	n.a.	n.a.
BaO	n.a.	0·078	0·209	0·019	0·125	0·082	0·046	n.a.	n.a.	n.a.
Total	97·74	99·63	100·24	99·35	100·67	98·12	98·67	100·39	100·97	99·73
glass mode	17·5	17·5	24	24	24		63	30	30	30
AI	1·22	1·07	1·11	0·93	0·44	0·94	1·03	1·14	1·06	0·45
T°C–H_2O (wt %)			981–0·5	983–0·5	1010–0·5	983–0·5	980–0·5	983–05	981–05	988–0·5
SiO_2 wr	49·22	49·22	58·11	58·11	58·11	n.a.	64·50	55·88	55·88	55·88

Sample/spot:	25x/m	h.r. 25 h/58 +microlites	20x/44 clear	20x/46 dark	27x/m	27x/6	16Bx/90	16Bx/92	h.r. 81 h	h.r. 32MS +microlites
Rock type:	sy.diorite		sy.gabbro	sy.gabbro	sy.diorite	sy.diorite	sy.gabbro	sy.gabbro		
H.r. type:	trachyte	trachyte	trachyte	trachyte	trachyte	trachyte	trachyte	trachyte	pantell.	pantell.
H.r.cycle:	II	II	II	II	II	II	II	II	IV	
wt %										
SiO_2	65·23	65·53	65·68	65·24	66·15	65·47	76·14	73·59	70·39	70·30
TiO_2	0·92	0·93	0·89	1·02	0·94	0·95	0·24	1·41	0·35	0·41
Al_2O_3	14·19	14·32	14·36	14·23	13·99	13·92	11·88	9·20	7·78	7·61
Fe_2O_3t	6·27	6·05	6·01	5·92	6·12	6·13	1·86	5·38	8·40	9·14
MnO	0·21	0·18	0·20	0·22	0·19	0·22	0·02	0·07	0·30	0·30
MgO	0·53	0·53	0·52	0·50	0·48	0·53	0·04	0·53	0·02	0·11
CaO	1·15	1·15	1·14	0·97	1·02	1·36	0·14	0·16	0·33	0·36
Na_2O	6·24	5·58	4·85	4·38	4·48	6·02	4·64	2·63	7·27	6·81
K_2O	4·68	4·64	5·17	5·20	5·22	5·13	4·70	4·18	4·48	4·59
Cl	0·58	n.a.	1·30	1·30	0·48	0·48	—	—	n.a.	0·92
SrO	0·049	b.d.l.	n.a.	n.a.	n.a.	n.a.	n.a.	n.a.	0·003	<0·002
BaO	0·038	b.d.l.	n.a.	n.a.	n.a.	n.a.	n.a.	n.a.	0·032	0·006
Total	100·08	98·90	100·12	98·98	99·07	100·21	99·65	97·14	99·34	100·55
glass mode	36	n.a.	10	10	19	19	tr	tr	95	91
AI	1·08	0·99	0·94	0·90	0·93	1·11	1·07	0·96	2·16	2·12
T°C–H_2O (wt %)	978–0·5	980–0·5	980–0·5	978–0·5	974–0·5	977–0·5	877–1·85	875–1·85	847–1·85	849–1·85
SiO_2 wr	58·29	n.a.	52·85	52·85	55·56	55·56	53·57	53·57	70·12	71·04

wr, whole-rock. Fe as total Fe_2O_3; also, in 21x/3 sample F content is 0·47 wt %. Italic values were obtained by mass-balance calculation; b.d.l., below 50 ppm content. tr, present but not determined in modal analysis; n.a., not analysed. The underlined data were calculated for Cl as perfect incompatible element in the whole-rock. AI, Agpaitic index. T°C, temperature calculated according to liquid geothermometer of Sisson & Grove (1993*b*) at H_2O (wt %) content.

Table 11: Results of Rayleigh fractional crystallization modelling of selected trace elements for some enclaves and volcanic rocks of Pantelleria within the Daly Gap

Parental magma:	basalt		basalt		hawaiite		mugearite		benmoreite		trachyte		syenite	
	1MB		1MB		28x		16Bx		22x		108x		81x	
Daughter magma:	basalt		hawaiite		mugearite		benmoreite		trachyte		pantellerite		pantellerite	
	Sic17aC		28x		16Bx		22x		108x		108 h		81 h	
Subtracted minerals (%)														
Fo_{80}-(1)	17·3	Fo_{80}-(1)	9·1	Fo_{80}-(1)	3·2	Fo_{41}-(25x)	12·5	Fo_{41}-(25x)	0·4	$Fo_{2·5}$-(81x)	6·5	$Fo_{2·5}$-(81x)	3·1	
Cpx-(1)	29·6	Cpx-(1)	39·2	Cpx-(1)	23·3	Cpx-(74x)	25·5	Cpx-(22x)	15·7	Cpx-(81x)	1·4	Cpx-(81x)	1·2	
An_{76}-(1)	53·1	An_{76}-(1)	41·0	An_{76}-(1)	55·1	An_{36}-(74x)	46·7	An_{26}-(22x)	20·2	An_{36}-(74x)	16·1	An_{36}-(74x)	12·4	
Mt-(1)		Mt-(1)	9·7	Mt-(1)	16·3	Mt-(25x)	12·7	Mt-(25x)	9·7	Anc-(81 h)	76·0	Amp-(81x)	9·6	
Ap-(1)		Ap-(1)	1·0	Ap-(1)	2·0	Ap-(231)	2·5	Ap-(32x)	1·4			Ap-(231)	0·4	
								Anc-(22x)	52·6			Anc- (81 h)	71·7	
												Ilm-(81x)	1·4	
F liq	0·87		0·65		0·80		0·57		0·37		0·44		0·18	
R^2	0·044		0·065		0·041		0·268		0·073		0·422		0·010	

	Obs	Calc	Obs.	Calc.	Obs.	Calc.	Obs.	Calc.	Obs.	Calc.	Obs.	Calc.
ppm												
V	282		286	97	181	43	112	8	111	1	56	1
Ni	49		72	29	58	17	6	2	1	1	6	1
Rb	18		24	21	20	26	26	45	41	112	150	236
Y	27		18	39	16	46	13	72	9	167	69	395
Zr	162		193	222	212	271	186	456	360	1173	1856	2637
Nb	34		57	74	80	91	61	156	116	408	n.a..	924
La	28		65	74	71	90	45	151	52	392	n.a..	866
Sm	7·3		9·9	13·0	n.a.	15·0	n.a.	25·0	n.a.	61·0	n.a.	138·0
Lu	0·3		0·6	0·4	n.a.	0·5	n.a.	0·8	n.a.	1·8	n.a.	4·1
Th	2·4		7·3	4·4	n.a.	5·3	n.a.	8·7	n.a.	20·5	n.a.	43·1

The sample number of the minerals is reported in parentheses; data sources for sample numbers: 1, Mahood & Baker (1986); 231, Mahood & Stimac (1990); Sic17aC, Civetta *et al*. (1998). For the basalt trace elements an average composition of literature data was used. x, enclave; h, host-rock; R^2 is the sum of the squares of the residuals. n.a., not analysed. Obs, observed; Calc., calculated. Distribution coefficients are from Luhr & Carmichael (1980), Villemant *et al*. (1981), Villemant (1988) and Peccerillo *et al*. (2003).

fractional crystallization models, with variants involving compositionally stratified magma chambers (e.g. Barberi *et al*., 1975; Civetta *et al*., 1998; Peccerillo *et al*., 2003). Other hypotheses suggest that the peralkaline silicic rocks and associated basalts represent two different magma types that are not petrogenetically related (Mahood *et al*., 1990; Lowenstern & Mahood, 1991).

Fractional crystallization modelling of the enclaves spanning the 'Daly Gap'

A step-by-step magmatic differentiation process from basalt to trachyte has been modelled, where at each stage the more progressively differentiated daughter magma represents the parental magma of the subsequent differentiation stage. The mineral compositions in the rocks 1MB basalt, 28x hawaiite, 16Bx mugearite, 22x benmoreite and 108x trachyte were used to model the phenocryst extract during progressive differentiation (Table 11). Using these mass-balance results, theoretical differentiation trends for both compatible and incompatible trace elements (Ni, V, Th, La, Sm, Lu, Nb, Y, Zr,) were calculated on the basis of Rayleigh fractionation for the complete step-by-step differentiation model covering the 'Daly Gap', and compared with the observed trends. Although a successful mass balance can be achieved for major element oxides, the trace element trends (Fig. 5c) cannot be reproduced.

We have also tested the fractional crystallization hypothesis by considering plots of an incompatible element vs the ratio of the same incompatible to a less-incompatible element (Joron & Treuil, 1989), such as the plots of Hf vs Hf/La, Zr vs Zr/Y, Th vs Th/Sm (Ce vs Ce/Yb, Cs vs Cs/Yb, Nb vs Nb/Y not shown) in Fig. 11. These diagrams illustrate that the enclaves, which range from mafic to felsic in composition, define a coherent, but much steeper, trend than the lavas.

Magma mixing modelling: hawaiite and trachyte as end-members of intermediate composition magmas

A linear array of data in major element variation diagrams can be interpreted as the result of mixing between two magmas with different compositions (Bacon, 1986; Frost & Mahood, 1987; Gourgaud & Villemant, 1992; Feeley & Dungan, 1996). In the Harker diagrams (Figs 5 and 12a) in the SiO_2 48–65% range, the enclaves show at least two distinctly different trends of MgO, P_2O_5, Cr, Ni and Sc (not shown). In the majority of the enclaves the MgO contents define a negative trend with good linear correlation, which intercepts the trend defined by the mafic lavas at SiO_2 ~48% and MgO ~4% (hawaiite) and the field of felsic lavas at SiO_2 65% and MgO <0·5% (trachyte) (Fig. 5a).

The calculated mafic end-member (Table 12) is a hawaiite that nearly coincides with the bulk-rock analysis of an enclave (103x) from the >50 ka volcanic rocks with MgO 3·85% (Trend I, Fig. 12a), and comparable with the composition of the differentiated magma ($F = 0{\cdot}50$, $T = 1082$°C and QFM conditions) calculated by Mahood & Baker (1986) on the basis of an experimental study at low pressure of a less evolved basalt (38MB). Applying the Sisson & Grove (1993*b*) geothermometer to the calculated mafic end-member gives a similar temperature if we consider that the original melt had 0·5–1·5 wt % H_2O. The felsic end-member corresponds to SiO_2 65% and MgO < 0·5%, and a calculated temperature of 1000–950°C.

The doleritic enclaves, the basalts with anorthoclase xenocrysts, hawaiite 33MB and two intermediate composition enclaves SIC11C and SIC52C, define a second array in Fig. 12 that intercepts the mafic lava trend at SiO_2 48% and MgO ≈7% (~1190°C) and the felsic trend at SiO_2 65% and MgO < 0·5%. This second trend (trend II in Fig. 12a) is probably formed by the mixing between an FM-1 basalt, probably rising along dykes, and overlying trachytic magma. The major and trace element contents of the mixing end-members, calculated by taking into consideration the 48% and 65% SiO_2 intercepts of the least-squares calculated linear trends, or by linear extrapolations, are given in Table 12.

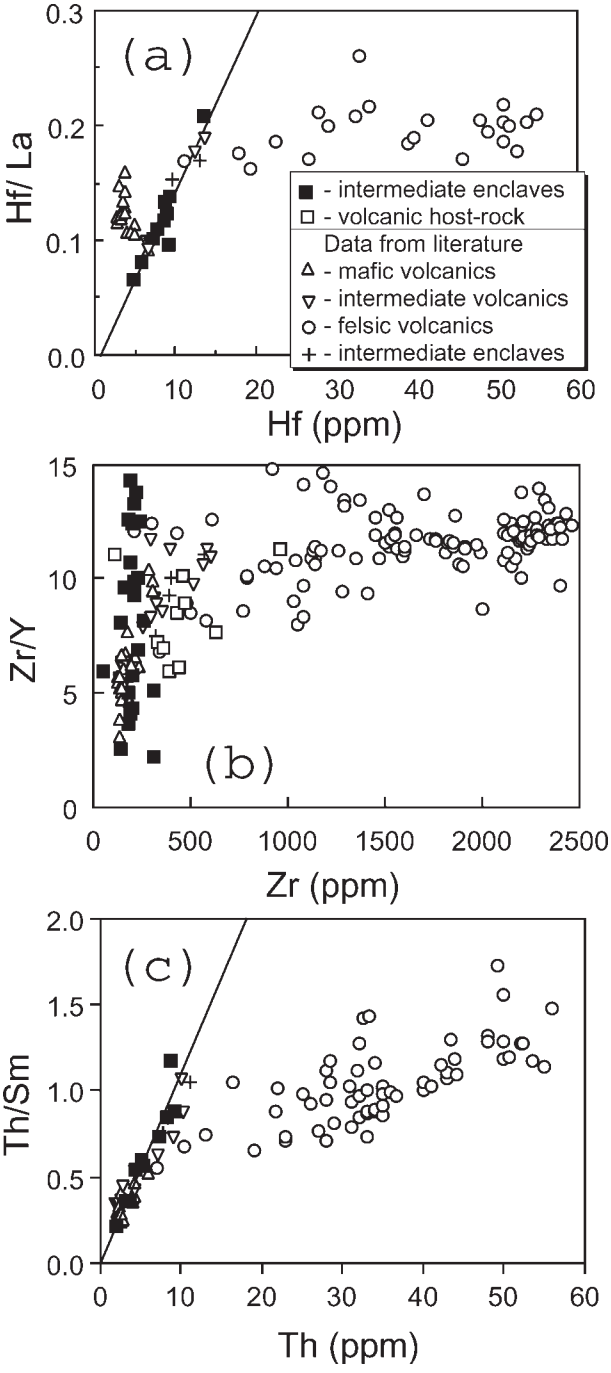

Fig. 11. Plots of an incompatible element vs the ratio of the same incompatible element to a less-incompatible element: (a) Hf vs Hf/La; (b) Zr vs Zr/Y; (c) Th vs Th/Sm.

The hypothesized mixing model between hawaiite and trachyte (trend I) is consistent for all the analysed elements (for the REE plot of intermediate enclaves see Fig. 13) and is in perfect agreement with all the analysed enclaves of intermediate composition. Some differences

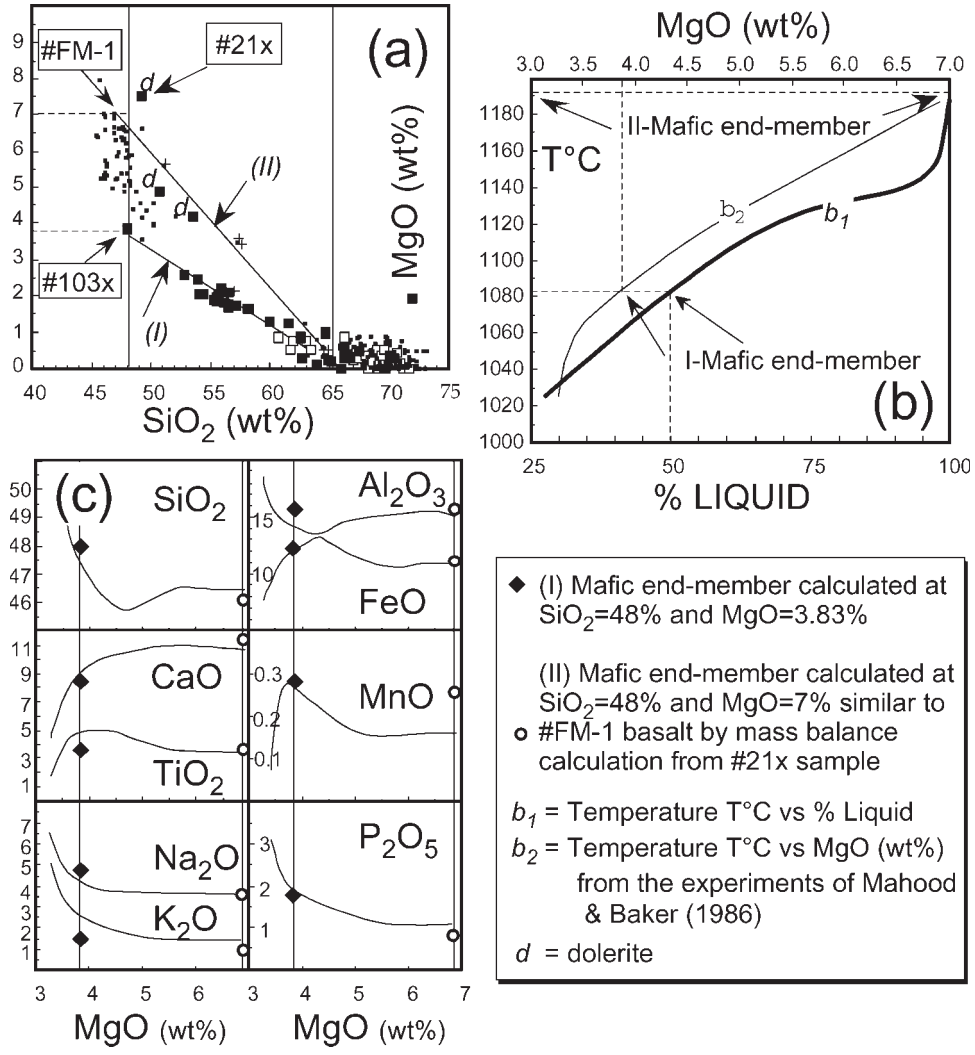

Fig. 12. Calculation of mafic end-member compositions of different trends on the MgO vs SiO_2 (wt %) diagram. (a) At SiO_2 48 wt %, there are two mafic end-member intercepts at MgO 3·8 wt % and MgO 7 wt %, respectively; symbols are as in Fig. 5a. (b) Percentage liquid and MgO content (wt %) in the liquid vs temperature for the 0·1 MPa crystallization experiments of Mahood & Baker (1986) on a partially melted basaltic rock. The (I) mafic end-member with MgO 3·8 wt % corresponds to a residual liquid (50%) with a temperature of 1082°C; the (II) mafic end-member with MgO 7 wt % nearly coincides with 100% of the basaltic melt at the liquidus temperature (≈1190°C) and is very similar to the FM-1 basalt calculated by mass balance from the 21x enclave (Table 12). (c) The (I) and the (II) mafic end-members are compared with the experimental curves at 0·1 MPa (= 1 bar) of Mahood & Baker (1986).

between the measured and calculated data are probably due to analytical bias for low trace element contents, or to overlaps of the data with trend II.

The origin of the glass in the enclaves

We can distinguish three different and simple hypotheses for the origin of the glass in the intermediate enclaves: (1) the enclave is partially crystallized after magma mixing, with the glass representing the chilled mixed melt, when it is incorporated in a partially molten/plastic state in the host magma; (2) the glass in the enclave derives from host magma infiltration; (3) the interstitial glass is the product of partial remelting of previously solid enclaves heated by the host magma. We will evaluate each of these hypotheses in turn.

(1) The glasses in the intermediate enclaves are compositionally very different from those of mixtures of hawaiitic and trachytic melts: they have trachytic or felsic compositions. The inhomogeneous melt is not comparable with an intercumulus liquid within a crystal mush according to the following considerations. (a) A syenogabbro enclave (16B), hosted by a nearly holocrystalline trachyte, is almost totally crystallized and shows textural

Table 12: Calculated mafic and silicic end-members of magma mixing and representative volcanic rocks of mafic and intermediate compositions

TAS classif.:	primitive basalt	basalt	basalt	basalt	hawaiite	hawaiite	hawaiite	hawaiite	hawaiite	mugearite	mixing	benmoreite	mixing	benmoreite	mixing	trachyte	mixing	trachyte	trachyte
Type:	calc.[1]			calc.[2]	enclave	experim.[3]			calc.	enclave	calc.[4]	enclave	calc.[5]	enclave	calc.[4]	enclave	calc.[4]		calc.
Sample:	FM-0	38	Opl120-b	FM-1	21x	PSU-10	135	FPN4	Tra-no. = 0 mafic end-member	20x	Tra-no. = 27%	17Bx	Tra-no. = 46%	40x	Tra-no. = 53·6%	81x	Tra-no. = 85%	119	Tra-no. = 100% felsic end-member
Data source:		MB	C			MB	MB	EC										MS	
wt %																			
SiO_2	45·45	46·00	46·15	45·95	49·22	47·90	49·58	50·26	48·00	52·85	52·59	55·88	55·82	57·14	57·11	62·65	62·45	64·54	65·00
TiO_2	3·19	3·50	3·40	3·54	2·81	4·55	3·15	2·98	3·41	2·71	2·66	2·21	2·14	1·97	1·93	0·86	1·06	0·72	0·64
Al_2O_3	14·34	14·90	15·05	15·93	15·17	14·60	15·83	17·16	16·09	15·57	16·10	16·16	16·10	16·27	16·10	15·80	16·11	16·26	16·11
FeOt	11·23	11·30	11·30	11·02	10·26	11·70	10·92	10·31	12·18	10·68	10·28	8·79	8·95	8·25	8·41	6·36	6·20	4·95	5·15
MnO	0·26	0·18	0·17	0·26	0·26	0·28	0·20	0·18	0·28	0·32	0·27	0·23	0·27	0·25	0·26	0·29	0·25	0·18	0·25
MgO	10·90	7·01	6·95	6·98	7·39	3·69	4·34	3·98	3·83	2·57	2·87	2·22	2·20	1·71	1·93	0·29	0·82	0·57	0·29
CaO	10·35	11·00	10·96	11·46	8·99	8·47	8·59	7·91	8·68	6·59	6·71	5·18	5·33	4·99	4·78	1·64	2·49	1·91	1·40
Na_2O	3·24	3·50	3·58	3·60	4·14	4·36	4·22	4·97	4·73	5·81	5·45	6·02	5·95	6·20	6·16	6·83	6·99	6·45	7·39
K_2O	0·38	1·44	1·46	0·42	1·18	2·82	1·95	1·83	1·21	1·75	1·98	2·55	2·53	2·45	2·74	5·11	3·64	4·25	4·07
P_2O_5	0·68	0·99	0·97	0·76	0·59	2·03	1·22	0·43	1·40	1·13	1·04	0·77	0·78	0·77	0·68	0·17	0·26	0·16	0·06
Total	100·02	99·82	99·99	99·92	100·01	100·40	100·00	100·01	99·81	99·98	99·95	100·01	100·06	100·00	100·10	100·00	100·27	99·99	100·36
mg-no.	0·65	0·58	0·58	0·56	0·58	0·41	0·43	0·43	0·38	0·32	0·35	0·33	0·32	0·29	0·31	0·08	0·20	0·18	0·10
ppm																			
Sc			20·7	17·7	16·0			21·2	36·0	29	28	16	22	25	20	16	11	5·3	6·0
V		291	273		176		281	264	215	214	160	167	121	104	105	32	41		10
Cr		166	183	8	6		13		12	8	9	17	7	13	7	4	4	<8	2
Ni		95	95	23	12		6	29	8	7	7	6	6	14	6	1	5		4
Rb			28	12	20			43	14	14	23	37	30	23	32	45	43	70	48
Sr		763	702	453	395		682	675	424	315	328	280	260	273	233	46	121	180	67
Y			32	26	33			42	33	14	39	16	43	35	44	10	51		54
Zr			306	190	227			356	125	176	178	221	216	203	231	111	293	472	323
Nb			61	35	47			79	37	62	50	76	59	57	62	68	77		84
Cs					0·19			0·17	0·19	0·20	0·21	0·37	0·22	0·10	0·22	0·12	0·24	0·70	0·25
Ba			421	352	612			686	1000	1251	1135	1005	1230	1194	1268	671	1425	968	1500
La			59·5	60·6	68·0			74·8	60·0	72·0	65·7	66·0	69·7	96·0	71·0	73·0	77·9	74·0	81·0
Ce			120·7	106·8	121·0			145·3	109·0	130·0	119·5	124·0	126·9	178·0	130·0	148·0	142·2	136·0	148·0
Nd			59·9	36·1	40·3		63·5	63·5	35·0	38·0	38·2	41·3	40·5	38·8	41·4	38·1	45·2	60·0	47·0
Sm			11·56	8·94	9·63		1·82	11·82	8·00	8·96	8·54	7·32	8·92	10·23	9·07	7·98	9·70	11·90	10·00
Eu			3·75	3·13	3·37		3·72	3·72	3·00	4·01	3·14	2·98	3·23	3·52	3·27	3·41	3·43	2·81	3·50
Dy			7·07	8·14	9·27			7·54	10·00	10·87	10·41	11·99	10·69	11·25	10·80	9·50	11·28		11·50
Er			2·95	5·30	5·83			3·42	6·00	6·40	6·14	5·73	6·23	8·15	6·27	5·65	6·43		6·50
Yb			2·31	4·13	4·55			2·86	4·00	3·98	4·30	4·40	4·51	5·79	4·59	5·18	4·94	5·10	5·10
Lu			0·32	0·45	0·49			0·43	0·39	0·39	0·43	0·42	0·46	0·48	0·48	0·52	0·53	0·76	0·55
Hf				8·32	8·98			6·74	7·00	7·29	7·66	13·56	8·13	9·25	8·31	8·99	9·08	13·80	9·45
Th			5·98	6·99	8·15			7·34	7·80	3·24	8·61	8·57	9·18	9·05	9·41	4·34	10·35	10·40	10·80

MB, Mahood & Baker (1986); MS, Mahood & Stimac (1990); EC, Esperança & Crisci (1995); C, Civetta *et al.* (1998), partial analyses; FM, this study.
[1]Primitive basalt calculated compositions (see Table 6).
[2]Basalt calculated composition (see Table 6).
[3]Liquid obtained at $T = 1076^{\circ}C$ according to experiments of Mahood & Baker (1986).
[4]Tra-no. (trachyte-number) = 100 × trachyte/(trachyte + hawaiite): the result of mixing on the basis of mass-balance calculation between hawaiite and trachyte end-members.
Some analyses are recalculated to 100% on anhydrous basis; mg-number = $Mg/(Mg + Fe^{2+})$; Fe^{3+}/Fe^{2+} ratio is calculated according to Kilinc *et al.* (1983).

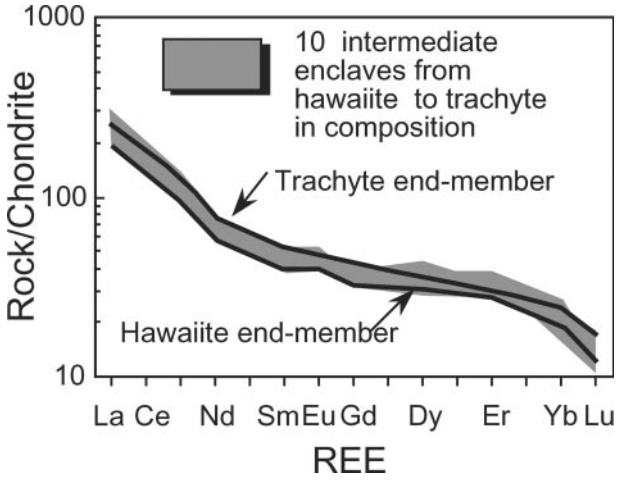

Fig. 13. Chondrite-normalized REE patterns of 10 intermediate enclaves spanning a range from hawaiite to trachyte in composition [normalization constants from Boynton (1984)] (Table 4). The patterns of the calculated hawaiite and trachyte end-members (Table 12) are also shown.

characteristics comparable with those of the other enclaves, except for the amount of glass. The traces of glass in the 16B enclave have a felsic composition with SiO_2 >70 wt %. (b) Several enclaves (e.g. 22x, 25x, 16bx) show radial intergrowths of Fe-augite and oligoclase plagioclase, which formed before anorthoclase crystallization. Such a radial texture of clinopyroxene and plagioclase in skeletal intergrowth (Fig. 3 g), although unusual, has been reported previously in medium-grained dolerite (MacKenzie *et al.*, 1982). The presence of euhedral plagioclase at the glass contact seems in contrast with the xenomorphic intergrowth with the clinopyroxene. (c) Acicular apatite appears to intersect different crystals of plagioclase and the intracrystalline glass (Fig. 3e and f). This fragile texture (by SEM imaging we observed 1160 μm × 1 μm dimensions) is not compatible with progressive crystallization of magma in the residual spaces between earlier formed crystals in a partially molten/plastic enclave. (d) The glass in the enclaves is inhomogeneous, varying in colour from dark brown to clear over short distances (Figs 3 and 4) between the part in contact with the crystals and the central area, but, nevertheless, in some cases has a constant major element composition (Table 10). Alternatively a glass area that appears homogeneous in colour can show inhomogeneity in composition. The colour changes of interstitial glass have been used as a criterion to identify areas of melt-mixing within enclaves (Zinngrebe & Foley, 1995). (e) A crystal mush according to Marsh (1988) can form when just 50% of the melt has crystallized. The glass composition is, therefore, incompatible with the presence of a large amount of crystalline solid (also >90%) (Table 10) and with a residual felsic melt, which solidified as a glass instead of forming a granophyric texture.

(2) The origin of glass in the enclaves by host magma infiltration does not fit with the observed glass inhomogeneity (Table 10). For example, the Sr content of the glass can be very variable, even in adjacent point analyses, from >1000 ppm to <40 ppm (below detection limit). The high contents of Sr, not shown, are clearly due to feldspar melting in the enclave, whereas the very low Sr contents are due to host melt infiltration: the lack of mixing between two similar melts can be due to the greater viscosity of the host magma with abundant microlites and kinetic considerations. The host trachyte magma tends to fracture, permeate and dismember the peripheral part of the enclave (Fig. 2d).

(3) *In situ* partial melting appears to be most realistic explanation for the presence of interstitial glass. In medium-grained enclaves needles of apatite are enclosed in both oligoclase and anorthoclase: the melting of the anorthoclase leaves the residual apatite needles and partially preserves the plagioclase. Apatite is often the only crystal in the intracrystalline glass. The glass can occasionally show square-shaped K-feldspar microlites, which are portions of mechanically dismembered anorthoclase (Table 8). The high Sr contents of the glass are clearly due to feldspar melting (e.g. 1500–5800 ppm Sr in feldspar of 22x). The glass with the highest silica content (SiO_2 >70%) occurs in the enclaves hosted within trachyte and, following Harris & Bell (1982), can be interpreted as the result of partial remelting of the majority of the low-temperature minerals, including quartz (no longer present). During this process the euhedral cores of more Ca-rich plagioclase crystals have been preserved. A least-squares mass-balance model, applied to the glass of sample 22, can be used to test this remelting hypothesis. The results are in excellent agreement with the hypothesis of partial melting of all the original low-temperature minerals in the enclave, particularly anorthoclase, with a contribution from late and interstitial minerals such as quartz and aegirine–augite, in essentially oxidizing conditions (Table 13). The calculated composition of the melted feldspar ($Ab_{56}An_4Or_{40}$) is similar to the alkali-feldspar (Or_{38}) found in syenite and in the recrystallized trachyte groundmass (Fig. 3 h). The Ab–Or–Qz haplogranitic system at 0·2 GPa shows that, after preliminary eutectic consumption of a small quantity of quartz, the melting process involves only the alkali feldspars. However, the high melting rate probably prevented the achievement of equilibrium conditions, leading to the formation of an inhomogeneous glass. In the Q–Ab–Or system (e.g. Bowen & Tuttle, 1950; Carmichael & MacKenzie, 1963) the glasses in the enclaves hosted by trachyte (excluding the glass in dolerite 21x) plot between the eutectic minimum (pantelleritic glass) and the thermal

Table 13: Composition of representative glass within a syenodiorite enclave as a result of the melting of suitable minerals, estimated by least squares mass-balance calculations

Sample:	22x/m	22x	73x	22x					
Type:	Glass	Ol-Fo_{39}	Aegirine–augite	Mt	Ab (wt %)	An (wt %)	Or (wt %)	Calculated minerals	wt %
wt %									
SiO_2	64·47	32·73	49·90	0·20	68·14	43·86	64·70	Olivine Fo_{39}	2·61
TiO_2	0·88	0·04	0·38	21·98	0·00	0·00	0·00	Aegirine–augite	5·18
Al_2O_3	14·50	0·02	0·23	1·11	19·92	36·05	18·40	Anc ($Ab_{56}An_4Or_{40}$)	74·26
FeOt	5·57	45·42	27·07	68·94	0·05	0·29	0·00	Ti-magnetite	4·13
MnO	0·22	2·27	0·58	1·26	0·00	0·00	0·00	Quartz	13·82
MgO	0·52	17·50	1·08	1·57	0·00	0·03	0·00		100·00
CaO	1·16	0·35	11·16	0·00	0·11	19·52	0·00	R^2	0·03
Na_2O	6·53	0·00	6·65	0·00	11·65	0·24	0·00		
K_2O	4·90	0·00	0·00	0·00	0·14	0·00	16·90		
Total	98·75	98·33	97·05	95·06	100·01	99·99	100·00		
SiO_2 wr	58·11								

R^2 is the sum of the squares of the residuals. Anc, anorthoclase. Some mineral types not recognized in sample 22x are present in hypidiomorphic enclaves as rims on other minerals or xenomorphic crystals. Pure Albite (Ab), Anorthite (An) and Orthoclase (Or) analyses (wt %) were used for the feldspar mass-balance calculation.

valley towards Or_{38} in the Or–Ab binary system (trachytic glass).

Melting conditions of the enclaves

As noted above, the presence of glass in the enclaves is strictly related to the nature of the host magma: glass occurs only when this is trachytic. The Pantelleria trachytes have an estimated liquidus temperature of 950–1000°C (Mahood, 1984; Lowenstern *et al.*, 1993); similar temperatures were obtained by applying the liquid geothermometer of Sisson & Grove (1993*b*) and considering for the original melt a H_2O content of ≈0·5–1·85 wt %. For the internal part of a solid enclave, under dry conditions and for a pressure range of 0·5–0·2 GPa, partial melting starts at 925–950°C. The Sisson & Grove (1993*b*) geothermometer, initially calibrated for liquids with SiO_2 <55 wt % and not alkalic composition, is applicable in the range 1300–1100°C, under dry conditions, and 1100–750°C under wet conditions. The estimated temperatures of formation for the silica-saturated glasses (SiO_2 64–66 wt % and AI ≈0·94) in the enclaves are almost 10–15°C lower than those of the host magma, ~876°C for the high-silica glass (SiO_2 >70 wt %), considering the maximum H_2O content of the melts to be close to that of the host magma. The pressure of a column of melt with a density d = 2·5–2·2 g/cm^3 in a magma chamber at 5 km depth (Mahood, 1984) falls within the range of 0·13–0·11 GPa; therefore, on the basis of the system Qz–Or–Ab–H_2O, the initial melt of the enclaves at 850°C should have a minimum water content of ~1·5 wt % (Johannes, 1985; Johannes & Holtz, 1990) and a water solubility limit of 4·2 wt % (Behrens & Jantos, 2001). The high-silica glass probably corresponds to incipient remelting, in conditions of partial equilibrium, whereas the other glasses result from the greater remelting of syenodioritic and syenogabbro enclaves in essentially H_2O very undersaturated conditions (Fig. 14).

The residence time of the enclaves within the melt

According to Geschwind & Rutherford (1995), the presence in a melt of acicular and skeletal microlites or fibrous terminations of microphenocrysts is due to rapid decompression of the magma in the higher parts of the volcanic conduit, and to the high rate of crystallization (2–9 days). The presence of two different kinds of glass with similar composition, but containing rare and abundant microlites, respectively, in the peripheral portions of the enclaves is considered evidence of different residence times of the microlites within the melt, certainly longer in the host melt.

Feldspars from most of the enclaves in the trachytes of the 'Cinque Denti' caldera are zoned, but the anorthoclase crystals do not show exsolution. Therefore, the temperatures reached in the enclaves must have been high enough to account for the partial re-homogenization

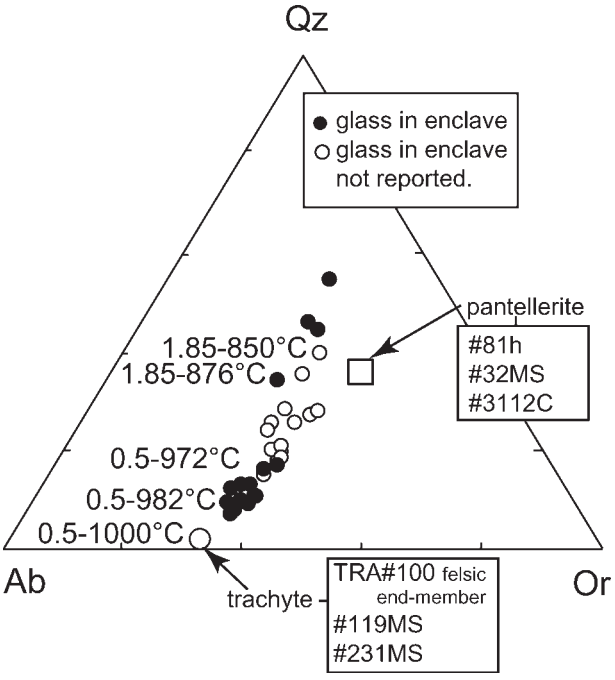

Fig. 14. Analyses of glasses in enclaves hosted by trachyte plotted in the Qz–Or–Ab normative diagram. ●, analysed glass in Table 10; ○, unreported data. H_2O (wt %) content and temperature are reported as pairs of numbers. The large circle on the Ab–Or side of the diagram indicates the composition of the calculated felsic end-member with trachyte-number = 100% (Table 12), and the trachyte volcanic rocks 119 and 231 from Mahood & Stimac (1990). The square indicates the composition of the pantellerites 81 h and 32 from Mahood & Stimac (1990), and 3112 from Carmichael (1991).

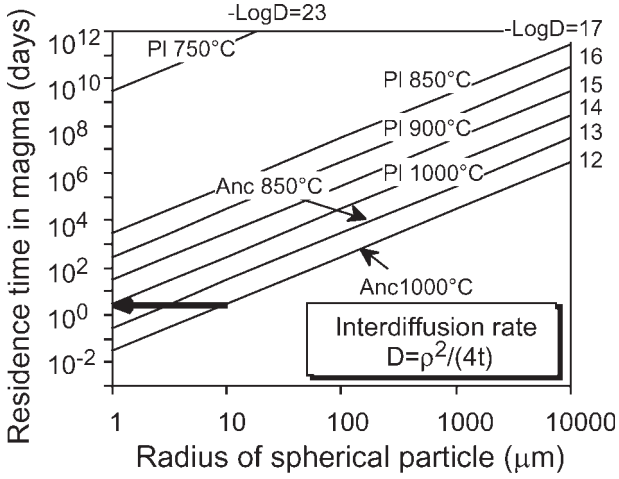

Fig. 15. Size of enclave (expressed as the radius of an equivalent spherical particle) vs days of residence of the enclave within the host magma. The diagram constrains the time needed to erase any chemical zoning in feldspar by diffusion. The interdiffusion diagram was calculated on the basis of the mean experimental data obtained for Or_{40} alkali-feldspar (anc) by Christofersen *et al.* (1983) and for plagioclase (pl) by Johannes (1985). The interdiffusion rate $D = \rho^2/(4t)$ is in cm^2/s for a sphere of ρ (cm) radius at t seconds. The contours in the diagram are for different interdiffusion rate values reported as (negative) exponents to the base 10.

of pre-existing perthites. According to Brown & Parsons (1984), 'only extremely rapidly chilled feldspars will remain homogeneous on cooling' (at rates of a few degrees/hour). For zoned anorthoclase-bearing hornfels xenoliths in the basaltic andesite lavas of Stromboli (Aeolian Islands, Sicily), a cooling rate of a few days has recently been estimated (Renzulli *et al.*, 2003).

As far as the zonation is concerned, the alkali feldspars have ovoid cores with sharp boundaries against the surrounding rims. Taking into account feldspar interdiffusion, which according to Christofersen *et al.* (1983) is not dependent on pressure and the H_2O content of the melt, we have tested the residence time of the enclaves in the trachytic magma at 1000°C, on the basis of the relation $D = \rho^2/(4t)$, where D is the interdiffusion rate (cm^2/s) of a sphere of ρ (cm) radius at t seconds (Johannes, 1985). Alkali feldspars have interdiffusion rates that vary with composition and crystallographic direction (Christofersen *et al.*, 1983); for a value of $D = 10^{-12}$ cm^2/s the homogenization rate is approximately 1 μm/h, 10 μm in 3 days or 1 mm in 79 years. Plagioclase, according to the D values calculated by Johannes (1985) of 10^{-13} cm^2/s at 1000°C, requires 10 times longer: 1 μm in 7 h, 10 μm in 29 days or 1 mm in 792 years (Fig. 15).

The interdiffusion rate within the (Or_{40}) alkali feldspar at the pantellerite liquidus temperature of ~850°C is approximately $D = 10^{-13.5}$ cm^2/s (Christofersen *et al.*, 1983), corresponding to a homogenization rate of 1 μm/day or 10 μm in 91 days (Fig. 15). Mesoperthite exsolution and evidence of cataclastic deformation induced by thermal shock (Ferla *et al.*, 1978) in the alkali feldspar in syenite enclaves within the host pantellerite are still preserved under these conditions.

On the basis of the above data, the residence time of the enclaves within the host magma is considered to be fairly short. Assuming thermal equilibrium, the lack of homogenization of the anorthoclase, on the basis of microscopical observations and electron microprobe analyses of sector zoning ~10 μm thick, implies that the residence time of the enclave within the melt at 1000°C can be estimated at 3–5 days, if we consider the range of feldspar compositions and a linear interdiffusion rate based on extrapolation of previous data.

The 'Daly Gap' at Pantelleria

The 'Daly Gap' at Pantelleria between the mafic and felsic volcanic rocks has been explained by a number of models including crustal melting induced by basalt heating (Rittmann, 1967). Crustal melting is not confirmed by the relatively constant $^{87}Sr/^{86}Sr$ of both

mafic and felsic volcanic rocks, which suggests that the felsic magmas could be derived from parental basalts by fractional crystallization (Barberi *et al.*, 1969; Civetta *et al.*, 1984, 1998). The latter hypothesis would be confirmed by the presence of enclaves of intermediate composition in the lavas (Villari, 1974; Civetta *et al.*, 1984). This model has been successfully applied to explain the petrogenesis of bimodal alkaline volcanic suites in a number of continental rifts (Barberi *et al.*, 1975; Peccerillo *et al.*, 2003) and oceanic islands such as Mururoa (Caroff *et al.*, 1993). In alternative hypotheses, pantellerites were thought to be derived from basalt unmixing (Lucido, 1982) or partial melting of a metasomatized mantle source (Bailey & Macdonald, 1987). Nevertheless, on the basis of isotopic studies, Mahood *et al.* (1990) have suggested for Pantelleria that trachypantellerite magmas were generated by partial fusion (5%, on the basis of mass-balance calculations; Ferla & Meli, in preparation) of crustal alkali-gabbros induced by intrusion of fresh basalt. The subsequent differentiation of the trachypantellerite magma resulted in the formation of anorthoclase-cumulate trachytes and residual pantellerite (Mahood & Baker, 1986; Mahood & Stimac, 1990; Mahood *et al.*, 1990; Lowenstern & Mahood, 1991). According to Mahood & Baker (1986) the 'benmoreitic' enclaves in the Pantelleria volcanic rocks are feldspathic cumulates and are not representative of magma of intermediate composition in the 'Daly Gap'.

Magma mixing and mingling can be significant processes in the generation of rocks of intermediate composition in the 'Daly Gap' of alkaline magmatic suites. However, although the chemical composition of the enclaves fills the 'Daly Gap', this does not indicate that there was ever a continuous liquid line of descent from mafic to felsic magma compositions.

The intermediate composition enclaves exhibit microscopic evidence for several generations of minerals that can either be rimmed or occur as single crystals: these include olivine, clinopyroxene, plagioclase, alkali feldspar and Fe–Ti oxides. The presence of forsteritic olivines in the enclaves, which are clearly xenocrystic, is consistent with the presence of mafic enclaves within a more felsic liquid. Normally zoned feldspars coexist with crystals with corroded cores of ternary feldspar, external euhedral part of the cores composed of plagioclase and outer zones of alkali-feldspar. According to Feeley & Dungan (1996), these textures can be explained by the inclusion of Na-rich crystals within a hotter, Ca-rich, melt, followed by crystallization of plagioclase from the hybridized magma, and eventually by the intercumulus-like crystallization of anorthoclase and alkali-feldspar from the residual melt.

Consequently we consider that the mineralogy of the enclaves is consistent with commingling between mafic and felsic magmas (i.e. Ferla, 1997). The more mafic enclaves are clearly highly differentiated mafic melts (hawaiite) containing relict 'basaltic' minerals such as forsteritic olivine, low Ti-augite, labradoritic plagioclase and Fe–Ti oxides. Subsequently, the commingling between hawaiite and trachyte melt containing cumulus anorthoclase took place. We suggest that this process began with an initial mixing (= blending) between the prevailing mafic magma and the felsic melt [according to the model of Frost & Mahood (1987)] (e.g. sample 21x enclave) and continued with further crystallization of the mafic components (Dorais *et al.*, 1990; Wiebe *et al.*, 1997) and incipient melting of the anorthoclase, as observed in the doleritic enclaves of hawaiitic composition.

The enclaves of intermediate composition, containing xenocrysts of the earlier stages of hawaiite and trachyte crystallization, provide the evidence for the commingling process, and undercooling inducing the crystallization, from an already hybrid melt, of intermediate composition acicular and skeletal olivine, Al- and Ti-rich rimmed pyroxene, radial intergrowths of pyroxene and oligoclase and acicular apatite. Late-stage crystallization of ternary feldspar, alkali-feldspar, quartz, aegirine–augite and, occasionally, Na-amphibole and biotite from the residual melt occurred in intercumulus-like conditions. The undercooling appears to be induced by the lower temperature of the original trachytic magma.

The mafic trachyte composition of the volcanic rocks hosting these enclaves falls within the linear array between the differentiated basalt and the trachyte in Harker variation diagrams. According to field and petrographic data, the host-rocks immediately surrounding the intermediate composition enclaves appear to be partially contaminated, enclosing solid and partially melted dismembered enclaves of small size, in agreement with the scheme proposed by Bacon & Metz (1984), Bacon (1986) and Feeley & Dungan (1996). These contaminated trachytes are the result of the mixing between fragmented intermediate enclave materias and a low-silica trachyte (Figs 2d and 6).

According to Mahood *et al.* (1990), Pantelleria provides proof of the existence of a stratified magma chamber with the pantellerite magma localized in the higher part, the anorthoclase-rich trachytic magma in the middle part and the basaltic magma localized below the trachyte in the lower part (Civetta *et al.*, 1984, 1988, 1998; Mahood & Hildreth, 1986). On the basis of the results presented here, an alternative hypothesis to the model of continuous magmatic differentiation from basalt through trachyte to pantellerite can be suggested for the Pantelleria magmatic suite. Following Bacon & Metz (1984) and Bacon (1986), we propose that the enclaves with intermediate compositions demonstrate the interaction between the lower, not basaltic but differentiated mafic magma (hawaiite) and the higher

trachyte containing anorthoclase, with the formation of a hybridized layer.

Some of the enclaves result from the intrusion of a fresh batch of basaltic magma into the more felsic part of a stratified magma chamber. The medium-grained enclaves have a more complex origin. The medium grain size of the enclaves, together with the presence of interstitial melt induced by heating from the host trachytic magma, most probably reflects fragmentation of the wall-rocks to the magma-chamber during the eruption of the 'Green Tuff' and accompanying caldera collapse. According to this hypothesis these enclaves would correspond to earlier crystallization products of the magma chamber system. During the 'Green Tuff' eruption, Pantelleria was covered by a large effusion of pantelleritic ignimbrite, followed by subordinate trachyte lavas (Civetta *et al.*, 1998; Mahood & Stimac, 1988). The emptying of the magmatic chamber, the collapse of the upper part of volcanic edifice, and the formation of Cinque Denti caldera were the result of this eruption. Volcanic activity continued, according to Mahood & Hildreth (1986), with the intra-caldera effusion of the trachytic lavas hosting the enclaves, which form the basis of this study.

Partial melting of some of the enclaves in contact with host magma at a temperature of 1000–950°C occurred under very low-pH_2O conditions, at pressures corresponding to a depth of between 2 and 5 km. Their residence time within the rising magma must have been less than 5 days, on the basis of the preserved zoning of the minerals. This is the calculated time for a magma rising from 2 km depth from the upper part of the chamber at a rate of approximately 12 m^3/s through a conduit radius of 25 m (Wallmann *et al.*, 1988).

Wall-rock enclaves, similar to those analysed in this study, should also occur within the intra-caldera ignimbritic pantellerites of more recent magmatic cycles. This appears to be the case for the 31x syenodioritic enclave and the 'benmoreitic' sample reported by Avanzinelli *et al.* (2004), which were both collected at the same locality (C.da Mida), within VI cycle pantellerite host-rocks.

ACKNOWLEDGEMENTS

The authors wish to thank C. Garbarino for his kind assistance with microprobe analysis at CNR laboratory of Cagliari (Italy), and S. Rotolo and P. Censi for helpful discussions. We are very grateful to C. W. Devey, F. Innocenti, G. A. Mahood, D. F. Parker, A. Provost, M. Stein, M. Wilson and two anonymous reviewers for constructive critical review and useful suggestions that greatly improved the manuscript. Financial support was provided by Italian 'Ministero Istruzione Università Ricerca' (MIUR, 60%).

REFERENCES

Avanzinelli, R., Bindi, L., Menghetti, S. & Conticelli, S. (2004). Crystallisation and genesis of peralkaline magmas from Pantelleria Volcano, Italy: an integrated petrological and crystal-chemical study. *Lithos* **73**, 41–69.

Bacon, C. R. (1986). Magmatic inclusions in silicic and intermediate volcanic rocks. *Journal of Geophysical Research* **91**, 6091–6112.

Bacon, C. R. & Hirschmann, M. M. (1988). Mg/Mn partitioning as test for equilibrium coexisting Fe–Ti oxides. *American Mineralogist* **73**, 57–61.

Bacon, C. R. & Metz, J. (1984). Magmatic inclusions in rhyolites, contaminated basalts, and compositional zonation beneath the Coso volcanic field, California. *Contributions to Mineralogy and Petrology* **85**, 346–365.

Bailey, D. K. & Macdonald, R. (1987). Dry peralkaline felsic liquids and carbon dioxide flux through the Kenya rift zone. In: Mysen, B. (ed.) *Magmatic Processes: Physicochemical Principles. Geochemical Society, Special Publication* **1**, 91–105.

Baker, I. (1968). Intermediate oceanic volcanic rocks and the 'Daly Gap'. *Earth and Planetary Science Letters* **4**, 103–106.

Baker, D. R. & Eggler, D. H. (1983). Fractionation paths of Atka (Aleutians) high-alumina basalts: constraints from phase relations. *Journal of Volcanology and Geothermal Research* **18**, 387–404.

Barberi, F., Borsi, S., Ferrara, G. & Innocenti, F. (1969). Strontium isotopic composition of some recent basic volcanites of southern Tyrrenian Sea and Sicily Channel. *Contributions to Mineralogy and Petrology* **23**, 157–172.

Barberi, F., Ferrara, G., Santacroce, R., Treuil, M. & Varet, J. (1975). A transitional basalt–pantellerite sequence of fractional crystallisation, the Boina Centre (Afar, Ethiopia). *Journal of Petrology* **16**, 22–56.

Behrens, H. & Jantos, N. (2001). The effect of anhydrous composition on water solubility in granitic melts. *American Mineralogist* **86**, 14–20.

Berman, R. G. (1988). Internally-consistent thermodynamic data for minerals in the system Na_2O–K_2O–CaO–MgO–FeO–Fe_2O_3–Al_2O_3–SiO_2–TiO_2–H_2O–CO_2. *Journal of Petrology* **29**, 445–522.

Berrino, G. & Capuano, P. (1995). Gravity anomalies and structures at the island of Pantelleria. *Acta Vulcanologica* **7**, 19–26.

Bohrson, W. A. & Reid, M. R. (1997). Genesis of silicic peralkaline volcanic rocks in an ocean island setting by crustal melting and open-system processes. *Journal of Petrology* **38,** 1137–1166.

Bonnefoi, C. C., Provost, A. & Albarède, F. (1995). The 'Daly gap' as a magmatic catastrophe. *Nature* **378**, 270–272.

Boynton, W. V. (1984). Geochemistry of rare earth elements: meteorite studies. In: Henderson, P. (ed.) *Rare Earth Element Geochemistry*. Amsterdam: Elsevier, pp. 63–114.

Bowen, N. L. & Tuttle, O. F. (1950). The system $NaAlSi_3O_8$–$KAlSi_3O_8$–H_2O. *Journal of Geology*, **58**, 489.

Brown, W. L. & Parsons, I. (1984). Exsolution and coarsening mechanisms and kinetics in an ordered cryptoperthite series. *Contributions to Mineralogy and Petrology* **86**, 3–18.

Cann, J. R. (1968). Bimodal distribution of rocks from volcanic islands. *Earth and Planetary Science Letters* **4**, 479–480.

Carapezza, M., Ferla, P., Nuccio, P. M. & Valenza, M. (1979). Caratteri petrologici e geochimici delle vulcaniti dell'Isola Ferdinandea. *Rendiconti della Società Italiana di Mineralogia e Petrologia* **35**, 377–388.

Carmichael, I. S. E. (1962). Pantelleritic liquids and their phenocrysts. *Mineralogical Magazine* **33**, 86–113.

Carmichael, I. S. E. (1967). The iron–titanium oxides of salic volcanic rocks and their associated ferromagnesian silicates. *Contributions to Mineralogy and Petrology* **14**, 36–64.

Carmichael, I. S. E. (1991). The redox states of basic and silicic magmas: a reflection of their source regions? *Contributions to Mineralogy and Petrology* **106**, 129–141.

Carmichael, I. S. E. & Ghiorso, M. S. (1990). The effect of oxygen fugacity on the redox state of natural liquids and their crystallizing phases. In: Nicholls, J. & Russell, J. K. (eds) *Modern Methods of Igneous Petrology: Understanding Magmatic Processes. Mineralogical Society of America, Reviews in Mineralogy* **24**, 191–212.

Carmichael, I. S. E. & MacKenzie, W. S. (1963). Feldspar–liquid equilibria in pantellerites: an experimental study. *American Journal of Science* **261**, 382–396.

Caroff, M., Maury, R. C., Leterrier, J., Joron, J. L., Cotten, J. & Guille, G. (1993). Trace element behavior in the alkali basalt–comenditic trachyte series from Mururoa atoll, French Polynesia. *Lithos* **30**, 1–22.

Catalano, R., Infuso, S. & Sulli, A. (1993). The Pelagian foreland and its northward foredeep: Plio-Pleistocene structural evolution. In: Max, M. D. & Colantoni, P. (eds) *Geological Development of the Sicilian–Tunisian Platform. UNESCO Report in Marine Science* **58**, 37–42.

Chayes, F. (1963). Relative abundance of intermediate members of the oceanic basalt–trachyte association. *Journal of Geophysical Research* **68,** 1519–1534.

Chayes, F. (1977). The oceanic basalt–trachyte relation in general and in the Canary Island. *American Mineralogist* **62**, 666–671.

Christofersen, R., Yund, R. A. & Tullis, J. (1983). Inter-diffusion of K and Na in alkali feldspars: diffusion couple experiments. *American Mineralogist* **68**, 1126–1133.

Civetta, L., Cornette, Y., Crisci, G., Gillot, P.-Y., Orsi, G. & Requejos, C. S. (1984). Geology, geochronology and chemical evolution of the island of Pantelleria. *Geological Magazine* **121**, 541–668.

Civetta, L., Cornette, Y., Gillot, P.-Y. & Orsi, G. (1988). The eruptive history of Pantelleria (Sicily Channel) in the last 50 ka. *Bulletin of Volcanology* **50**, 47–57.

Civetta, L., D'Antonio, M., Orsi, G. & Tilton, G. R. (1998). The geochemistry of volcanic rocks from Pantelleria Island, Sicily channel: petrogenesis and characteristics of the mantle source region. *Journal of Petrology* **39**, 1453–1491.

Clague, D. A. (1978). The oceanic basalt–trachyte association: an explanation of the Daly Gap. *Journal of Geology* **86**, 739–743.

Colby, J. W. (1967). *MAGIC IV, a computer program for quantitative electron microbrobe analyses*. Allentown, PA: Bell Telephone Laboratories.

Colombi, B., Giese, P., Luongo, G., Morelli, C., Riuscetti, M., Scarascia, S., Schute, K., Strowald, J. & de Visintini, G. (1973). Preliminary report on the seismic refraction profile Gargano–Salerno–Palermo–Pantelleria. *Bollettino di Geofisica Teorica e Applicata* **15**, 225–254.

Cornette, Y., Crisci, G. M., Gillot, P.-Y. & Orsi, G. (1983). The recent volcanic history of Pantelleria: a new interpretation. In: Sheridan, M. F. & Barberi, F. (eds) *Explosive Volcanism. Journal of Volcanology and Geothermal Research* **17**, 361–373.

Deer, W. A., Howie, R. A. & Zussman, J. (1978). *Rock Forming Minerals. Single-chain Silicates*. Harlow: Longman, 668 pp.

De La Roche, H., Leterrier, J., Grandclaude, P. & Marchal, M. (1980). A classification of volcanic and plutonic rocks using R1R2-diagram and major-element analyses—its relationships with current nomenclature. *Chemical Geology* **29**, 183–210.

De Vivo, B., Frezzotti, M. L. & Lima, A. (1993). Immiscibility in magmatic differentiation and fluid evolution in granitoid xenoliths: fluid inclusion evidence. *Acta Vulcanologica* **3**, 195–202.

Dorais, M. J., Whitney, J. A. & Roden, M. F. (1990). Origin of mafic enclaves in the Dinkey Creek Pluton, Central Sierra Nevada, California. *Journal of Petrology* **31**, 853–881.

Esperança, S. & Crisci, G. M. (1995). The island of Pantelleria: a case for the development of DMM–HIMU isotopic compositions in a long-lived extensional setting. *Earth and Planetary Science Letters* **136**, 167–182.

Feeley, T. C. & Dungan, M. A. (1996). Compositional and dynamic controls on mafic–silicic magma interactions at continental arc volcanoes: evidence from Cordon El Guadal, Tatara–San Pablo Complex, Chile. *Journal of Petrology* **37**, 1547–1577.

Ferla, P. (1997). The role of magma mixing in enclaves covering the 'Daly gap' in alkaline suite at Pantelleria (Italy) (abstract). *Plinius (Italian Supplement to European Journal of Mineralogy)* **16**, 113–115.

Ferla, P., Nuccio, P. M. & Valenza, M. (1978). Fenomeni termochimici nell'interazione fra magma e xenoliti arenacei nella lava etnea del 1886. *Mineralogica et Petrografica Acta* **22**, 71–84.

Franzini, M., Leoni, L. & Saitta, M. (1975). Revisione di una metodologia analitica per fluorescenza X basata sulla correzione completa degli effetti matrice. *Rendiconti della Società Italiana de Minerologia e Petrologia* **31**, 365–378.

Frost, P. T. & Mahood, G. A. (1987). Field, chemical and physical constraints on mafic–felsic magma interaction in the Lamarck Granodiorite, Sierra Nevada, California. *Geological Society of America Bulletin* **99**, 272–291.

Geschwind, C. H. & Rutherford, M. J. (1995). Crystallisation of microlites during magma ascent: the fluid mechanics of 1980–1986 eruptions at Mount St. Helens. *Bulletin of Volcanology* **57**, 356–370.

Ghiorso, M. S. & Sack, R. O. (1991). Fe–Ti oxide geothermometry: thermodynamic formulation and the estimation of intensive variables in silicic magmas. *Contributions to Mineralogy and Petrology* **108**, 485–510.

Gourgaud, A. & Villemant, B. (1992). Evolution of magma mixing in an alkaline suite: the Grande Cascade sequence (Monts-Dore, French Massif Central). Geochemical modelling. *Journal of Volcanology and Geothermal Research* **52**, 255–275.

Grove, T. L., Gerlach, D. C. & Sando, T.W. (1982). Origin of calc-alkaline series lava at Medicine Lake volcano by fractionation, assimilation and mixing. *Contributions to Mineralogy and Petrology* **80**, 160–182.

Harris, C. & Bell, J. D. (1982). Natural partial melting of syenite blocks from Ascension Island. *Contributions to Mineralogy and Petrology* **79**, 107–113.

Huebner, J. S. & Sato, M. (1978). The oxygen fugacity–temperature relationships of manganese oxide and nickel oxide buffers. *Amercan Mineralogist* **55**, 934–952.

Johannes, W. (1985). The significance of experimental studies for the formation of migmatites. In: Ashworth, J. R. (ed.) *Migmatites*. Glasgow: Blackie, pp. 36–85.

Johannes, W. & Holtz, F. (1990). Formation and composition of H_2O undersaturated granitic melts. In: Ashworth, J. R. & Brown, M. (eds) *High-temperature Metamorphism and Crustal Anatexis*. London: Unwin Hyman, pp. 87–104.

Joron, J. L. & Treuil, M. (1989). Hygromagmaphile element distributions in oceanic basalts as fingerprints of partial melting and mantle heterogeneities: a specific approach and proposal of an identification and modelling method. In: Saunders, A. D. & Norry, M. J. (eds) *Magmatism in the Ocean Basins. Geological Society, London, Special Publications* **42**, 277–299.

Kilinc, A., Carmichael, I. S. E., Rivers, M. L. & Sack, R. O. (1983). The ferric–ferrous ratio of natural silicate liquids equilibrated in air. *Contributions to Mineralogy and Petrology* **83**, 136–140.

Leake, B. E. (Chairman), Woolley, A. R. (Secretary), Arps, C. E. S., Birch, W. D., Gilbert, C. M., Grice, J. D., *et al.* (1997). Nomenclature of amphiboles: Report of the Subcommittee on Amphiboles of the International Mineralogical Association,

Commission on New Minerals and Mineral Names. *American Mineralogist* **82**, 1019–1037.

Le Maitre, R. W., Bateman, P., Dudek, A., Keller, J., Lameyre, J., Le Bas, M. J., Sabine, P. A., Schmid, R., Sorensen, H., Streckeisen, A., Woolley, A. R. & Zanettin, B. (1989). *A Classification of Igneous Rocks and Glossary of Terms: Recommendations of the International Union of Geological Sciences Subcommission on the Systematics of Igneous Rocks*. Oxford: Blackwell Scientific.

Leoni, L. & Saitta, M. (1976). X-ray fluorescence analysis of 29 trace elements in rock and mineral standards. *Rendiconti della Società Italiana de Mineralogia e Petrologia* **32**, 497–510.

Leoni, L., Menichini, M. & Saitta, M. (1982). Determination of S, Cl and F in silicate rocks by X-ray fluorescence analyses. *X-ray Spectrometry* **11**, 156–158.

Loucks, R. R. (1996). A precise olivine–augite Mg–Fe-exchange geothermometer. *Contributions to Mineralogy and Petrology* **125**, 140–150.

Lowenstern, J. B. & Mahood, G. A. (1991). New data on magmatic H_2O contents of pantellerites, with implications for petrogenesis and eruptive dynamics at Pantelleria. *Bulletin of Volcanology* **54**, 78–83.

Lowenstern, J. B., Mahood, G. A., Herving, R. L. & Sparks, J. (1993). The occurrence and distribution of Mo and molybdenite in unaltered peralkaline rhyolites from Pantelleria, Italy. *Contributions to Mineralogy and Petrology* **114**, 119–129.

Lucido, G. (1982). Liquid immiscibility: a possible genetic process may explain the volcanites of Pantelleria (Channel of Sicily). *Mineralogica et Petrografica Acta* **26**, 15–26.

Luhr, J. F. & Carmichael, I. S. E. (1980). The Colima Volcanic Complex, Mexico. *Contributions to Mineralogy and Petrology* **71**, 343–372.

Macdonald, R. (1974). Nomenclature and petrochemistry of the peralkaline oversaturated extrusive rocks. In: Bailey, D. K., Barberi, F. & Macdonald, R. (eds) *Oversaturated Extrusive Peralkaline Volcanic Rocks. Bulletin Volcanologique (Special Issue)* **38**, 498–516.

Macdonald, R. & Bailey, D. K. (1973). The chemistry of the peralkaline oversaturated obsidians. *US Geological Survey, Professional Papers* **440-N**(Part 1), 1–37.

MacKenzie, W. S., Donaldson, C. H. & Guilford, C. (1982). *Atlas of Igneous Rocks and their Textures*. Harlow: Longman.

Mahood, G. A. (1984). Pyroclastic rocks and calderas associated with strongly peralkaline magmatism. *Journal of Geophysical Research* **89**, 8540–8552.

Mahood, G. A. & Baker, D. R. (1986). Experimental constraints on depths of fractionation of mildly alkalic basalts and associated felsic rocks: Pantelleria, Strait of Sicily. *Contributions to Mineralogy and Petrology* **93**, 251–264.

Mahood, G. A. & Hildreth, W. (1983). Nested calderas and trap-door uplift at Pantelleria, Strait of Sicily. *Geology* **11**, 103–106.

Mahood, G. A. & Hildreth, W. (1986). Geology of the peralkaline volcano at Pantelleria, Strait of Sicily. *Bulletin of Volcanology* **48**, 143–172.

Mahood, G. A. & Stimac, J. A. (1990). Trace-element partitioning in pantellerites and trachytes. *Geochimica et Cosmochimica Acta* **54**, 2257–2276.

Mahood, G. A., Halliday, A. N. & Hildreth, W. (1990). Isotopic evidence for the origin of pantellerites in a rift-related alkalic suite: Pantelleria, Italy. *International Volcanology Congress of the International Association of Volcanology and Chemistry of the Earth's Interior, Mainz, Abstracts Volume*. Mainz: IAVCEI.

Marsh, B. D. (1988). Crystal capture, sorting, and retention in convecting magma. *Geological Society of American Bulletin* **100**, 1720–1737.

Mathez, E. A. (1973). Refinement of the Kudo–Weill plagioclase thermometer and its application to basaltic rocks. *Contributions to Mineralogy and Petrology* **41**, 61–72.

Morimoto, N. (1988). Nomenclature of pyroxenes. *Fortschritte der Mineralogie* **66**, 237–252.

Mungall, J. E. & Martin, R. F. (1995). Petrogenesis of basalt–comendite and basalt–pantellerite suites, Terceira, Azores, and some implications for the origin of oceanic rhyolites. *Contributions to Mineralogy and Petrology* **119**, 43–55.

Nimis, P. (1995). A clinopyroxene geobarometer for basaltic systems based on crystal-structure modeling. *Contributions to Mineralogy and Petrology* **121**, 115–125.

Olmi, F. (1997). La microsonda elettronica e particolari problemi di microanalisi. *Plinius (Italian Supplement to European Journal of Mineralogy)* **18**, 237–245.

Orsi, G., Ruvo, L. & Scarpati, C. (1991). The recent explosive volcanism at Pantelleria. *Geologische Rundschau* **80**, 187–200.

Papike, J. J., Cameron, K. & Baldwin, K. (1974). Amphiboles and pyroxenes; characterization of other than quadrilateral components and estimates of ferric iron from microprobe data. *Geological Society of America, Abstracts with Programs* **6**, 1053–1050.

Peccerillo, A., Barberio, M. R., Yirgu, G., Ayalew, D., Barbieri, M. & Wu, T. W. (2003). Relationships between mafic and peralkaline silicic magmatism in continental rift setting: a petrological, geochemical and isotopic study of the Gedemsa Volcano, Central Ethiopian Rift. *Journal of Petrology* **44**, 2003–2032.

Putirka, K., Johnson, M., Kinzler, R., Longhi, J. & Walker, D. (1996). Thermobarometry of mafic igneous rocks based on clinopyroxene–liquid equilibria, 0–30 kbar. *Contributions to Mineralogy and Petrology* **123**, 92–108.

Renzulli A., Tribaudino, M., Salvioli-Mariani, E., Serri, G. & Holm, P. H. (2003). Cordierite–anorthoclase hornfels xenoliths in Stromboli lavas (Aeolian Island, Sicily): an example of a fast cooled contact aureole. *European Journal of Mineralogy* **15**, 665–679.

Reuther, C. D. & Eisbacher, G. H. (1985). Pantelleria rift: crustal extension in a convergent intraplate setting. *Geologische Rundschau* **74**, 585–597.

Rittmann, A. (1967). Studio geovulcanologico e magmatologico dell' isola di Pantelleria. *Rivista Mineraria Siciliana* **106–108**, 147–204.

Roeder, P. L. & Emslie, R. F. (1970). Olivine–liquid equilibrium. *Contributions to Mineralogy and Petrology* **29**, 275–289.

Romano, R. (1969). Sur l'origine de l'excès de sodium (ns) dans certaines laves de i'Ile de Pantelleria. *Bulletin Volcanologique* **33**, 694–700.

Sisson, T. W. & Grove, T. L. (1993*a*). Experimental investigation of the role of H_2O in calc-alkaline differentiation and subduction sone magmatism. *Contributions to Mineralogy and Petrology* **113**, 143–166.

Sisson, T. W. & Grove, T. L. (1993*b*). Temperature and H_2O contents of low high-alumina basalts. *Contributions to Mineralogy and Petrology* **113**, 167–184.

Snyder, D. A. & Carmichael, I. S. E. (1992). Olivine–liquid equilibria and the chemical activities of FeO, NiO, Fe_2O_3, and MgO in natural basic melts. *Geochimica et Cosmochimica Acta* **56**, 303–318.

Spray, J. G. & Rae, D. A. (1995). Quantitative electron-microprobe analysis of alkali silicate glasses: a review and user guide. *Canadian Mineralogist* **33**, 323–332.

Villari, L. (1974). The island of Pantelleria. *Bulletin of Volcanology* **38**, 680–724.

Villemant, B., Jaffrezic, H., Joron, J. L. & Treuil, M. (1981). Distribution coefficient of major and trace elements, fractional

crystallisation in the alkali basalt series of Chaîne des Puys (Massif Central, France). *Geochimica et Cosmochimica Acta* **45**, 1997–2016.

Wallmann, P. C., Mahood, G. A. & Pollard, D. D. (1988). Mechanical models for correlation of ring-fracture eruptions at Pantelleria, Strait of Sicily, with glacial sea-level drawdown. *Bulletin of Volcanology* **50**, 327–339.

Washington, H. S. (1913–1914). The volcanoes and rocks of Pantelleria: I, II, III. *Journal of Geology* **21**, 653–670; **21**, 683–713; **22**, 16–27.

Webster, J. D. (1997). Chloride solubility in felsic melts and the role of chloride in magmatic degassing. *Journal of Petrology* **38**, 1793–1807.

Wiebe, R. A., Smith, D., Sturm, M., King, E. M. & Seckler, M. S. (1997). Enclaves in Cadillac Mountain Granite (coastal Maine): samples of hybrid magma from the base of the chamber. *Journal of Petrology* **38**, 393–423.

Wolff, J. A. & Wright, J. V. (1981). Formation of the Green Tuff, Pantelleria. *Bulletin of Volcanology* **44**, 681–690.

Yoder, H. S. (1973). Contemporaneous basaltic and rhyolitic magmas. *American Mineralogist* **58**, 153–171.

Zies, E. G. (1966). A new analysis of cossyrite from the Island of Pantelleria. *American Mineralogist* **51**, 200–205.

Zinngrebe, E. & Foley, S. F. (1995). Metasomatism in mantle xenoliths from Gees, West Eifel, Germany: evidence for the genesis of calc-alkaline glasses and metasomatic Ca-enrichment *Contributions to Mineralogy and Petrology* **122**, 79–96.

APPENDIX: SAMPLE LOCATIONS

Sample	Latitude (N)		Longitude (E)	
	degrees	minutes	degrees	minutes
12	36	47·26	11	59·77
15	36	46·76	11	59·97
16B	36	46·62	11	59·91
17B	36	46·55	11	59·90
18	36	46·52	11	59·91
20	36	46·53	11	59·83
21	36	46·63	11	59·83
22	36	46·55	11	59·78
23	36	46·55	11	59·77
25	36	46·61	11	59·67
27A	36	46·58	11	59·70
27B	36	46·63	11	59·67
28	36	46·81	11	59·42
30	36	47·57	11	59·40
31	36	47·59	11	59·73
40	36	47·71	12	00·27
41	36	47·71	12	00·27
42	36	47·71	12	00·27
62A	36	46·50	12	00·19
62B	36	46·51	12	00·19
63	36	46·57	11	58·88
72	36	45·84	11	59·73
73	36	47·58	11	59·33
759	36	47·94	11	59·40
77	36	48·46	11	58·09
79	36	48·46	11	58·10
80A	36	48·54	11	58·23
80C	36	48·54	11	58·23
81	36	44·63	11	59·92
85	36	45·82	11	59·23
89	36	46·13	11	58·56
90	36	48·09	11	57·45
97	36	49·33	12	00·32
102	36	49·12	11	59·01
103	36	49·12	11	59·05
105	36	49·12	11	59·02
108	36	45·51	12	01·00
118	36	46·47	12	01·42
120	36	48·63	12	01·38
121	36	48·63	12	01·43